PERMANENT MAGNETS

SHORT COURSE

SNOWMASS, CO.
JULY 2001

R. Schlueter

PERMANENT MAGNETS

I MAGNETOSTATICS BASICS

- B, H
- MAXWELL
- B-H IRON
- $B, \tilde{H}, \tilde{V}, A$

II PURE PM THEORY

- B-H PM
- EM & PM EQUIVALENCE IN SOLENOID
- ADVANTAGES OF PM
- EXPANSIONS, TAYLOR, LAURENT
- MULTIPOLES, ALLOWED
- PM MULTIPOLES, STRENGTH, QUALITY
- 2D EASY AXIS ROTATION TH.
- 3D PURE PMs
- 3D EASY AXIS ROTATION Tth.

III HYBRID THEORY

SCALAR POT = CONST. SURFACES + CHARG

DIRECT FIELDS, INDIRECT FIELDS

HYBRID DIPOLE

Schwarz-Christoffel, excess flux

IV APPLICATIONS

A. HYBRID

QUADRUPOLE, TUNING

FERRITE VS RARE EARTHS

PM PROPERTIES LIST

COMBINED FCN. MAGNET

HYBRID IDs

TIP SHAPES

B. PURE PM

PURE PM IDS

ID ENDS

SEPTUMS

SOLENOIDS

HARMONIC GEN./CORRECTOR RING

FORCES

NI

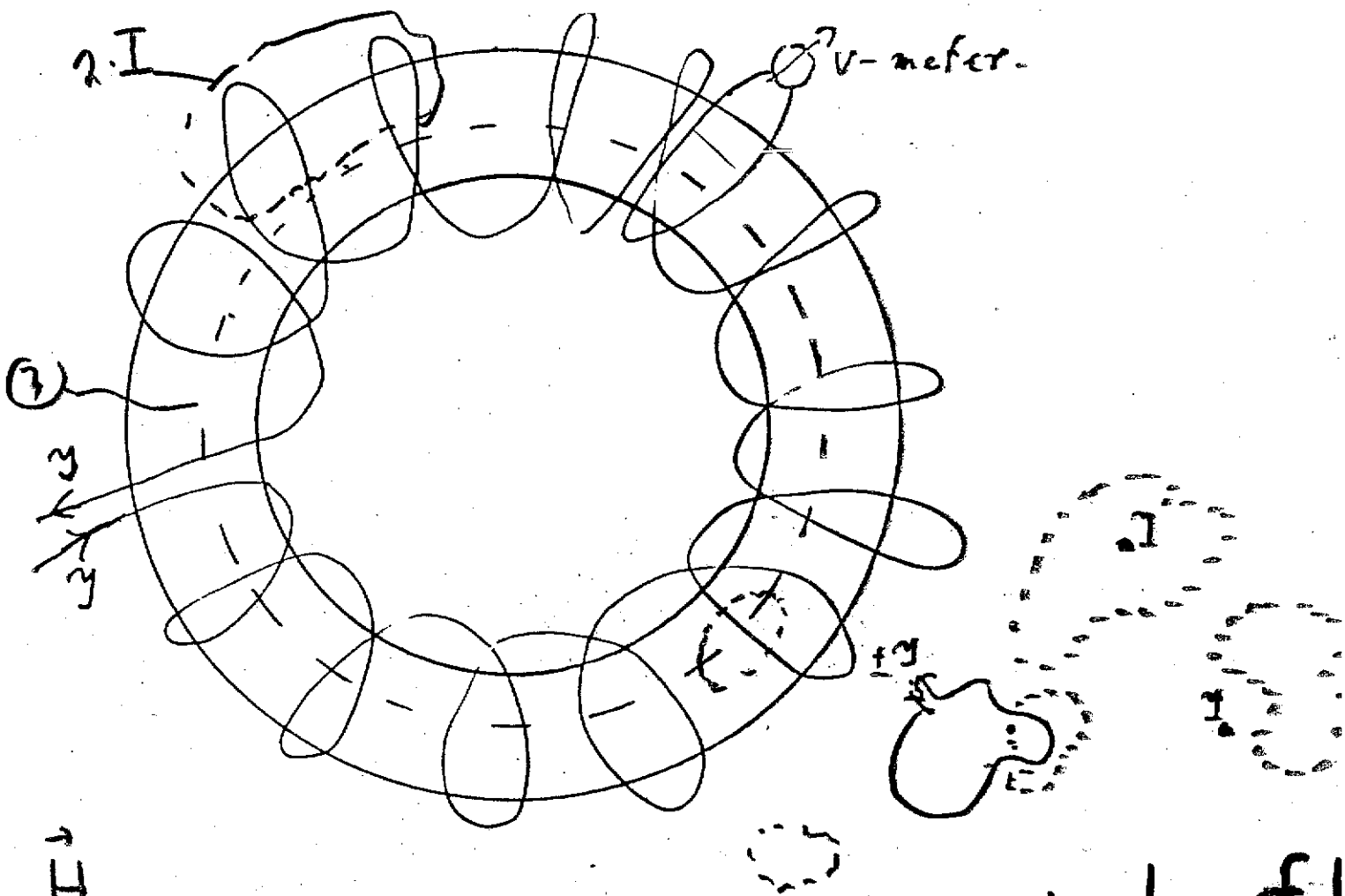

$\vec{H}$

$\oint H \cdot ds = I_{enclosed} \Rightarrow H\,[A/m] \times$ unit value of l

$V = \oint E \cdot ds = -\frac{d\int \mu_0 H \cdot da}{dt}$ [VACUUM]

$\mu_0 = 4\pi \cdot 10^{-7}\ Vs/A \cdot m$

$V = -\frac{d\int B da}{dt}$

$B = B(H)$

B ≡ magnetic flux density $[T] \equiv Vs/m^2$

$B = \mu \mu_0 H$

└ dimensionless number

MAXWELL:

INTEGRAL FORMULATION (macroscopic scale)		DIFFERENTIAL FORMULATION (microscopic scale)
Ampere	$\oint \vec{H}\cdot d\vec{s} = I(t) = \int \vec{j}\cdot d\vec{a}$	$\Leftrightarrow \quad \vec{\nabla}\times\vec{H} = \vec{j}$
FARADAY	$V_{IND} = \oint \vec{E}\cdot d\vec{s} = -\int \vec{B}\cdot d\vec{a} = -\dot{\Phi}$	$\Leftrightarrow \quad \vec{\nabla}\times\vec{E} = \dot{\vec{B}} \Rightarrow$
$(\dot{} \equiv \frac{\partial}{\partial t})$	$\vec{\nabla}\cdot\dot{\vec{B}} = 0 \Rightarrow$	$\vec{\nabla}\cdot\vec{B} = \rho_M = 0$

In vacuum: $\vec{B} = \mu_0 \vec{H} \equiv \vec{\vec{H}}$; $\mu_0 = 4\pi \frac{Gcm}{A} = 4\pi\cdot 10^{-7} \frac{Vs}{Am}$

In general: $\vec{B} = \mu_0 \mu \vec{H} \equiv \mu \vec{\vec{H}}$; $\sim \equiv \cdot\mu_0$

Continuity across an interface:

$\vec{\nabla}\cdot B = 0 \Rightarrow \Delta B_\perp = 0$

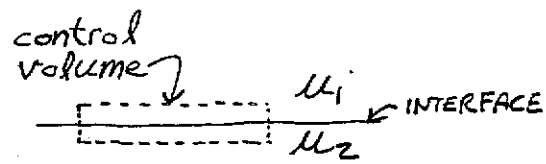

$\vec{\nabla}\times H = 0 \Rightarrow \Delta H_{//} = 0$

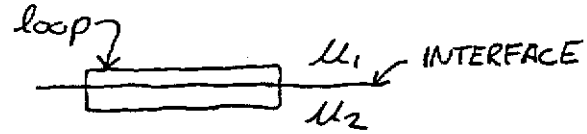

Application - for isotropic media of μ_2, μ_1:

HW find $\alpha_1 = f(\mu_2, \mu_1, \alpha_2)$

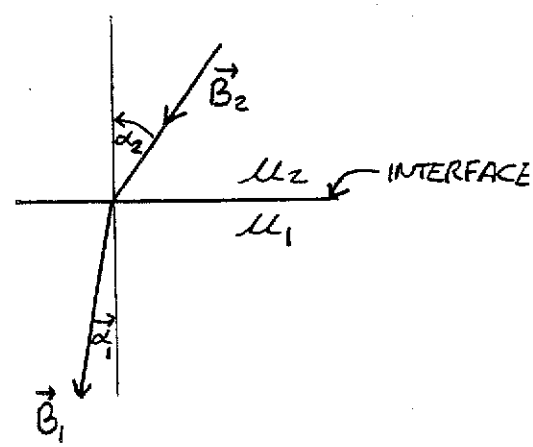

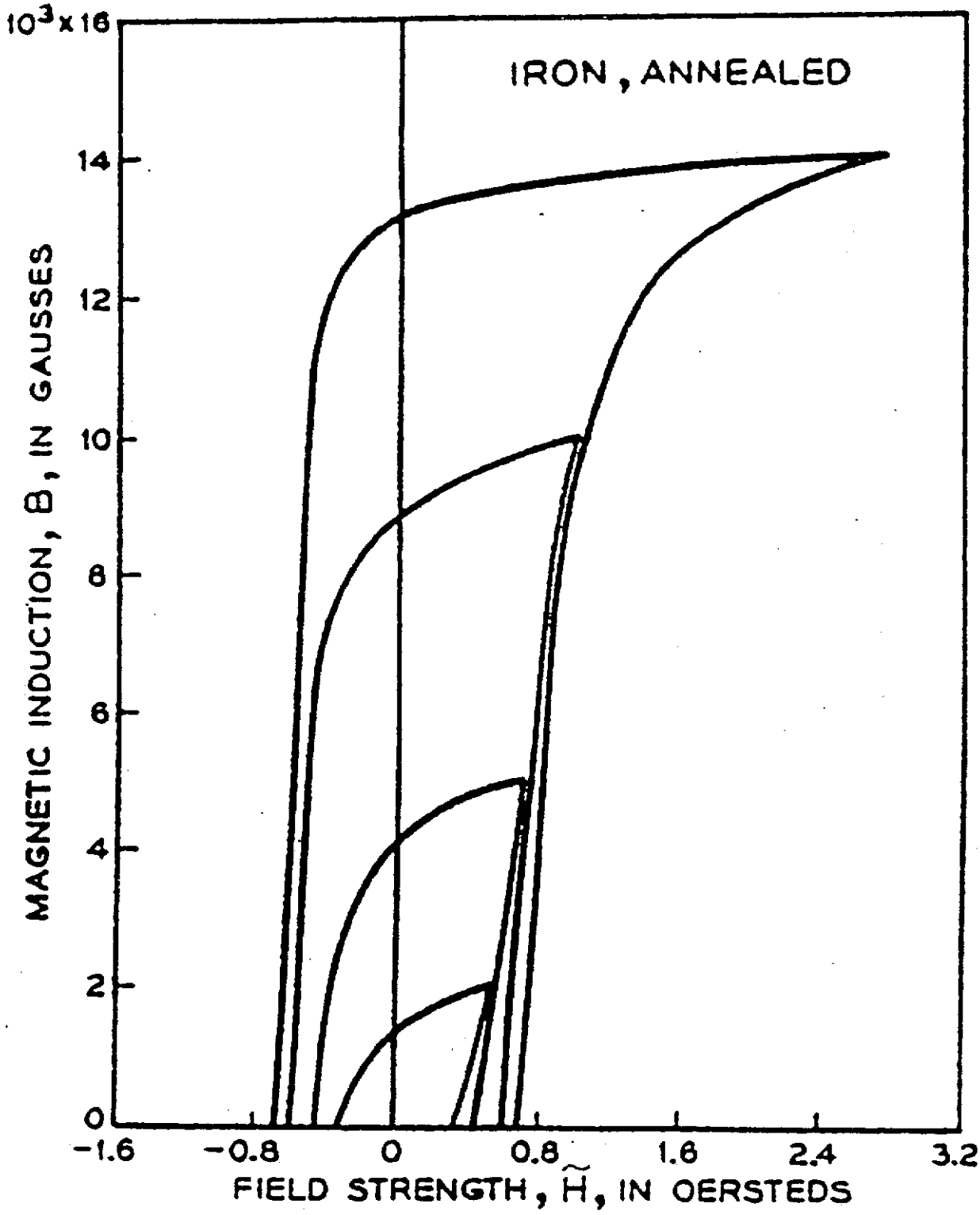

Upper halves of hysteresis loops of ordinary annealed iron

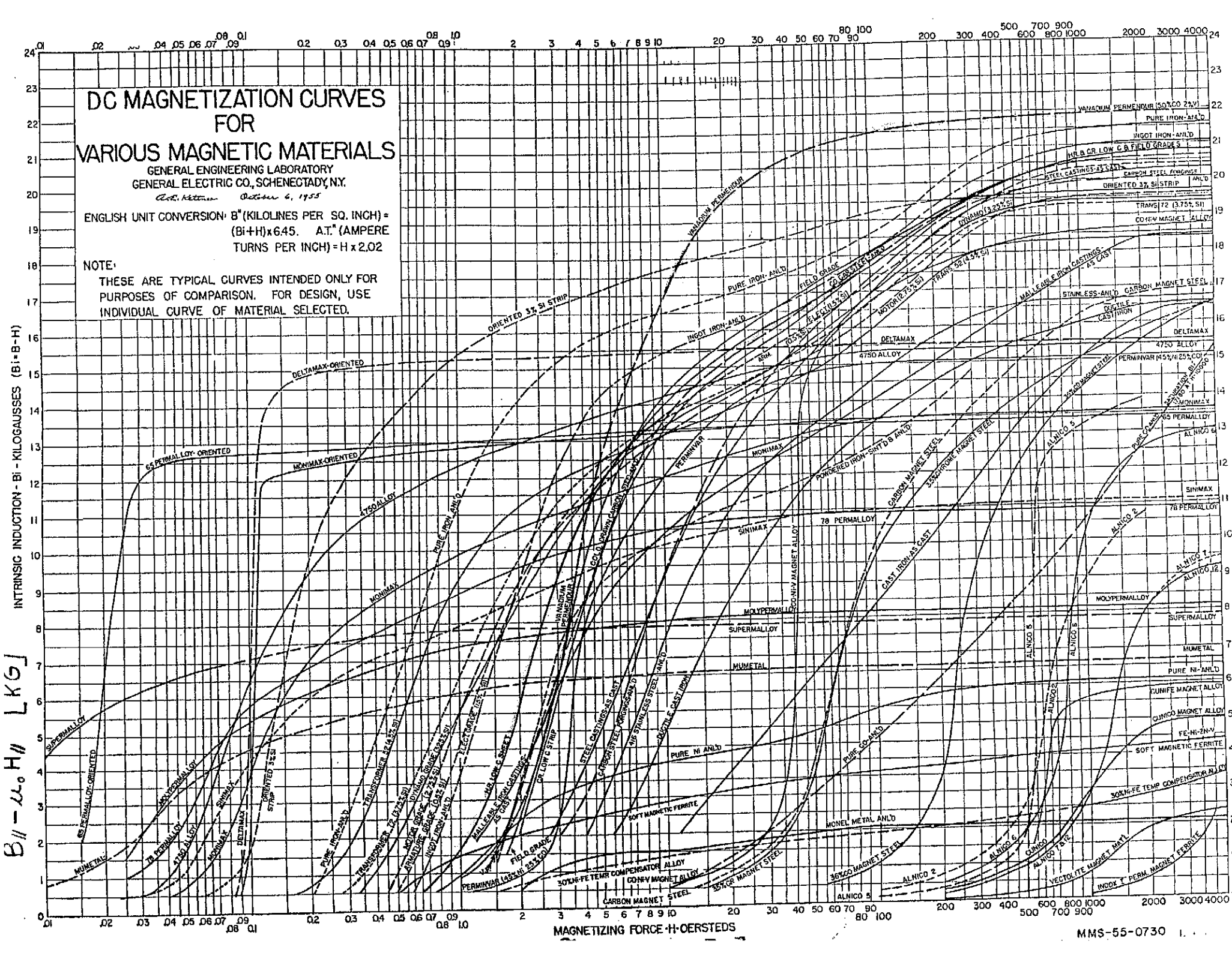
DC MAGNETIZATION CURVES FOR VARIOUS MAGNETIC MATERIALS
GENERAL ENGINEERING LABORATORY
GENERAL ELECTRIC CO., SCHENECTADY, N.Y.
Oct. 6, 1955
ENGLISH UNIT CONVERSION: B" (KILOLINES PER SQ. INCH) = (Bi+H)x6.45. A.T." (AMPERE TURNS PER INCH) = H x 2.02
NOTE:
THESE ARE TYPICAL CURVES INTENDED ONLY FOR PURPOSES OF COMPARISON. FOR DESIGN, USE INDIVIDUAL CURVE OF MATERIAL SELECTED.
INTRINSIC INDUCTION - Bi - KILOGAUSSES (Bi = B - H)
B// - μ0 H// [KG]
MAGNETIZING FORCE - H - OERSTEDS
VANADIUM PERMENDUR (50% CO 2% V)
PURE IRON - ANL'D
INGOT IRON - ANL'D
HR & CR LOW C & FIELD GRADES
STEEL CASTINGS - AS CAST
CARBON STEEL FORGINGS - ANL'D
ORIENTED 3% SI STRIP
TRANS. 72 (3.75% SI)
CONI-V MAGNET ALLOY
DYNAMO (3.25% SI)
MALLEABLE IRON CASTINGS - AS CAST
STAINLESS - ANL'D CARBON MAGNET STEEL
DUCTILE CAST IRON
DELTAMAX
4750 ALLOY
PERMINVAR (45% NI 25% CO)
MONIMAX
65 PERMALLOY
ALNICO 5
POWDERED IRON - SINT'D & ANL'D
CARBON MAGNET STEEL
3.5% CHROME MAGNET STEEL
SINIMAX
78 PERMALLOY
ALNICO 2
ALNICO 1
ALNICO 12
MOLYPERMALLOY
SUPERMALLOY
MUMETAL
PURE NI - ANL'D
CUNIFE MAGNET ALLOY
CUNICO MAGNET ALLOY
FE-NI-ZN-V
SOFT MAGNETIC FERRITE
30% NI-FE TEMP COMPENSATOR ALLOY
PURE CO - ANL'D
MONEL METAL ANL'D
36% CO MAGNET STEEL
35% CR MAGNET STEEL
CARBON MAGNET STEEL
ALNICO 6
CUNICO
ALNICO 7 & 12
VECTOLITE MAGNET MAT'L
INDOX 1 PERM. MAGNET FERRITE
TRANSFORMER (4.5% SI)
ARMATURE GRADE (2.25% SI)
ELECTRICAL (1.5% SI)
MOTOR (2.5% SI)
FIELD GRADE (.5% SI)
PERMINVAR (45% NI 25% CO)
MS LOW C SHEET
MS STAINLESS STEEL ANL'D
DUCTILE CAST IRON
MMS-55-0730

SCALAR & VECTOR POTENTIALS:

For $\vec{j}=0$ & $\frac{d}{dt}=0 \Rightarrow$

1) $\vec{\nabla}\times\vec{H}=0$ & $\vec{\nabla}\times\vec{\nabla}V=0$ $\quad\therefore\quad \vec{H}=-\vec{\nabla}V$
(V: scalar)

2) $\vec{\nabla}\cdot\vec{B}=0$ & $\vec{\nabla}\cdot\vec{\nabla}\times\vec{A}=0$ $\quad\therefore\quad \vec{B}=\vec{\nabla}\times\vec{A}$
($\vec{A}$: vector)

LAPLACE EQN. for $\tilde{V}$:

$\nabla^2 \equiv \frac{\partial^2}{\partial x^2}+\frac{\partial^2}{\partial y^2}+\frac{\partial^2}{\partial z^2}$

$$\vec{B}=\vec{\tilde{H}}=-\vec{\nabla}\tilde{V}\ ;\ \vec{\nabla}\cdot\vec{B}=0 \Rightarrow \vec{\nabla}\cdot\vec{\nabla}\tilde{V}=\nabla^2\tilde{V}=0$$

LAPLACE EQN. for cartesian components of $\vec{\tilde{H}}=(\tilde{H}_x,\tilde{H}_y,\tilde{H}_z)$:

$$0=\nabla^2\tilde{V} \Rightarrow \frac{\partial}{\partial x}\overset{0=}{\nabla^2\tilde{V}} = \nabla^2\frac{\partial\tilde{V}}{\partial x} = -\nabla^2\tilde{H}_x$$

similarly $0=\nabla^2\tilde{H}_y$, $0=\nabla^2\tilde{H}_z$

IMPORTANT IMPLICATION: EXTREMA ON SURFACE OF VOLUME;
FURTHERMORE, SINCE $H_{y\,IDEAL}$ & $H_{y\,ACTUAL}$ obey MAXWELL,
THEN SO DOES $H_{y\,ERROR} = H_{y\,ACTUAL} - H_{y\,IDEAL}$

$\Rightarrow$ If we specify field quality on a surface enclosing a volume, then field quality will be at least as good everywhere within this volume, the "GOOD FIELD REGION"

LAPLACE EQN. for $\vec{A}$ in 2-D case where $\frac{\partial}{\partial z}=0$:

$$\vec{\tilde{H}}=\vec{B}=\vec{\nabla}\times\vec{A}\ ;\ \vec{\nabla}\times\vec{\tilde{H}}=0 \Rightarrow \vec{\nabla}\times\vec{\nabla}\times\vec{A}=\nabla^2 A=0$$

here $\nabla^2\equiv\frac{\partial^2}{\partial x^2}+\frac{\partial^2}{\partial y^2}$; $\vec{A}=(0,0,A)$

2-D Scalar & Vector Potentials

$$\vec{\tilde{H}} = \vec{\tilde{B}} = (B_x, B_y) = \left(\frac{\partial A}{\partial y}, -\frac{\partial A}{\partial x}\right) = \left(-\frac{\partial \tilde{V}}{\partial x}, -\frac{\partial \tilde{V}}{\partial y}\right) \qquad [\text{Gauss}]$$

2-D Differential Equations in Vacuum:

$$\vec{\nabla} \times \vec{\tilde{H}} = 0 \Rightarrow \left(\frac{\partial \tilde{H}_y}{\partial x} - \frac{\partial \tilde{H}_x}{\partial y}\right)_{\hat{k}} = 0$$

$$\nabla \cdot B = 0 \Rightarrow \frac{\partial B_x}{\partial x} + \frac{\partial B_y}{\partial y} + \cancel{\frac{\partial B_z}{\partial z}} = 0$$

$= 0$ in 2-D case

3-D Differential Equations in Vacuum:

Define $\tilde{\mathcal{H}}_x(x,y) \equiv \int_{z_1}^{z_2} \tilde{H}_x(x,y,z)\, dz$; $\tilde{\mathcal{H}}_y$, $\tilde{\mathcal{H}}_z$ similarly

then: $\frac{\partial \tilde{\mathcal{H}}_y}{\partial x} - \frac{\partial \tilde{\mathcal{H}}_x}{\partial y} = 0$ &

$$\frac{\partial \tilde{\mathcal{H}}_x}{\partial x} + \frac{\partial \tilde{\mathcal{H}}_y}{\partial y} = \tilde{H}_z(x,y,z_2) - \tilde{H}_z(x,y,z_1)$$

$\therefore$ If $\tilde{H}_{z_2} = \tilde{H}_{z_1}$ then the variables $\tilde{\mathcal{H}}_x$ & $\tilde{\mathcal{H}}_y$, integrated over the 3rd dimension obey the 2-D differential equations.

Flux through a surface: $\phi = \int \vec{B} \cdot d\vec{a} = \int \vec{\nabla} \times \vec{A} \cdot d\vec{a} = \oint \vec{A} \cdot d\vec{s}$

In 2-D: $\phi_{1\text{-}2} = L(A_2 - A_1)$

where L is length in 3rd dimension

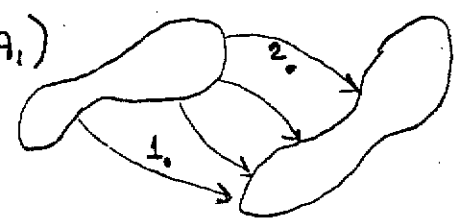

NON-UNIQUENESS OF V when currents are present

$$\oint_{abca} \vec{\tilde{H}} \cdot d\vec{s} = \tilde{I}$$

1st quadrant H-magnet →

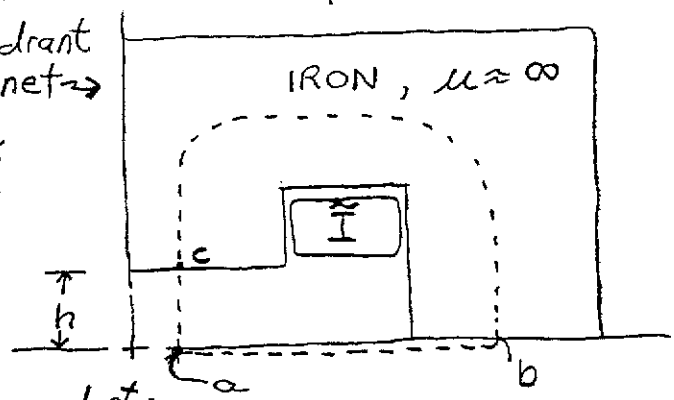

$$0 + \tilde{H}_{IRON}^{\,0} L_{IRON} + \tilde{H}_{gap} \cdot h = \tilde{I}$$

$$B_{gap} = -\tilde{I}/h$$

can still use V, but path dependent:

a-c 1) $\tilde{V}_a = 0$; $B_y = -\frac{\partial \tilde{V}}{\partial y} \Rightarrow \tilde{V}_c = -B_y \cdot h = \tilde{I}$

a-b-c 2) $\tilde{V}_a = 0$; $B_x = -\frac{\partial \tilde{V}}{\partial x} \Rightarrow \tilde{V}_b = 0$, $\tilde{V}_c = 0$

Notation:

$\begin{cases} \eta \equiv x + iy \\ z \equiv 3^{RD} \text{ Dimension} \end{cases}$

$\begin{cases} H_z, H_3 \equiv \text{heights [cm]} \\ H, H_c, H_{PM} \equiv \text{field strengths [A/cm]} \end{cases}$

$\begin{cases} ' \equiv \frac{d}{d\eta} \quad \text{sometimes} \\ ' \equiv \text{per unit length in } 3^{RD} \text{ dimension some other times} \end{cases}$

$\cdot \equiv \frac{d}{dt}$

$\tilde{V}, \tilde{H} \equiv \mu_o V, \mu_o H$ $\qquad$ $\tilde{V}$ [G-cm] , A[G-cm]

V [A] , I [A] , B [G]

$\mu_o = .4\pi$ G cm/Amp

Let $F(\eta) = A(x,y) + i\tilde{V}(x,y)$ be an analytical function of the complex variable $\eta \equiv x+iy$ with real part $A(x,y)$ and imaginary part $\tilde{V}(x,y)$.

CAUCHY-RIEMANN: $\left(' \equiv \frac{d}{d\eta}\right)$

$$\left.\begin{aligned} \frac{\partial F}{\partial x} &= \frac{\partial A}{\partial x} + i\frac{\partial \tilde{V}}{\partial x} = \frac{dF}{d\eta}\frac{\partial \eta}{\partial x} = F'\cdot 1 \\ \frac{\partial F}{\partial y} &= \frac{\partial A}{\partial y} + i\frac{\partial \tilde{V}}{\partial y} = \frac{dF}{d\eta}\frac{\partial \eta}{\partial y} = F'\cdot i \end{aligned}\right\} \Rightarrow \begin{aligned} \frac{\partial A}{\partial x} &= \frac{\partial \tilde{V}}{\partial y}, \\ -\frac{\partial A}{\partial y} &= \frac{\partial \tilde{V}}{\partial x} \end{aligned}$$

$$\frac{\partial^2 F}{\partial x^2} = \frac{d^2F}{d\eta^2}\ ;\ \frac{\partial^2 F}{\partial y^2} = \frac{d^2F}{d\eta^2}(-1) \Rightarrow \frac{\partial^2 F}{\partial x^2} + \frac{\partial^2 F}{\partial y^2} = \nabla^2 F = 0$$

$A + \tilde{V}$ here satisfy same equations that vector potential A + scalar potential $\tilde{V}$ describing fields B_x, B_y did.

So we have (2-D) $F \equiv A + i\tilde{V}$

- $\tilde{V}$ ← magnetic scalar potential
- A ← magnetic vector potential
- F ← complex potential

Relationship between complex potential + magnetic field

HW

ADVANTAGES of PM SYSTEMS

- strongest fields when small
- compact
- immersible in other fields
- analytical material
- no power supplies
- no cooling
- no energy bill

REPRESENTATIONS OF PM MATERIAL:

in PM: $\left.\begin{aligned} B_{\parallel} &= \mu_{\parallel} H_{\parallel} + B_r \\ B_{\perp} &= \mu_{\perp} H_{\perp} \end{aligned}\right\} \quad \left.\begin{aligned} \vec{B} &= \hat{\mu}\vec{H} + \vec{B}_r \\ \vec{H} &= \hat{\gamma}\vec{B} - \vec{H}_c \end{aligned}\right.$

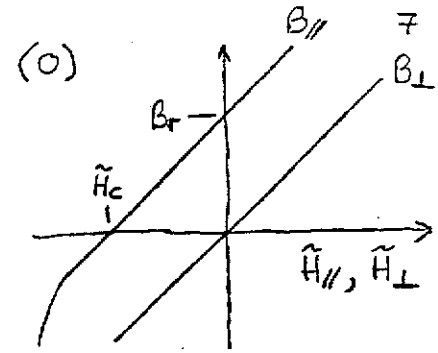

(1) $\vec{\nabla}\times\vec{H} = 0 \Rightarrow \vec{\nabla}\times\hat{\gamma}\vec{B} = \vec{\nabla}\times\vec{H}_c \equiv \vec{j}_{eq}$

AND $\vec{\nabla}\cdot\vec{B} = 0$

$(\gamma \equiv 1/\mu)$

ALTERNATIVELY,

(2) $\vec{\nabla}\cdot\vec{B} = 0 \Rightarrow \vec{\nabla}\cdot\hat{\mu}\vec{H} = -\vec{\nabla}\cdot\vec{B}_r \equiv \rho_{eq}$

AND $\vec{\nabla}\times\vec{H} = 0$

$\hat{\mu} \approx 1$

$\therefore$ PM = passive material ($\hat{\gamma}$ or $\hat{\mu}$) with active terms ($\vec{j}_{eq}$ or ρ_{eq})

FOR PM HOMOGENEOUSLY MAGNETIZED:

(1) $\vec{\nabla}\times\vec{H}_c = 0$ everywhere except at $\perp$ surface $\Rightarrow$ current sheet

(2) $\vec{\nabla}\cdot\vec{B}_r = 0$ everywhere except at $\parallel$ surface $\Rightarrow$ charge sheet

$\therefore$

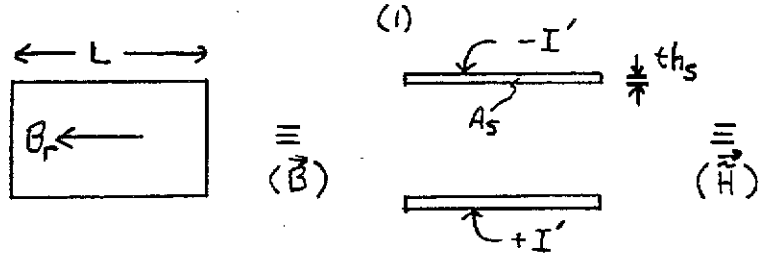

PM CURRENT SHEETS CHARGE SHEETS

(2) $-\vec{\nabla}\cdot\vec{B}_r = \rho_{eq} = \frac{Q}{Vol} = \frac{\pm B_r}{th_e} \Rightarrow Q = \underbrace{\rho_{eq}}_{Q/Vol}\cdot\underbrace{th_e}_{Vol}\cdot A_e = \underbrace{\pm B_r}_{Q/Area}\cdot\underbrace{A_e}_{Area}$

convenient to use $\sigma \equiv Q/A_e = \rho_{eq}\cdot th_e = \pm B_r$

(1) $\vec{\nabla}\times\vec{H}_c \equiv \vec{j}_{eq} = \frac{I}{A_s} = \frac{\pm H_c}{th_s} \Rightarrow I = \underbrace{j_{eq}}_{I/Area}\cdot\underbrace{th_s}_{Area}\cdot L = \underbrace{\pm H_c}_{I/Len.}\cdot\underbrace{L}_{Length}$

convenient to use $I' \equiv I/L = j_{eq}\cdot th_s = \pm H_c$

APPLICATIONS OF VARIOUS REPRESENTATIONS:

PLOTTING $\vec{B}$:

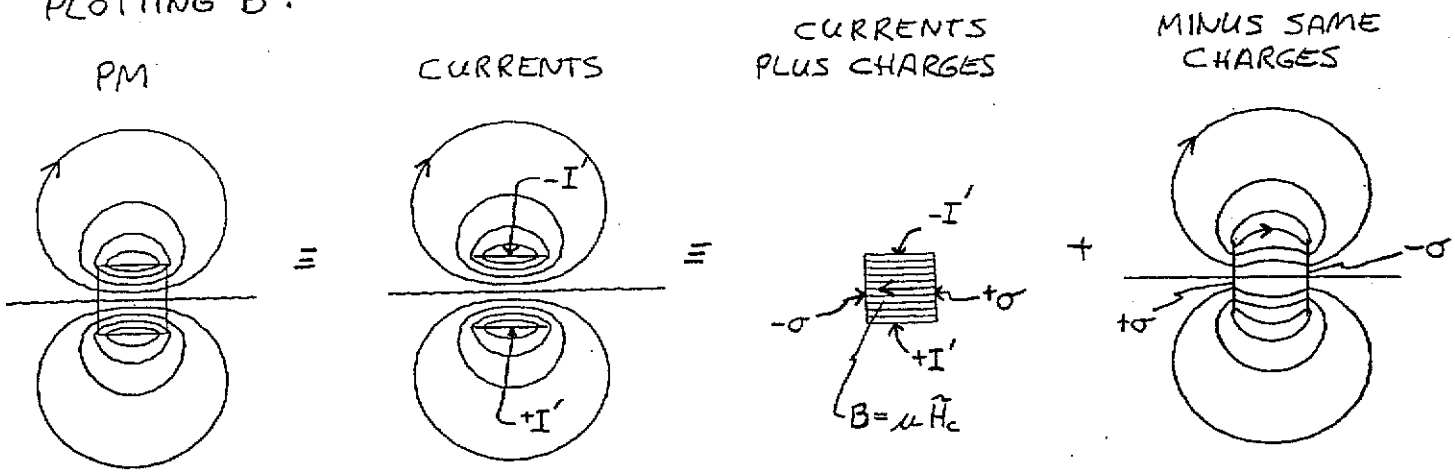

PLOTTING $\vec{H}$:

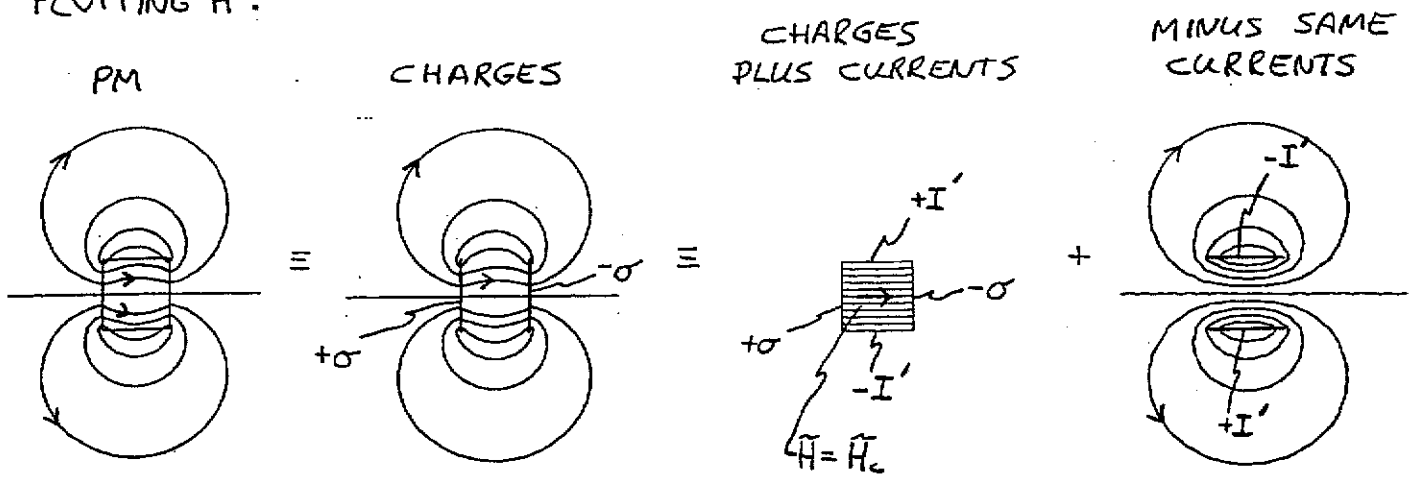

CAN USE CHARGE SHEETS TO REPRESENT ELECTROMAGNETS TOO!

EXAMPLE: USE CHARGE SHEET MODEL TO CALCULATE $\vec{B}$ ON-AXIS IN A SEMI-INFINITE SOLENOID

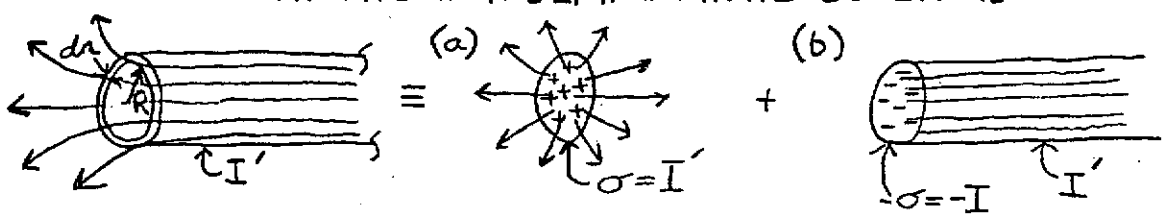

✓ 1st

on annulus dr:

$dq = 2\pi r\,dr\cdot\sigma$,

$d\tilde{V} = \frac{1}{4\pi}\frac{dq}{l} = \frac{\sigma r\,dr}{2\sqrt{r^2+z^2}}$

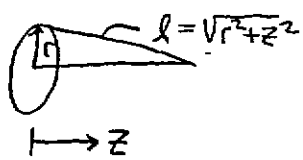

2ND

DIPOLE -

TAYLOR VS. LAURENT EXPANSI

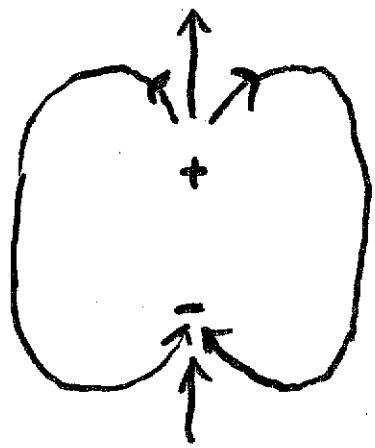

THE SILVERTREE HOTEL
P.O. Box 5009, Snowmass Village, Colorado 81615
(970) 923-3520; FAX (970) 923-5192
www.silvertreehotel.com • e-mail: reservations@silvertreehotel.com

2 Magnetostatics Basics

The LEB magnets will operate in iron-dominated, resistive regimes. In the current-free region inside the beam tube, fields can be described by Maxwell's equations as follows:

$$\nabla \times E = -\frac{\partial B}{\partial t} \Longrightarrow \nabla \cdot B = 0, \qquad \nabla \times H = 0 \tag{1}$$

where $B = \mu_0 H$. H (and thus B) can be expressed as the gradient of a scalar potential V or, alternatively as the curl of a vector potential A:

$$\mu_0 H = -\nabla V, \qquad B = \nabla \times A \tag{2}$$

Away from magnet ends fields are two dimensional; A and V satisfy the Cauchy-Riemann equations $A'_x = V'_y$ and $V'_x = -A'_y$, and can thus be represented as the real and imaginary parts of an analytic function F of the complex variable $z = x + iy$:

$$F \equiv A + iV \tag{3}$$

It follows directly from Eqns. (2) and (3) that the complex conjugate $B^*(z)$ of the field is analytic in z and is given by:

$$B^*(z) = i\frac{dF}{dz} \tag{4}$$

It is convenient to expand the complex ~~scalar~~ potential F in a power series about a point (say $z = 0$) and analyze the 'harmonic' components:

$$F(z) = \sum_{n=1}^{\infty} \left(\frac{z}{r_p}\right)^n c_n \; ; \qquad B^*(z) = i\sum_{n=1}^{\infty} \left(\frac{z}{r_p}\right)^{n-1} \frac{nc_n}{r_p} \tag{5}$$

where r_p is the magnet aperture radius ($\longrightarrow$ half gap h for a dipole). For magnets exhibiting midplane symmetry, the coefficients $c_n \equiv a_n + ib_n$ are pure real (or pure imaginary if A, rather than V, is constant along the midplane). For symmetric multipole magnets (i.e. rotatable by $360°/2m$ with a change of polarity), of order m (e.g. $m = 1$ for dipole, 2 for quadrupole, etc.) the complex potential F and flux density $B^*(z)$ are

$$F(z) = \sum_{n=1}^{\infty} \left(\frac{z}{r_p}\right)^{m(2n-1)} a_{m(2n-1)} \; ; \quad B^*(z) = i\sum_{n=1}^{\infty} \left(\frac{z}{r_p}\right)^{m(2n-1)-1} \frac{m(2n-1)a_{m(2n-1)}}{r_p} \tag{6}$$

Allowed harmonics (Poisson notation)
For design rotatable by $\theta^\circ = 360°/m'$:

Dipole: m = 0, Quad m = 1, etc.
Where $m' \equiv m + 1$, $n' \equiv n + 1$

m'	cur. change sgn. n' = m'(2M-1)/2	cur. same sign n' = m'M
1		1 2 3 4 5
2	1 3 5 7 9	2 4 6 8 10
3		3 6 9 12 15
4	2 6 10 14 18	4 8 12 16 20
5		5 10 15 20 25
6	3 9 15 21 27	6 12 18 24 30

M = 1,2,3,4...

Multipole Magnet	Vac. Ch Shape	Allowed Harmonics	Corrector Coils (Approp. Located)	Remaining Harmonics
Dipole a)	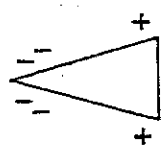	n' 1 2 3 4 5 r (1) s (rotate, m', same sign)	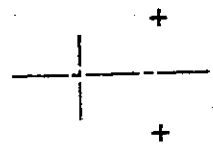	n' x x 3 4 5
b)	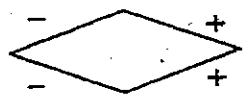	1 3 5 7 9 r (2) c		x x 5 7 9
Quad. c)		2 4 6 8 10 r (2) s		x x 6 8 10
d)	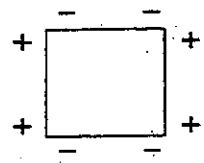	2 6 10 14 18 r (4) c	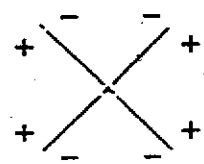	x x 10 14 18
Sext. e)	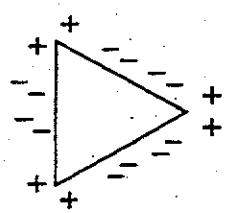	3 6 9 12 15 r (3) s	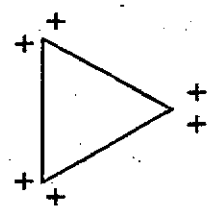	x x 9 12 15
f)	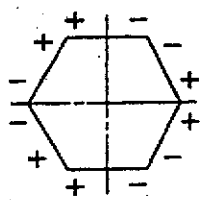	3 9 15 21 27 r (6) c	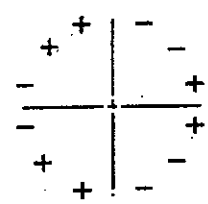	x x 15 21 27
g)	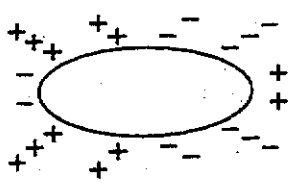	1 3 5 7 9 r (2) c		x x 5 7 9

TIP-02529

Figure 11. Summary of Eddy Current-Induced Harmonics and Passive Suppression for Multipole Magnets With Various Generic Vacuum Chamber Shapes.

NUCLEAR INSTRUMENTS AND METHODS 169 (1980) 1-10; © NORTH-HOLLAND PUBLISHING CO.

DESIGN OF PERMANENT MULTIPOLE MAGNETS WITH ORIENTED RARE EARTH COBALT MATERIAL*

K. HALBACH

University of California, Lawrence Berkeley Laboratory, Berkeley, CA 94720, U.S.A.

Received 20 August 1979

By taking advantage of both the magnetic strength and the astounding simplicity of the magnetic properties of oriented rare earth cobalt material, new designs have been developed for a number of devices. In this article on multipole magnets, special emphasis is put on quadrupoles because of their frequent use and because the aperture fields achievable (1.2–1.4 T) are rather large. This paper also lays the foundation for future papers on: (a) linear arrays for use as "plasma buckets" or undulators for the production of synchrotron radiation; (b) structures for the production of solenoidal fields; and (c) three-dimensional structures such as helical undulators or multipoles.

1. Introduction

For some applications, the most important of the many advantages of permanent magnets is the fact that they can be made very small without reduction of magnetic field strength. In conventionally powered magnets, the current density in the coils is inversely-proportional to the linear dimension, leading to insurmountable cooling problems and attendant reduction of field strength as size decreases.

We will discuss new designs that, with the currently available oriented rare earth cobalt (REC) material, produce, in some devices, fields that are as strong or stronger than those achievable with conventional magnets of any size.

Thus, REC magnets will have a performance advantage over conventional magnets regardless of size, shifting the decision between the two to different areas, such as convenience of strength adjustment, price, etc.

The advantage of REC is not only its strength, but also the simplicity of its magnetic properties. This simplicity makes REC systems easy to understand and to treat analytically, which in turn leads directly to improved designs. For this reason, we devote some space to REC properties, and how they can be best described in the magnetostatic equations, despite the fact that these properties have been known by workers in the field since Strnat[1]) started the development of REC.

For the sake of completeness, we include similarly the derivation of some theorems that are, at least in principle, textbook material, but are used so infrequently that they cannot be expected to be at the fingertips of most readers.

* This work was supported by the Los Alamos Scientific Laboratory and the Lawrence Berkely Laboratory of the US Department of Energy under contract No. W-7405-ENG-48.

2. Basic formulae, notation

For three dimensional (3D) calculations, we use the standard Cartesian coordinates x, y, z. Most of the two dimensional (2D) calculations are done with complex numbers that are identified by underlining the symbols. Specifically $\underline{z}$ is defined by $\underline{z}=x+iy=re^{i\varphi}$, with $i^2=-1$. The complex conjugate of a quantity is indicated by an asterisk.

In a vacuum region, the two dimensional field components B_x, B_y (or H_x, H_y) can be derived from either a scalar potential V or a vector potential that only needs to have a component A in the z direction:

$$B_x = \partial A/\partial y = -\partial V/\partial x, \tag{1a}$$

$$B_y = -\partial A/\partial x = -\partial V/\partial y. \tag{1b}$$

The relationships between the derivatives of A and V are the same as the Cauchy–Riemann conditions of the real and imaginary part of an analytical function of the complex variable $\underline{z}$, i.e., the complex potential $\underline{F}(\underline{z})=A+iV$ is such a function, and if we use $\underline{B}=B_x+iB_y$ to describe the two-dimensional vector $\boldsymbol{B}$, it follows from eq. (1) that

$$\underline{B}^* = i\,\mathrm{d}\underline{F}/\mathrm{d}\underline{z} \tag{2}$$

is also an analytical function of $\underline{z}$. The field at location $\underline{z}_0$, generated by a current filament, I, at location $\underline{z}$, is given by

$$\underline{B}^*(\underline{z}_0) = \frac{\mu_0 I}{2\pi i}\,\frac{1}{\underline{z}_0-\underline{z}} \tag{3}$$

The coefficients of the Taylor series expansion of $\underline{F}$ and $\underline{B}^*$ are in the customary fashion identified by

the subscript of the expansion of $\underline{F}$:

$$\underline{F}(z_0) = \sum_{n=1} \underline{a}_n z_0^n, \tag{4a}$$

$$\underline{B}^*(z_0) = \sum_{n=1} \underline{b}_n z_0^{n-1}; \qquad \underline{b}_n = i n \underline{a}_n. \tag{4b}$$

The same expansions, but with $n<0$, will be used to describe fields in the region radially outside the magnets. MKS units are used throughout, with $\mu_0 = 4\pi \times 10^{-7}\ \mathrm{V\,s\,A^{-1}\,m^{-1}}$.

3. Properties of REC

3.1. The manufacturing process

To get a rough understanding of the reasons for the REC properties described in section 3.2, we describe very briefly the major steps in one of the major manufacturing processes used today to produce REC. For details, the reader is referred to the book by McCaig[2]).

After a molten mixture of roughly five (atomic) parts cobalt to one (atomic) part of some rare earth metal(s) is solidified by rapid cooling, a crushing and milling process produces a powder that consists of particles with linear dimensions of the order of 5 μm. These grains are magnetically highly anisotropic, "wanting" to be polarized only along one crystalline direction. The powder is then exposed to a strong magnetic field and subjected to high pressure, causing the individual grains to physically rotate until their magnetically preferred axes are parallel to the applied field. These aligned blocks of material are then sintered, and machined or ground if necessary. Finally the material is exposed to a very strong magnetic field in a direction parallel or antiparallel to the previously established preferred direction, orienting practically all alignable magnetic moments along the direction of magnetization, commonly called the easy axis. The property that makes REC so valuable is that this magnetization is very strong, and that it can be changed in a substantial way only by applying a strong field in the direction opposite to the one used to magnetize the material.

3.2. The $B(H)$ relationship of REC

The relationship between $B_\parallel$ and $H_\parallel$ in the direction parallel to the easy axis is schematically shown in fig. 1. The most important characteristics of the $B_\parallel(H_\parallel)$ curve are the following:

(a) It is, for all intents and purposes, a straight line over a very wide range, with a typical slope $dB_\parallel/dH_\parallel\mu_0 = \mu_\parallel \approx 1.04$–$1.08$. The point where the slope becomes significantly larger depends on the details of the manufacturing process, but is usually well within the third quadrant, at $-H_\parallel/H_c \approx 1.5$–$2$.

(b) The offset of the $B_\parallel(H_\parallel)$ curve from the origin, the remanent field B_r, is typically 0.8–0.95 T, with the coercive field $\mu_0 H_c$ about 4–8% less than B_r.

(c) As long as one stays on the straight line part of the $B_\parallel(H_\parallel)$ curve, moving along the curve does not change this straight line.

In the range of interest here, the relationship between $B_\parallel$ and $H_\parallel$ can be represented by:

$$B_\parallel = \mu_0 \mu_\parallel H_\parallel + B_r \tag{5a}$$

or, with $\gamma = 1/\mu$:

$$H_\parallel = \gamma_\parallel B_\parallel/\mu_0 - H_c. \tag{5b}$$

In the direction perpendicular to the easy axis, the relationship between $B_\perp$ and $H_\perp$ is, to a very good approximation, described by:

$$B_\perp = \mu_0 H_\perp + B_r(H_\perp/H_A)$$

or, with

$$\mu_\perp = 1/\gamma_\perp = 1 + B_r/\mu_0 H_A,$$

$$B_\perp = \mu_0 \mu_\perp H_\perp. \tag{6}$$

The high degree of anisotropy of good materia manifests itself in the large values of the anisotropy field $\mu_0 H_A$: typical values are 12–40 T, giving values of 1.02 to 1.08 for $\mu_\perp$, and eq. (6) is usually valid up to several Tesla.

Aside from the REC material discussed so far, resin bonded REC material is also available, with qualitatively the same properties, but lower values of B_r and H_c. Some of the oriented ferrites also have similar properties, but with $B_r \leqslant 0.35$ T and larger values ($\gtrsim 1.1$) for the permeabilities $\mu_\parallel$ and $\mu_\perp$.

The designs discussed in this paper can also be

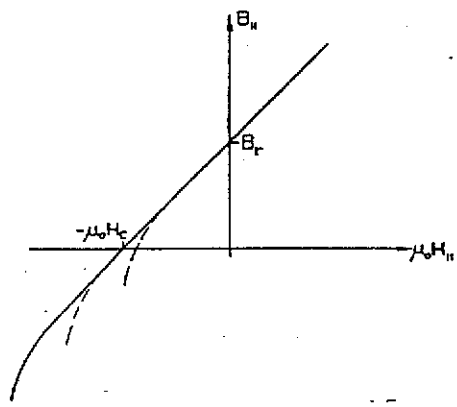

Fig. 1. $B(H)$-curve in the direction parallel to the easy axis.

implemented with these materials; we always refer to REC magnets because it is the unique strength of the REC materials, combined with the other properties described in this section, that will open the door to new and exciting applications.

3.3. Description of REC properties in the magnetostatic equations

Equations (5a) and (6) can be combined into the vector equation:

$$B = \mu_0 \mu * H + B_r. \tag{7a}$$

In this equation, B_r is the vector with the magnitude of the remanent field B_r in the direction of the easy axis, and $\mu * H = \mu_\perp H_\perp + \mu_\parallel H_\parallel$. Eqs. (5b) and (6) can be similarly combined into

$$H = \gamma * B/\mu_0 - H_c. \tag{7b}$$

If we derive H from a scalar potential, we have to satisfy $\operatorname{div} B = 0$, yielding with eq. (7a)

$$\operatorname{div}(\mu_0 \mu * H) = \rho = -\operatorname{div} B_r. \tag{8a}$$

If we derive B similarly from a vector potential, we get from eq. (7b) and Ampères law

$$\operatorname{curl} \gamma * B/\mu_0 = j = \operatorname{curl} H_c. \tag{8b}$$

The anisotropy of the material shows up in two different ways: in the inhomogeneous terms on the right sides of eqs. (8a, b), and in the slight anisotropy associated with the weak differential permeability of REC. Because the permeabilities are so close to one, we assume, unless stated otherwise, that $\mu_\parallel = \mu_\perp = 1$. This very good approximation, together with the assumption of constant H_c and B_r, means that the material can be treated as vacuum with either an imprinted charge density — $\operatorname{div} B_r$ or an imprinted current density $\operatorname{curl} H_c$. This in turn has the consequence that the fields produced by different pieces of REC superimpose linearly, and that they can be calculated with fairly little effort when no soft magnetic material is present. It should be noted that in the case of homogeneously magnetized material, i.e., $H_c, B_r = \text{const.}$ within the material, $\operatorname{curl} H_c$ and $\operatorname{div} B_r$ are zero everywhere except at the surface, where one encounters delta functions that signify the presence of current sheets or charge sheets.

3.4. Calculation of three dimensional (3D) fields produced by REC

In the absence of soft material, we derive the field at the location outside the material from a scalar potential,

$$H(r_0) = -\operatorname{grad} V, \tag{9}$$

with V given by an integral over the volume of the material:

$$\mu_0 V(r_0) = \frac{1}{4\pi} \int \frac{\rho(r)}{|r - r_0|} \, dv. \tag{10}$$

In the case of a homogeneously magnetized REC piece, one has a charge sheet at its surface. With eq. (8a) one therefore obtains in that case V from an integral over the surface of the material:

$$V = \frac{1}{4\pi} \int \frac{H_c \cdot da}{|r - r_0|} = \frac{H_c}{4\pi} \cdot \int \frac{da}{|r - r_0|}. \tag{11}$$

For our model, $B_r = \mu_0 H_c$ has been used. A particularly appealing property of this formula is the fact that the integral is independent of H_c.

For the case of continuously varying H_c, we use, with $K(r) = 1/|r - r_0|$ the identity

$$\rho K/\mu_0 = -K \operatorname{div} H_c = H_c \operatorname{grad} K - \operatorname{div}(K H_c).$$

Because $H_c = 0$ outside the material,

$$\int \operatorname{div}(K H_c) \, dv = \int K H_c \cdot da = 0.$$

With

$$\operatorname{grad} K = -(r - r_0)/|r - r_0|^3,$$

we obtain

$$V = -\frac{1}{4\pi} \int \frac{H_c \cdot (r - r_0)}{|r - r_0|^3} \, dv. \tag{12}$$

3.5. Calculation of two-dimensional (2D) fields produced by REC

For a REC assembly that is sufficiently long in the z-direction and whose magnetization vector B_r has no z component, the fields outside the material can, in the absence of soft steel, to a good approximation be described by:

$$\underline{B}^*(z_0) = \frac{\mu_0}{2\pi i} \int \frac{j}{z_0 - z} \, dx \, dy, \tag{13}$$

with

$$\mu_0 j = \partial B_{ry}/\partial x - \partial B_{rx}/\partial y. \tag{14}$$

We have again used $B_r = \mu_0 H_c$.

It is shown in the Appendix that eq. (13) can, without restrictions on $\underline{B}_r = B_{rx} + i B_{ry}$, be written as

$$\underline{B}^*(z_0) = \frac{1}{2\pi} \int \frac{\underline{B}_r}{(z_c - z)^2} \, dx \, dy. \tag{15}$$

This formula can be considered the 2D equivalent of eq. (12), because it expresses the field by an

integral that contains the magnetization itself, and not a combination of its spatial derivatives.

Equation (15) has a property that is highly significant for many applications: if two REC assemblies are identical, except that in the second system the easy axis is rotated everywhere by the angle $+\beta$ relative to the easy axis orientation in first system, then the right hand side of eq. (15) for the second system equals that of the first system, but is multiplied by $e^{i\beta}$. This allows us to state the *Easy Axis Rotation Theorem*. – If in a 2D, soft–steel free, REC system all easy axes are rotated by the angle $+\beta$, then all magnetic fields outside the REC rotate by the angle $-\beta$ without a change in amplitude. – Fig. 2 illustrates this theorem. The theorem is qualitatively easy to understand if one realizes that each volume element of REC produces a dipole field for which this theorem is valid for obvious reasons.

For a homogeneously magnetized piece of REC, $\underline{B}_r$ can be taken outside the integral in eq. (15). Integrating first over x, one obtains:

$$\underline{B}^*(z_0) = \frac{\underline{B}_r}{2\pi} \oint \frac{dy}{z_0 - \underline{z}}. \tag{16a}$$

Integration over y first yields

$$\underline{B}^*(z_0) = -\frac{\underline{B}_r}{2\pi i} \oint \frac{dx}{z_0 - \underline{z}}, \tag{16b}$$

and eqs. (16a) and (16b) can be combined into

$$\underline{B}^*(z_0) = -\frac{\underline{B}_r}{4\pi i} \oint \frac{dz^*}{z_0 - \underline{z}}. \tag{16c}$$

The last three equations are given because, depending on the geometrical shape of the REC piece, one of these integrals may be easier to evaluate than the others or the integral in eq. (15).

Equation (16b) [and similarly eq. (16a)] can also be derived by using the current sheet model for a REC piece with its easy axis parallel to the x-a: and then invoking the easy axis rotation theoren

To calculate fields inside the material, the techr ques developed in ref. 3 can be used. We summa ize here only the result for the case of a homoge eously magnetized piece of REC: by first removi a circular cylinder of material around the point z any one of the eqs. (16a–c) can be used, with a integration path as shown in fig. 3. (Notice that th integrals over the straight lines cancel.) To obtai $\underline{B}^*$, one has to add the contribution $\underline{B}_r/2$ caused by th removal of the cylinder. To obtain $\mu_0\underline{H}^*$ inside th material, one has to use $\mu_0\underline{H}^* = \underline{B}^* - \underline{B}_r^*$.

Even though it is possible to write down explici ly the fields produced by the multipole magnet discussed below, it is more convenient, and give more insight, to use the Taylor expansions intro duced in eqs. (4a, b). To obtain the expansion coef ficients, one has to use in eqs. (16a–c)

$$\frac{1}{z_0 - \underline{z}} = -\sum_{n=1}^{\infty} \frac{z_0^{n-1}}{\underline{z}^n}, \tag{17a}$$

and for use in eq. (15), one obtains by differentia tion of eq. (17a):

$$\frac{1}{(z_0 - \underline{z})^2} = \sum_{n=1}^{\infty} \frac{n z_0^{n-1}}{\underline{z}^{n+1}}. \tag{}$$

For a field expansion radially outside the magn one has to use

$$\frac{1}{z_0 - \underline{z}} = \sum_{n=0}^{-\infty} \frac{z_0^{n-1}}{\underline{z}^n} \tag{17b}$$

and

$$\frac{1}{(z_0 - \underline{z})^2} = -\sum_{n=-1}^{-\infty} \frac{n z_0^{n-1}}{\underline{z}^{n+1}}. \tag{18b}$$

4. REC multipole magnets

4.1. Multipoles with continuous easy axis orientation

To produce a strong $2N$–multipole magnet with good field quality, one wants to arrange the REC in

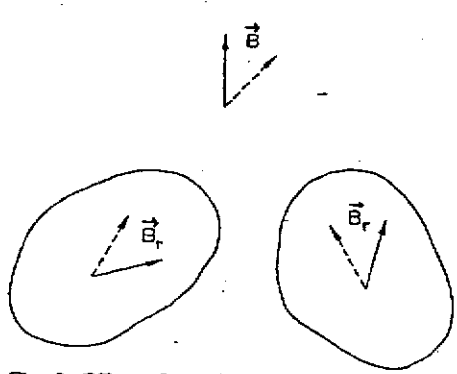

Fig. 2. Effect of rotation of easy axes on magnetic field.

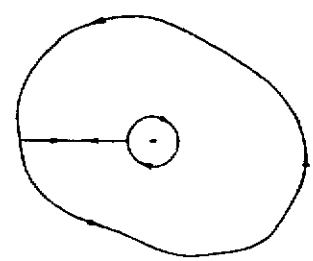

Fig. 3. Integration path for calculation of field inside the F material.

such a way that in eq. (4b), $\underline{b}_N$ is large, and that all other $\underline{b}_n$ are as small as possible. Using eq. (18a) in eq. (15), we obtain

$$\underline{b}_n = \frac{n}{2\pi} \cdot \int \frac{\underline{B}_r}{\underline{z}^{n+1}} \, da .$$

With $\underline{B}_r = B_r e^{i\beta(\varphi)}$, and $\underline{z} = re^{i\varphi}$, we get

$$\underline{b}_n = \frac{n}{2\pi} \int \frac{B_r \exp\{i[\beta(\varphi) - (n+1)\varphi]\}}{r^{n+1}} \, r\,dr\,d\varphi . \quad (19)$$

From this equation follows directly that the largest possible real $\underline{b}_N$ is obtained by choosing

$$\beta(\varphi) = \varphi(N+1) . \quad (20)$$

Equation (19) also shows the expected fact that a piece of REC contributes the more to the multipole strength the closer it is to the point $\underline{z} = 0$.

If the space between the two circles $|\underline{z}| = r_1$ and $|\underline{z}| = r_2$ is filled with REC, with B_r a constant and $\beta(\varphi)$ given by eq. (20), $\underline{b}_n = 0$ for $n \neq N$, giving for $|\underline{z}_0| < r_1$

$$\underline{B}^*(\underline{z}_0) = \left(\frac{\underline{z}_0}{r_1}\right)^{N-1} B_r \frac{N}{N-1}\left[1 - \left(\frac{r_1}{r_2}\right)^{N-1}\right] \quad \text{for } N \geq 2; \quad (21a)$$

$$\underline{B}^*(\underline{z}_0) = B_r \ln(r_2/r_1) \quad \text{for } N = 1 . \quad (21b)$$

Inspection of the field for $|\underline{z}| > r_2$, using eq. (18b) instead of eq. (18a), shows that the field outside this multipole magnet is exactly zero.

The fact that "recipe" eq. (20) leads to a perfect multipole is not surprising when one realizes that as a direct consequence of eq. (20), the current density j [in eq. (8b)] inside the material has only the component $j_c = H_c(N+1) \sin N\varphi/r$, with the current sheets at the inside and outside boundaries of the REC also being proportional to $\sin N\varphi$.

Equations (21) were given for $N = 1, 2$ by Blewett[4]) in an unpublished report in 1965. However that report does not mention the anisotropy of the material, and consequently does not give the design recipe represented by eq. (20).

The multipole just discussed obviously produces the strongest and cleanest multipole field possible within a circular aperture of a pure REC multipole with a given amount of material. A study of the field inside the material shows that one can find closed curves that are perpendicular to $\boldsymbol{H}$ everywhere. Replacing the material inside such a closed curve by soft steel with very large permeability will reduce the amount of REC without significantly changing the field in the aperture. It is my subjective judgement that the potential savings are too small to be worth the resulting complication of construction in the case of strong multipoles, and this avenue has therefore not been pursued in the study of the segmented multipoles.

Since the above mentioned steel contours can range into the aperture region, this approach can be used to design multipoles that have steel poles controlling the field in the aperture and use fairly little REC. However, with the exception of dipoles, those magnets have weaker pole tip fields than the pure REC multipoles. While it is my opinion that incorporation of steel into the design will not increase the upper limit of the achievable multipole strength, given by eq. (21a), I have no proof for this assessment.

In order to satisfy eq. (20), we require strong magnetic fields during the alignment process with a distribution of local direction given by eq. (20). Since a 2D vacuum field satisfying that condition must behave like $\underline{B}^* \sim 1/\underline{z}^{N+1}$ in the region of interest, it is highly unlikely that one can produce REC with precisely the desired easy axis distribution, particularly for small magnets. Fortunately, the segmented magnet design discussed below has a performance very close to that of the ideal REC multipole.

4.2. The segmented multipole magnet

To get a reasonable approximation to eq. (20), we segment the magnet into M geometrically identical pieces such that, ignoring the direction of the easy axes, the structure is invariant to rotation by the angle $2\pi/M$ about $\underline{z} = 0$. Throughout each piece, the easy axis points in the same direction, but that direction advances (in the $x-y$ coordinate system) by $(N+1)2\pi/M$ from one piece to the next. This means that relative to a coordinate system fixed in the piece, the easy axis advances by $N2\pi/M$ from one piece to the next.

Using eqs. (17), (16c) and (4b), $\underline{b}_n$ produced by one such piece can be expressed (for both positive and negative n) by

$$\underline{b}_n = \operatorname{sgn}(n) \frac{\underline{B}_r}{4\pi i} \oint \frac{d\underline{z}^*}{\underline{z}^n} . \quad (22)$$

If the contribution to $\underline{b}_n$ coming from a reference piece is $\underline{C}_n$, then the contribution from a piece rotated by α relative to the reference piece is $\underline{C}_n e^{i\alpha(N+1)} e^{-i\alpha(n+1)}$, where the first exponential factor comes from the rotation of the easy axis by

$\alpha(N+1)$, and the second factor from the integral in eq. (22). With $\alpha = m2\pi/M$, we get for the whole assembly

$$\underline{b}_n = \underline{C}_n \sum_{m=0}^{N-1} \exp\left[i\,2\pi m(N-n)/M\right].$$

If $(N-n)/M$ is zero or a positive or negative integer, the sum equals M. If $(N-n)/M$ is not an integer, the geometrical series is zero, yielding

$$\underline{B}^*(z_0) = M \sum_{\nu} \underline{C}_n z_0^{n-1}; \qquad n = N+\nu M. \tag{23}$$

Depending whether one wants to know the fields in the aperture region or outside the magnet, one takes the sum over either positive or negative n.

Figure 4 shows the geometry for a trapezoidal reference piece that is bisected by the x-axis and whose magnetization is characterized by $\underline{B}_r$. We allow discussion of a smaller than maximum possible angular size $(2\pi/M)$ by making the angular size of the reference piece $\varepsilon 2\pi/M$.

For $n>0$, $\underline{C}_n$ is most easily obtained by using eq. (17a) in eq. (16b). Using the latter $\underline{C}_n$ in eq. (23) gives:

$$\underline{B}^*(z_0) = \underline{B}_r \sum_{\nu=0}^{\infty} \left(\frac{z_0}{r_1}\right)^{n-1} \frac{n}{n-1}\left[1-\left(\frac{r_1}{r_2}\right)^{n-1}\right] K_n$$

$$n = N+\nu M$$

$$K_n = \cos^n(\varepsilon\pi/M)\frac{\sin(n\varepsilon\pi/M)}{n\pi/M} \tag{24a}$$

$$\left(\frac{n}{n-1}\left[1-(r_1/r_2)^{n-1}\right)\right)_{n=1} = \ln(r_2/r_1)$$

For the geometry indicated by dashed lines in fig. 4, i.e., for circular arcs of radii r_1, r_2 (the inner and outer boundaries) $\underline{C}_n$ is most easily calculated with eqs. (15) and (18a), and K_n in eq. (24a) has to be replaced by

$$K_n = \frac{\sin\left[(n+1)\,\varepsilon\pi/M\right]}{(n+1)\,\pi/M}. \tag{24b}$$

It follows from eq. (24) that for a given B_r, and

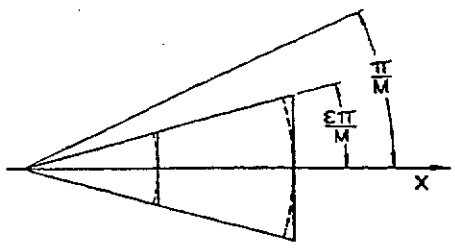

Fig. 4. One piece of a segmented REC multipole.

for $n = N > 1$, there always exists an upper limit the field strength at the magnet aperture, while the dipole this upper limit is controlled in essen by the $B_{\parallel}(H_{\parallel})$ curve in the third quadrant.

Comparison of eqs. (24) with eqs. (21) show that the fundamental harmonic of the segmente multipole is smaller by a factor K_N than the equiv alent ideal REC multipole and that for $\varepsilon = 1$ on comes close to the ideal strength if the number REC pieces per period.

$$M' = M/N, \tag{2

is equal to or larger than eight.

In the somewhat unusual case that one elects t use a small value like 2 for M', it follows in gener from eqs. (15) and (18a) [and specifically, of cours from eqs. (24a, b)] that K_N is largest not when equals one, but for

$$\varepsilon = \frac{M}{2(N+1)} = \frac{M'}{2(1+N^{-1})}, \tag{26}$$

provided this value is smaller than one.

From eqs. (24a, b) we can extract the amplitud of the field due to the harmonic $n = N+\nu M$ rela tive to the amplitude of the fundamental N. For th qualitatively representative case of trapezoidal R pieces, we obtain from eq. (24a) for that ratio at $|z| = r$, and for $\varepsilon = 1$

$$Q(\nu) = \left(\frac{r}{r_1}\right)^{\nu M} \frac{N-1}{n-1} \cos^{\nu M}\pi/M \frac{1-(r_1/r_2)^{n-1}}{1-(r_1/r_2)^{N-1}}. \tag{27}$$

For $r = r_1$, the values for $Q(\nu)$ are uncomfortabl large. Fortunately in most applications the larges r/r_1 of concern is, while close to one, still smal enough so that the factor $(r/r_1)^{\nu M}$ reduces $Q(\nu)$ t acceptable levels even for the most unfavorabl case, $\nu = 1$. Should, however, $Q(1)$ be larger tha acceptable, $Q(1)$ can be made to vanish by choos ing

$$\varepsilon = 1/(1+N/M) = 1-1/(1+M'). \tag{28}$$

For that value of ε, $Q(\nu)$ becomes

$$Q(\nu) = \left(\frac{r}{r_1}\right)^{\nu M} \frac{N-1}{n-1} \cos^{\nu M}\varepsilon\pi/M \times$$

$$\times \left(\sin\pi\frac{\nu-1}{1+M'} \Big/ \sin\frac{\pi}{1+M'}\right) \times$$

$$\times \left[1-\left(\frac{r_1}{r_2}\right)^{n-1} \Big/ 1-\left(\frac{r_1}{r_2}\right)^{N-1}\right] \tag{29}$$

For reasonably large values of M, it is unlikely

the worst of these harmonics ($n = N+2M$) will ever cause any problems.

The design represented by eq. (28) means that one has a wedge-shaped non-magnetic space between adjacent pieces of REC. While these gaps could be implemented by having appropriate notches in the magnet assembly fixture, an alternate method of making $Q(1)=0$ would be the use of a non-magnetic spacer between adjacent REC pieces. For that kind of design it would be advantageous to have spacers of uniform thickness D. Referring to fig. 5 for the definition of the symbols, application of eq. (16a) and (17a) gives for the field in that case

$$\underline{B}^*(\underline{z}_0) = \underline{B}_r \sum_{\nu=0}^{\infty} \left(\frac{\underline{z}_0}{r_1}\right)^{n-1} \frac{\cos\alpha_0 \cos^{n-1}\alpha_1}{(n-1)\alpha_0} \times$$

$$\times \left[\sin[\alpha_0+\alpha_1(n-1)] - \left(\frac{r_1\cos\alpha_2}{r_2\cos\alpha_1}\right)^{n-1} \times\right.$$

$$\left. \times \sin[\alpha_0+\alpha_2(n-1)]\right], \qquad (30a)$$

with

$$D/r_1 = 2\cos\alpha_0(\tan\alpha_0-\tan\alpha_1) \approx 2(\alpha_0-\alpha_1)/\cos\alpha_0. \qquad (30b)$$

$$\tan\alpha_2 = \tan\alpha_0-(r_1/r_2)(\tan\alpha_0-\tan\alpha_1). \qquad (30c)$$

To eliminate the harmonic $n=N+M$ in the case where the term proportional to $(r_1/r_2)^{n-1}$ in eq. (30a) can be neglected, one has to satisfy

$$\alpha_1 = (\pi-\alpha_0)/(n-1) = \alpha_0 \frac{M-1}{N+M-1}, \qquad (31a)$$

giving, with eq. (30b),

$$D/r_1 = \frac{2N}{N+M-1} \frac{\pi/M}{\cos\pi/M}. \qquad (31b)$$

Formulas for reference pieces with shapes other than trapezoids are easily derived following the same general procedure, but are not given here. From these expressions follows the general rule that the allowed harmonics $n=N+\nu M$ tend to be the smaller the better the inside REC boundary approximates a circle.

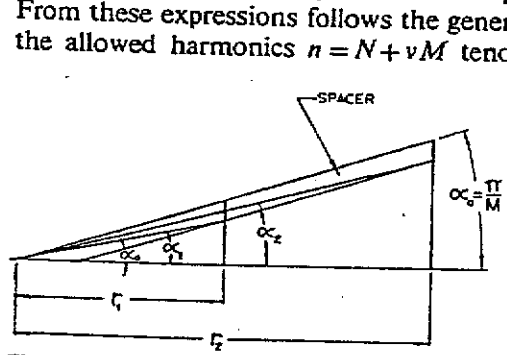

Fig. 5. One piece of a segmented REC multipole with flat sheet spacer.

To describe the fields (radially) outside the multipole, we expand $\underline{B}^*$ in $1/\underline{z}_0$. By using eqs. (17b) and (18b) instead of eqs. (17a) and (18a), we get instead of eqs. (24a, b):

$$\underline{B}^*(\underline{z}_0) = \sum_{\nu} \underline{b}_{-n} \underline{z}_0^{-n-1}$$

$$= \underline{B}_r \sum_{\nu=1}^{\infty} \left(\frac{r_2}{\underline{z}_0}\right)^{n+1} \frac{n}{n+1}\left[1-\left(\frac{r_1}{r_2}\right)^{n+1}\right] K_{-n}$$

$$n = \nu M-N \qquad (32a)$$

$$K_{-n} = \cos^{-n}(\varepsilon\pi/M) \frac{\sin n\varepsilon\pi/M}{n\pi/M} \text{ (Trapezoid)},$$

$$K_{-n} = \frac{\sin[(n-1)\varepsilon\pi/M]}{(n-1)\pi/M} \text{ (circular arcs)}. \qquad (32b)$$

Equation (32a) is valid for $|\underline{z}_0| > r_2/\cos(\varepsilon\pi/M)$ for the trapezoid, and for $|\underline{z}_0| > r_2$ for the circular arc case. Without going into details, it is clear that at these limits $\underline{B}(\underline{z}_0)$ is somewhat smaller than it is at $|\underline{z}_0| = r_1$. Since $n_{\min} = M-N = N(M'-1)$, the field decays very rapidly with increasing $|\underline{z}_0|$ provided that M is reasonably large. Shielding the space radially outside the multipole against these fields will therefore be rarely necessary. We therefore give the expansion for the field perturbation caused by a circular steel shell with $\mu=\infty$ and $|\underline{z}|=R$ without derivation:

$$\left.\begin{aligned} \Delta\underline{B}^*_{\text{Steel}}(\underline{z}_0) &= \sum_{\nu=1}^{\infty} \underline{z}_0^{n-1}(\underline{b}_{-n})^*/R^{2n} \\ n &= -N+\nu M, \end{aligned}\right\} \qquad (33)$$

$\underline{b}_{-n}$ are the expansion coefficients of the unperturbed field in $1/\underline{z}_0$ as used in eq. (32a). Notice that the fundamental ($n=N$) is not affected by the shield unless M has the exceptionally low value $2N$.

The results of this section show very clearly that the following properties are important for the design of a good segmented multipole magnet:

(1) the REC should be placed, with the largest possible volume filling factor, as closely to the "business" region as possible, "hugging" the aperture circle as well as possible.

(2) In order to produce strong fields of high quality, one should approximate eq. (20) reasonably well, with $M'=8$ easy axis orientations per period being a good guide number.

To arrive at a design, one has to combine these

two essential requirements with considerations like availability, or ease of production, of REC pieces of various shapes; ease of assembly, etc. Trapezoidal segments, as discussed above, seem to be a good choice, but it is quite possible that assemblies of tightly packed small rods with circular, hexagonal, or other, cross sections may be preferable under some circumstances.

4.3. The segmented REC quadrupole

Because of their special importance for accelerators, we discuss some details of quadrupoles, adding to the summaries published elsewhere[5,6]. Since quadrupoles with trapezoidal segments are quite typical, we restrict the discussion to this specific class of magnets.

From eq. (24a) follows for the fundamental harmonic for $\varepsilon = 1$:

$$\underline{B}^*(\underline{z}_0) = \frac{\underline{z}_0}{r_1} B_r 2\left(1 - \frac{r_1}{r_2}\right) K_2$$

$$K_2 = \cos^2(\pi/M)\,\frac{\sin 2\pi/M}{2\pi/M}. \qquad (34)$$

Table 1 shows that in order to get a strong quadrupole, one should choose $M = 12$ or 16. The gradients achievable with a 16-piece quadrupole are impressive, particularly when they are compared with those of conventional quadrupoles. For $M = 16$, $r_2/r_1 = 4$, (which is still quite compact) and $B_r = 0.95$ T (which is commercially available), one obtains an aperture field of 1.34 T. In contrast, a high quality conventional quadrupole is very difficult to make with more than 1 T at the aperture, and even that is possible only for fairly large aperture magnets. High aperture fields are of particular importance for linear accelerators with small apertures. For an aperture with $r_1 = 2$ mm, it it possible to achieve a gradient $B' = 6\ \mathrm{T\,cm^{-1}}$, and the diameter of such a quadrupole could be smaller than 2 cm. Clearly, it is impossible to achieve anything resembling this with conventional magnets and conventional REC quadrupole designs fall short of this gradient by at least a factor of 2.

Figure 6 shows a schematic cross section of a 16-piece quadrupole, with the easy axis direction indicated in each piece. It follows from that

Table 1

$M =$	4	8	12	16	20	24
$K_2 =$	0.32	0.77	0.89	0.94	0.96	0.97

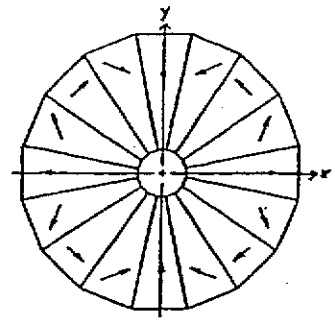

Fig. 6. Schematic cross section of a 16-piece REC quadrupole.

diagram that one needs pieces with five differen orientations of the easy axis relative to the trapezoi dal shape to make this 16-piece quadrupole. If on rotates all easy axes by 22.5° in the same direction only four different pieces are required, which ma be advantageous for the manufacturer. Since on has, in either case, a reasonably large number o pieces that are supposed to be identical, it may b advantageous to measure magnetization directio and magnitude for each piece, and then assemble the quadrupole in such a way that magnetizatio errors do the least harm to the field quality. Fo this reason, it may be a blessing in disguise t with present manufacturing techniques, the indi ual REC pieces are fairly small. This often force the use of several layers of REC in the axial direction, increasing the number of pieces and therefore improving the error cancelling statistics.

For a 16-piece quadrupole with $r_1/r_2 = 0.25$, the first undesirable harmonic ($n = 18$) field has, at $|\underline{z}| = r_1$, an amplitude that is approximately 6% of the fundamental [see eq. (27) for $N = 2$]. Eliminating that harmonic with a flat sheet of the thickness given by eq. (31b), the first non-vanishing harmonic is $n = 34$, with a relative amplitude of about 3% at the full aperture. The order of this harmonic is high enough that no attempt has yet been made to also eliminate it.

The fringe fields at the end of a segmented quadrupole (or other multipole) are fairly easily calculated by using the charge sheet model and eq. (11). If the cross sections of the REC pieces are trapezoidal, the charge sheets have rectangular cross sections and the integrals can be expressed by elementary transcendental functions, making the 3D field calculation rather easy. The relevant formulas are not reproduced here because the fringe fields of REC multipole magnets have some rather remarkable properties (to be discussed in sec

4.4) that make fringe field calculations necessary in only very rare instances.

Holsinger has built a prototype quadrupole with $r_1 = 1.1$ cm; $r_2 = 3$ cm; $M = 16$; and consisting of three 16-piece layers in the axial direction. Comparisons were made between measurements of that magnet, computer runs of that magnet with PANDIRA[7]), and the predictions made with the simple theory presented here. The results obtained with these procedures agreed very well with regard to the amplitude of the quadrupole field and the allowed higher harmonic $n = 18$. The only significant, but expected, discrepancy was the presence of the harmonics $n = 6, 10, 14$ in the computer model and the real magnet, while these harmonics do not exist in the simple model that assumes $\mu_\perp = \mu_\parallel = 1$. At $|z| = r_1$ the amplitudes of these harmonics were, relative to the quadrupole field, 0.2% for $n = 6$; 0.1% for $n = 14$; and $\leqslant 0.1\%$ for $n = 10$. While these errors are so small that they are unlikely to cause problems in most applications, one can easily imagine methods to eliminate these harmonics, if necessary. If, for instance, one has a gap between adjacent pieces for the elimination of $n = 18$, one would incorporate movable thin strips of soft steel into these gaps to tune away these undesired harmonics. The real magnet also had an approximately 0.5% sextupole, as well as some other multipoles, present. Since the individual REC pieces were not measured, it is expected that these harmonics can be significantly reduced when this is done and properly taken into account in the assembly. Another obvious tuning method would be the removal or addition of small amounts of REC at appropriate locations, but it is unlikely that such efforts will really be necessary.

4.4. Important practical consequences of applicability of linear superposition principle

It is obvious that the linear superposition principle is of crucial importance not only for specific important theorems, like the easy axis rotation theorem or the selection rule for possible harmonics [eq. (24a)], but to the whole mathematical description of REC magnets presented here. However, there are some very important practical consequences of the linear superposition principle that are obtainable without any mathematical derivations.

We consider first the following combination of two REC multipole magnets: one quadrupole is located, tightly fitting, inside the aperture region of another quadrupole. If each of these quadrupoles alone produces the same gradient, and both quadrupoles are rotated about the common axis by equal amounts in opposite directions, then the gradient in the aperture can be continuously changed between zero and twice the strength of the individual quadrupole. By similarly pairing of two dissimilar multipoles, one can make combined function magnets.

Care has to be taken for these combinations of REC magnets, and in particular for combinations of conventional steel magnets with REC magnets, that the REC is not driven into the nonlinear part of the $B_\parallel(H_\parallel)$ curve. A combination of magnets that would be fairly immune from this danger is a multipole inside the momogeneous field of a coaxial solenoid, since in this case the solenoidal field is everywhere perpendicular to the easy axis.

A different method to modify the effective strength of a REC quadrupole would be to assemble it from quadrupoles of relatively short axial lengths whose quadrupole field orientations can be adjusted. While this would be fairly easy to do, such a scheme obviously modifies the optical properties of the system in a non-trivial way, and this aspect of such a system is currently under investigation[8]).

Another important application of the superposition principle is the treatment of the fringe fields at the ends of multipole magnets. We deal here with two distinctly different aspects of fringe fields that are both very simple and important.

First we consider a multipole of finite physical length L whose left end is cut off in an arbitrary fashion, and whose right end is shaped such that the left end would fit it perfectly, without forming any gap. (See fig. 7). Another way to express that geometry is to state that the length of REC along any line parallel to the axis is either L or zero. Keeping the left end of the multipole fixed in space, we first consider the field quantity $G_1(r, \varphi, z)$ produced by a semi-infinite multipole, with $G_0(r, \varphi)$ representing the 2D field deep inside where it does not depend on z. Then the field quantity $G(r, \varphi, z)$

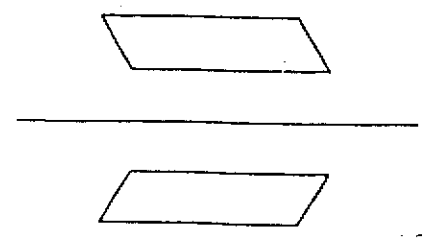

Fig. 7. Geometry of specific finite length REC multipole.

produced by a multipole of length L is given by

$$G(r,\varphi,z) = G_1(r,\varphi,z) - G_1(r,\varphi,z-L). \quad (35)$$

If we now calculate the optically important

$$\int_{-\infty}^{\infty} G(z)\,dz,$$

it is easy to see that eq. (35) leads to

$$\int_{-\infty}^{\infty} G(r,\varphi,z)\,dz = LG_0(r,\varphi). \quad (36)$$

This equation says not only that the effective length for the fundamental harmonic of interest equals the physical length of the multipole, but also that the integral over a field quantity vanishes if that field quantity is zero in the 2D cross section!

Next, we consider the properties of the fringe fields produced by a semi-infinite multipole, produced by cutting an infinite multipole by the x–y plane at $z=0$ (see fig. 8), i.e., we look at the fringe field function $G_1(z)$ for the specific case of the "square" end. If $V_1(r,\varphi,z)$ is the scalar potential produced by the multipole located at $z>0$, then the scalar potential produced by the multipole located at $z<0$ must be $V_1(r,\varphi,-z)$. If $V_0(r,\varphi)$ is the scalar potential inside the infinitely long multipole, the following obviously must hold:

$$V_1(r,\varphi,z) + V_1(r,\varphi,-z) = V_0(r,\varphi). \quad (37)$$

Applying the appropriate operator to this equation to get the field quantity $G_1(r,\varphi,z)$ of interest, we get, if no derivative with respect to z is involved:

$$G_1(r,\varphi,z) + G_1(r,\varphi,-z) = G_0(r,\varphi) = 2G_1(r,\varphi,0). \quad (38)$$

From this it follows that

$$\int_{-\infty}^{z_1} G_1(r,\varphi,z)\,dz = z_1\,G_0(r,\varphi) \quad (39)$$

if z_1 is sufficiently large. This means that the effective boundary is at $z=0$, and that the fringe field integral over a field quantity vanishes if that quantity is zero in the 2D cross section. Notice that this statement is stronger than the one made above with respect to eq. (36), which required integration over the fringe fields of both ends.

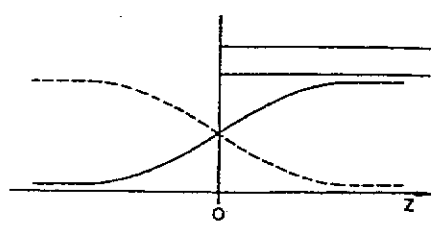

Fig. 8. Fields at the end of a REC multipole.

If the operator to obtain the field quantity of interest is proportional to $(\partial/\partial z)^m$, we get instead of eq. (38)

$$G_1(r,\varphi,z) = -(-1)^m G_1(r,\varphi,-z). \quad (40)$$

Integrating this $G_1(r,\varphi,z)$ over the fringe field region gives zero when $m \geq 2$, but not necessarily when $m=1$.

Appendix

Using eqs. (14) in eq. (13), one of the two integrals that have to be evaluated in eq. (13) is

$$I_1 = \frac{1}{2\pi i}\int \frac{\partial H_{cy}/\partial X}{z_0 - x - iy}\,dx\,dy.$$

Carrying out the integration over x first, and integrating by parts, one obtains

$$I_1 = \frac{1}{2\pi i}\oint \frac{H_{cy}}{z_0 - z}\,dy - \frac{1}{2\pi i}\int \frac{H_{cy}}{(z_0 - z)^2}\,dx\,dy.$$

Included in the integration area is a thin strip of vacuum outside the REC. $H_{cy}=0$ there, so that the line integral over y vanishes. Applying the same technique to the other integral necessary for the evaluation of the integral in eq. (13), one obtains eq. (15).

I would like to thank J. A. Farrell, T. D. Howard, E. A. Knapp (Los Alamos Scientific Laboratory) and R. L. Gluckstern (University of Maryland) for their active interest, support and discussions of this work. K. Strnat very kindly proofread the section dealing with the material production and properties.

M. Kaviany (Lawrence Berkeley Laboratory) made some useful computer runs and R. Holsinger shared the results of his computer runs and practical experiences and contributed greatly with several useful suggestions and many stimulating discussions.

References

1) K. J. Strnat and G. I. Hoffer, Techn. Report, AFML-TR-65-446, Wright Paterson Air Force Base, (1966); J. B. Y. Tsui, D. J. Iden, K. J. Strnat and A. J. Evers, *IEEE* Trans. Magn. 2 (1972) p. 188.
2) M. McCaig, *Permanent magnets in theory and practice*, (J. Wiley, London, 1977).
3) K. Halbach, Nucl. Instr. and Meth. 78 (1970) 185.
4) J. P. Blewett, BNL Internal Report, AADD-89 (1965).
5) K. Halbach, Proc. 1979 *Particle accelerator conf.*, IEEE Trans. Nucl. Sci. NS-26 (1979) 3882.
6) R. F. Holsinger and K. Halbach, Proc. 4 Int. Workshop on *Rare earth cobalt permanent magnets* (1979) p. 37.
7) R. F. Holsinger and K. Halbach, to be published.
8) R. L. Gluckstern, private communication.

Three-Dimensional Pure Permanent Magnet Undulator Design Theory

R. D. Schlueter and S. Marks
Lawrence Berkeley Laboratory, Berkeley, California 94720

Reprinted from
IEEE TRANSACTIONS ON MAGNETICS
Vol. 32, No. 4, July 1996

Three-Dimensional Pure Permanent Magnet Undulator Design Theory

R.D. Schlueter and S. Marks
Lawrence Berkeley Laboratory, Berkeley, California 94720

Abstract—**Expressions for fields due to a point charge in 3D and due to a line charge in 2D are compared. Extensions to dipoles are made with emphasis on the relationship between dipole orientation and field component magnitudes. Differences between the effects on fields of dipole rotations in 2D and in 3D are highlighted and formulas for maximizing individual field components are given. A final macrogeometry extension is made and a closed-form expression is developed to calculate the field due to an arbitrary 3D configuration of permanent magnet (PM) blocks. The field optimization theory is applied to the design of the ALS elliptically polarizing undulator (EPU). Utilizing 3D field enhancement, peak on-axis field in practical designs can be increased typically by 5% to 40% or more over their 2D counterparts. The theory is generally applicable to any pure (i.e., no soft magnetic material) PM design.**

I. Introduction

The theory of pure permanent magnet (PM) design in two dimensions has been described thoroughly [1,2]. Design of both nominally 2D pure PM structures, e.g., linearly polarizing undulators, and inherently 3D pure PM structures, e.g., Sasaki-type [3,4] planar elliptically polarizing undulators, can benefit from the extension of these concepts and optimization techniques to $\Re^3$. Herein, the PM material with $\mu = 1$ is represented by magnetic charge sheets on surfaces [5,6].

II. PM Point Charges and Dipoles

A. Point charge.

In $\Re^3$ the scalar potential and field from a point charge q [G-cm^2] located at $\mathbf{r}_q \equiv (x_q, y_q, z_q)$ are, respectively,

$$4\pi V(\mathbf{r}) = q/|\mathbf{r}-\mathbf{r}_q|;\ 4\pi\mathbf{B}(\mathbf{r}) = q(\mathbf{r}-\mathbf{r}_q)/|\mathbf{r}-\mathbf{r}_q|^3, \quad (1)$$

Manuscript received June 13, 1995.
This work was supported by the Director, Office of Energy Research, Office of Basic Energy Sciences, Mat. Sci. Div., of the U.S. Dept. of Energy, Contract No. DEAC03-76SF00098.

For a line charge of strength q' [G-cm^2/cm] per unit length in z, the field is 2D and is given by

$$4\pi\mathbf{B}(\mathbf{r}) = \int_{-\infty}^{\infty} \frac{q'(\mathbf{r}-\mathbf{r}_q)}{|\mathbf{r}-\mathbf{r}_q|^3}dz = \frac{2q'(x-x_q, y-y_q)}{|\mathbf{r}-\mathbf{r}_q|^2}. \quad (2)$$

The field conjugate is an analytic function of the complex variable $t \equiv x + iy$: $B^*(t) \equiv B_x - iB_y = q'/2\pi(t-t_q)$.

B. Dipole.

Extension to a dipole, where at $\mathbf{r}_q$ point charges of strength $\pm q$ separated by l are oriented (See Fig. 1.) via direction cosines $\hat{\eta}_q \equiv (\cos\chi, \cos\psi, \cos\theta)$, gives in 3D:

$$\frac{4\pi|\mathbf{r}_q-\mathbf{r}|^5}{ql}\begin{pmatrix} B_x(\mathbf{r}) \\ B_y(\mathbf{r}) \\ B_z(\mathbf{r}) \end{pmatrix} = \quad (3)$$

$$\begin{pmatrix} 2\hat{x}_q^2-\hat{y}_q^2-\hat{z}_q^2 & 3\hat{x}_q\hat{y}_q & 3\hat{x}_q\hat{z}_q \\ 3\hat{x}_q\hat{y}_q & 2\hat{y}_q^2-\hat{x}_q^2-\hat{z}_q^2 & 3\hat{y}_q\hat{z}_q \\ 3\hat{x}_q\hat{z}_q & 3\hat{y}_q\hat{z}_q & 2\hat{z}_q^2-\hat{x}_q^2-\hat{y}_q^2 \end{pmatrix}\begin{pmatrix} \cos\chi \\ \cos\psi \\ \cos\theta \end{pmatrix}$$

where $\hat{x}_q \equiv x_q - x$, etc. For a permanent magnet $q = \mathbf{B}_r \cdot \mathbf{a}$, where $\mathbf{B}_r$ is the remanent field and $\mathbf{a}$ is the surface normal.

For a line dipole of strength $q' = \mathbf{B}_r \cdot \mathbf{a}'$ in 2D:

$$\frac{2\pi|\hat{\mathbf{r}}_q|^4}{q'l}\begin{pmatrix} B_x(\mathbf{r}) \\ B_y(\mathbf{r}) \end{pmatrix} = \begin{pmatrix} \hat{x}_q^2-\hat{y}_q^2 & 2\hat{x}_q\hat{y}_q \\ 2\hat{x}_q\hat{y}_q & \hat{y}_q^2-\hat{x}_q^2 \end{pmatrix}\begin{pmatrix} \cos\chi \\ \cos\psi \end{pmatrix} \quad (4)$$

Since $\hat{\eta}_q = e^{i\chi}$, field conjugate $B^*(t) = q'le^{i\chi}/2\pi(t_q-t)^2$. Note that for a 2D line dipole oriented in, say, the x-direction, there is no B_x component at $\mathbf{r} = 0$ when that line charge is located along the line $y_q = \pm x_q$. At this location, this orientation also maximizes $B_y(0,0)$. This contrasts with the 3D case of a point dipole so oriented, which gives rise to a pure B_y component on-axis at $z = z_q$ when it lies along the line $y_q = \pm\sqrt{2}x_q$, though at this location $B_y(\mathbf{r}=0)$ is not maximized by this orientation.

C. Easy axis rotation.

In 2D, dipole rotation by an angle $\Delta\chi$ has the effect of rotating $\mathbf{B}$ by $-\Delta\chi$, while $|B|$ remains unchanged [1]:

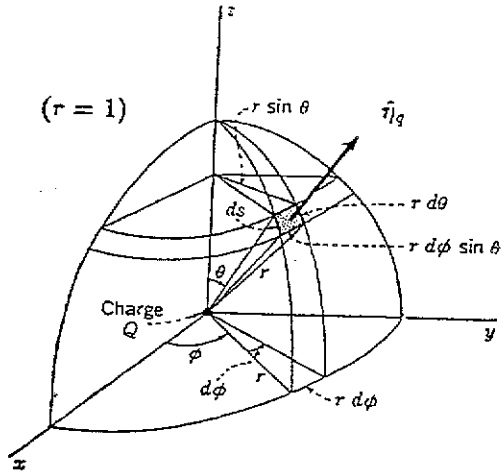

$\hat{\eta}_q \equiv (\cos\chi, \cos\psi, \cos\theta) = (\sin\theta\cos\phi, \sin\theta\sin\phi, \cos\theta)$

Fig. 1. Direction cosines of dipole at $\mathrm{r}_q = 0$

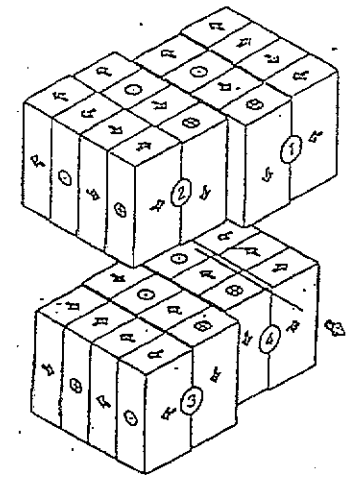

Fig. 2. ALS EPU periodic structure

$$B_2^* = \frac{q'le^{i(\chi+\Delta\chi)}}{2\pi(t_q-t)^2} = B_1^* e^{i\Delta\chi};\ \ \mathrm{B}_2 = \mathrm{B}_1 e^{-i\Delta\chi}. \qquad (5)$$

This 2D easy-axis rotation theorem implies that dipole orientation maximizing a field component nulls the orthogonal component. In 3D, without loss of generality, coordinates can be oriented such that the point of interest is at the origin and the dipole is at $(0,0,z_q)$. On-axis field $\mathbf{B}(0)$ is

$$(4\pi z_q^3/ql)\mathbf{B}(0) = (-\cos\chi, -\cos\psi, 2\cos\theta). \qquad (6)$$

In contrast to the 2D case, in 3D the magnitude $|B(0)|$ can vary by a factor of two, depending on the dipole orientation, being largest when the dipole is oriented in the direction of $\mathbf{r} - \mathbf{r}_q$:

$$(4\pi z_q^3/ql)|\mathbf{B}(0)| = \sqrt{3\cos^2\theta + 1}. \qquad (7)$$

Rotation of the dipole by $\Delta\phi_q$ in the x-y plane leaves B_z, $|B|$, and the sum $B_x^2 + B_y^2$ unchanged; individually, B_x and B_y are proportional to $\cos\phi_q$ and $\sin\phi_q$, respectively. Rotation by $\Delta\theta_q$ in any plane containing the z-axis leaves the ratio B_x/B_y unchanged; both B_x and B_y are proportional to $\sin\theta_q$, B_z is proportional to $\cos\theta_q$, and $|B| \propto \sqrt{3\cos^2\theta + 1}$. (See Fig. 1.)

D. Maximizing field components.

The formulas above are useful in determining the optimal orientation of magnetic moments in space to achieve a desired 3D field distribution. For example, in a 3D pure PM structure, using $|\hat{\eta}_q| = 1$, on-axis $B_y = f(\cos\psi, \cos\theta)$ and is given by:

$$\frac{4\pi|\mathbf{r}_q|^5}{ql} B_y(0,0,z) = 3x_q y_q \sqrt{1-\cos^2\psi - \cos^2\theta}$$

$$+ (2y_q^2 - x_q^2 - \hat{z}_q^2)\cos\psi + 3y_q\hat{z}_q\cos\theta. \qquad (8)$$

It is maximized for $\hat{\eta}_q$ given by:

$$\begin{pmatrix} \cos\chi \\ \cos\psi \\ \cos\theta \end{pmatrix} = \left[(3x_q y_q)^2 + (2y_q^2 - x_q^2 - \hat{z}_q^2)^2 + (3y_q\hat{z}_q)^2\right]^{-1/2} \begin{pmatrix} 3x_q y_q \\ 2y_q^2 - x_q^2 - \hat{z}_q^2 \\ 3y_q\hat{z}_q \end{pmatrix}. \qquad (9)$$

Thus to maximize on-axis $B_y(0,0,z)$, easy-axis orientation of a dipole at, for example, location $z_q = z$ and

$$\left\{ \begin{array}{c} x_q = 0 \\ 2y_q^2 - x_q^2 = 0 \\ y_q = 0 \end{array} \right\} \text{ is } \hat{\eta}_q = \left\{ \begin{array}{c} (0,+1,0) \\ (+1,0,0) \\ (0,-1,0) \end{array} \right\}. \qquad (10)$$

At the other extreme, as $\hat{z}_q \longrightarrow \infty$ at any (x_q, y_q), the easy-axis orientation of a dipole that maximizes on-axis $B_y(0,0,z)$, is $\cos\psi = -1$.

Implications for pure PM ID design are tremendous. One can increase on-axis B by $\sim 20\%$ in the inherently 3D ALS EPU structure ($\lambda = 5$cm, gap=1.8cm) by rotating the PM easy-axis as one moves off-axis in x. (See Fig. 2.)

On-axis fields of conventional linear polarizing pure PM devices also can be increased dramatically by taking advantage of this third-dimension easy-axis directionality optimization. For example, for pure PM IDs of gap-period ratios of 0.5 and 0.07, 4 blocks-per-period, and block height $L = \lambda/2$, maximum B_y of a practical structure utilizing easy-axis orientation variation in the x-direction (with just three rows of blocks in x) increases by 5% and 40%, respectively, over their 2D counterparts. (See Fig. 3.) For large period devices, peak fields greater than 2.5T are achievable. Finer subdivsion of blocks can in principle more than double these percentage increases, but manufacturing and assembly becomes increasingly cumbersome. If fabrication simplicity is paramount, peak on-axis field can actually be increased beyond the 2D 'ideal' field

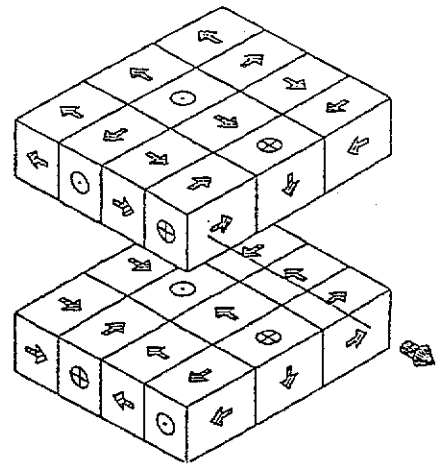

Fig. 3. Linear polarizing pure PM device with 3D field enhancement (one of many possible discretizations)

by merely truncating the PM blocks in the x-direction, since easy-axis orientation for maximizing peak on-axis B_y rotates through 180° as the x-coordinate of the dipole location varies within the interval $0 \leq x_q \leq \infty$.

Maximization of $B_x = f(\cos\psi, \cos\theta)$ is analogous:

$$\frac{4\pi|\mathbf{r}_q|^5}{ql} B_x(0,0,z) = (2x_q^2 - y_q^2 - \hat{z}_q^2)\sqrt{1-\cos^2\psi - \cos^2\theta} + 3x_q y_q \cos\psi + 3x_q \hat{z}_q \cos\theta. \quad (11)$$

It is maximized for $\hat{\eta}_q$ given by:

$$\begin{pmatrix} \cos\chi \\ \cos\psi \\ \cos\theta \end{pmatrix} = \left[(2x_q^2 - y_q^2 - \hat{z}_q^2)^2 + (3x_q y_q)^2 + (3x_q \hat{z}_q)^2\right]^{-1/2} \begin{pmatrix} 2x_q^2 - y_q^2 - \hat{z}_q^2 \\ 3x_q y_q \\ 3x_q \hat{z}_q \end{pmatrix}. \quad (12)$$

Thus to maximize on-axis $B_x(0,0,z)$, easy-axis orientation of a dipole at, for example, location $z_q = z$ and

$$\left\{ \begin{array}{c} x_q = 0 \\ 2x_q^2 - y_q^2 = 0 \\ y_q = 0 \end{array} \right\} \text{ is } \hat{\eta}_q = \left\{ \begin{array}{c} (-1,0,0) \\ (0,+1,0) \\ (+1,0,0) \end{array} \right\}. \quad (13)$$

At the other extreme, as $\hat{z}_q \longrightarrow \infty$ at any (x_q, y_q), the easy-axis orientation of a dipole that maximizes on-axis $B_x(0,0,z)$, is $\cos\chi = -1$.

III. PM BLOCKS & PERIODIC STRUCTURES

The field $\mathbf{B}(x,y,z)$ due to a uniformly magnetized block can be determined from a charge sheet model over the block surface where $q = \mathbf{B}_r \cdot \mathbf{a}$, where $\mathbf{B}_r$ is the remanent field and a is the magnet's surface area. Referring to the PM block in Fig. 4, charge sheets may exist on any of the block's six faces, depending on the magnetization

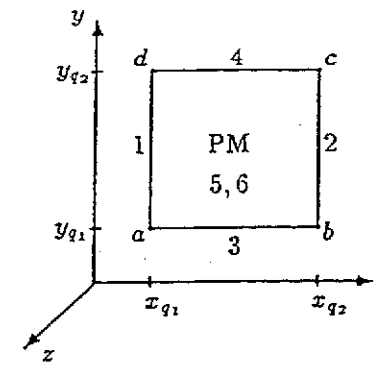

Fig. 4. PM block orientation and surfaces

orientation [5,6]. For a positive charge sheet on a single face:

$$\frac{4\pi}{B_r} B_u(x,y,z) = \int \frac{u - u_q}{|\mathbf{r} - \mathbf{r}_q|^3} da_q;$$

$$da_q = \left\{ \begin{array}{c} dx_q dy_q \\ dx_q dz_q \\ dy_q dz_q \end{array} \right\}; \quad \mathbf{B}_r \parallel \left\{ \begin{array}{c} z \\ y \\ x \end{array} \right\}, \quad (14)$$

where $u = x, y,$ or z. Summing contributions from the individual faces for each PM block in a system yields the vector components of B at any arbitrary location(s), e. along the axis in a pure PM undulator. For blocks whose surfaces are not parallel to the cartesian axes, one can always perform coordinate transformations by axes rotation; thus the development herein is completely general. Two types of integrals must be evaluated: those where the charge sheet surface normal and the calculated field component are parallel ($\mathbf{a}_q \times \hat{\eta}_{B_u} = 0$) and when they are perpendicular ($\mathbf{a}_q \cdot \hat{\eta}_{B_u} = 0$). (See Appendix A for solution details using either varible substitutions or Green's theorem.) The first integral type is:

$$\frac{4\pi}{B_r} B_u(x,y,z) = \int\int \frac{-\hat{u}_q}{|\hat{\mathbf{r}}_q|^3} du_q dv_q \equiv O_1(u_q, v_q) = \quad (15)$$

$$\ln\left(\frac{[\hat{v}_{q_2} + |\hat{\mathbf{r}}_q(u_{q_2}, v_{q_2}, w_q)|][\hat{v}_{q_1} + |\hat{\mathbf{r}}_q(u_{q_1}, v_{q_1}, w_q)|]}{[\hat{v}_{q_2} + |\hat{\mathbf{r}}_q(u_{q_1}, v_{q_2}, w_q)|][\hat{v}_{q_1} + |\hat{\mathbf{r}}_q(u_{q_2}, v_{q_1}, w_q)|]} \right)$$

where u is the cartesian coordinate of the field component of interest, with u, v, w each being any one of the cartesian coordinates x, y, z. The normal to the charged block surface is parallel to the w axis and is defined by the region w_q=constant, $u_{q_1} \leq u_q \leq u_{q_2}$, and $v_{q_1} \leq v_q \leq v_{q_2}$. B_r is the surface charge sheet density and $|\hat{\mathbf{r}}_q(u_q, v_q, w_q)| \equiv \sqrt{(u_q - u)^2 + (v_q - v)^2 + (w_q - w)^2}$. The second integral type is:

$$\frac{4\pi}{B_r} B_u(x,y,z) = \int\int \frac{-\hat{u}_q}{|\hat{\mathbf{r}}_q|^3} dv_q dw_q \equiv O_2(u_q) = \quad (16)$$

$$\arctan\left(\frac{\hat{v}_{q_2}\hat{w}_{q_1}}{\hat{u}_q|\hat{r}_q(u_q,v_{q_2},w_{q_1})|}\right)+\arctan\left(\frac{\hat{v}_{q_1}\hat{w}_{q_2}}{\hat{u}_q|\hat{r}_q(u_q,v_{q_1},w_{q_2})|}\right)$$

$$-\arctan\left(\frac{\hat{v}_{q_1}\hat{w}_{q_1}}{\hat{u}_q|\hat{r}_q(u_q,v_{q_1},w_{q_1})|}\right)-\arctan\left(\frac{\hat{v}_{q_2}\hat{w}_{q_2}}{\hat{u}_q|\hat{r}_q(u_q,v_{q_2},w_{q_2})|}\right)$$

where u is the cartesian coordinate of the field component, the block surface defined by the region u_q= const., $v_{q_1} \le v_q \le v_{q_2}$, and $w_{q_1} \le w_q \le w_{q_2}$ is normal to the v-w plane.

The field in a 3D structure of PM blocks, then, is

$$\frac{4\pi}{B_r}\begin{pmatrix} B_x(\mathbf{r}) \\ B_y(\mathbf{r}) \\ B_z(\mathbf{r}) \end{pmatrix} = \tag{17}$$

$$\begin{pmatrix} \sum_x O_2(x_q) & +\sum_y O_1(x_q,z_q) & +\sum_z O_1(x_q,y_q) \\ \sum_x O_1(y_q,z_q) & +\sum_y O_2(y_q) & +\sum_z O_1(y_q,x_q) \\ \sum_x O_1(z_q,y_q) & +\sum_y O_1(z_q,x_q) & +\sum_z O_2(z_q) \end{pmatrix},$$

where the summation Σ_x is over all charge sheet surfaces whose normal is parallel to the x axis, etc.

In the expression in Eq. (17), there is a singularity in the logarithm when $\hat{v}_q = -|\hat{r}_q|$. These singularities occur in pairs and can be handled numerically taking the limit:

$$\lim_{\epsilon\longrightarrow 0}\ln\left(\frac{-a+\sqrt{a^2+\epsilon^2}}{-b+\sqrt{b^2+\epsilon^2}}\right)=\ln(b/a). \tag{18}$$

We have used the 3D optimization techniques of the previous section to design the ALS EPU shown in Figure 2, using the closed-form expressions of this section. Program CPU [7] allows input of multiple rows of periodic arrays of PM blocks with specified magnetization orientations to rapidly calculate fields anywhere in the gap region of the proposed ALS EPU.

Having two blocks in each quadrant enables another beneficial design feature, i.e., a thinner vacuum chamber wall, and thus smaller magnetic gap, over the portion of the chamber directly above/below the beam axis than otherwise possible with a uniform-in-x chamber thickness due to strength limits. This further increases the attainable peak on-axis field. Note that with the 3D field enhancement, field rolloff in x is rapid, thus complicating focusing effects.

IV. APPENDIX A: INTEGRAL DERIVATIONS

For the integral type of Eq. (17), using Green's theorem and noting that $B_x = -\partial V/\partial x = \partial V/\partial x_q$, gives

$$\frac{4\pi}{B_r}B_x(x,y,z)=\int\int\frac{-\hat{x}_q}{|\hat{\mathbf{r}}_q|^3}dx_q dy_q=\frac{4\pi}{B_r}\int\int\frac{\partial V}{\partial x_q}dx_q dy_q$$

$$=\frac{4\pi}{B_r}\oint V dy_q=\frac{4\pi}{B_r}\left(\int_b^c V dy_q+\int_d^a V dy_q\right), \tag{19}$$

where points a, b, c, d are shown in Fig. 4. Integral contributions along a-b and c-d are zero since y is constant along these line segments. Integrating Eq. (21) with V given by Eq. (1) yields Eq. (17). Alternatively,

$$\frac{4\pi}{B_r}B_x(x,y,z)=\int_{x_{q_1}}^{x_{q_2}}\left(\frac{\hat{x}_q}{\hat{x}_q^2+\hat{z}_q^2}\right)\left(\frac{\hat{y}_q}{|\hat{\mathbf{r}}_q|}\right)\Bigg|_{y_{q_1}}^{y_{q_2}}dx_q. \tag{20}$$

Now

$$\int\left(\frac{\hat{x}_q}{\hat{x}_q^2+c_1}\right)\left(\frac{1}{\sqrt{\hat{x}_q^2+c_2}}\right)dx_q=\int\frac{dp}{p^2-(c_2-c_1)}$$

$$=\frac{-1}{\sqrt{c_2-c_1}}\ln\left|\frac{\sqrt{c_2-c_1}+\sqrt{\hat{x}_q^2+c_2}}{i\sqrt{\hat{x}_q^2+c_1}}\right|, \tag{21}$$

where $p \equiv \sqrt{\hat{x}_q^2+c_2}$, $c_1 = \hat{z}_q^2$, and $c_2-c_1 = \hat{y}_q^2$. Making the substitutions again yields Eq. (17).

Similarly, for the integral type of Eq. (18),

$$\frac{4\pi}{B_r}B_x(x,y,z)=\int_{z_{q_1}}^{z_{q_2}}\left(\frac{\hat{x}_q}{\hat{x}_q^2+\hat{z}_q^2}\right)\left(\frac{\hat{y}_q}{|\hat{\mathbf{r}}_q|}\right)\Bigg|_{y_{q_1}}^{y_{q_2}}dz_q. \tag{22}$$

Now

$$\int\left(\frac{1}{\hat{z}_q^2+c_1}\right)\left(\frac{1}{\sqrt{\hat{z}_q^2+c_2}}\right)dz_q=\int\frac{dp}{p^2(c_2-c_1)+c_1}$$

$$=\frac{1}{\sqrt{c_1}\sqrt{c_2-c_1}}\arctan\left(p\sqrt{\frac{c_2}{c_1}-1}\right), \tag{23}$$

where $p \equiv \hat{z}_q/\sqrt{\hat{z}_q^2+c_2}$, $c_1 = \hat{x}_q^2$, and $c_2-c_1 = \hat{y}_q^2$. Making the substitutions yields Eq. (18).

ACKNOWLEDGMENT

We are happy to thank Klaus Halbach for teaching us the magnetics fundamentals on which this work is based.

REFERENCES

[1] K. Halbach, "Design of permanent multipole magnets with oriented rare earth cobalt material", *Nucl. Instr. Meth.* vol. 169, p. 1, 1980.

[2] K. Halbach, "Physical and optical properties of rare earth cobalt magnets", *Nucl. Instr. Meth.* vol. 187, p. 109, 1981.

[3] S. Sasaki, "Design of a new type of planar undulator for generating variably polarized radiation", *Nucl. Instr. Meth.* vol. A331, p. 763, 1993.

[4] S. Sasaki, "Analysis for a planar variably polarizing undulator", *Proc. 8th Nat. Conf. on Synch. Rad. Instr.* Gaithersburg, MD, 1993.

[5] K. Halbach, "Insertion device design", LBL Report V8811-1.1-16, 1989.

[6] R.D. Schlueter, "Field errors in hybrid insertion devices", *Halbach Symposium on Magnet Technology* vol. 1, LBL Report 36839, p. 55, 1995.

[7] R.D. Schlueter, *Code CPU*, Lawrence Berkeley Lab., 1995.

3D FIELD DISTRIBUTION DUE TO A HOMOGENEOUSLY MAGNETIZED PM: CLOSED FORM EXPRESSIONS (5,6)

RDS 2/95

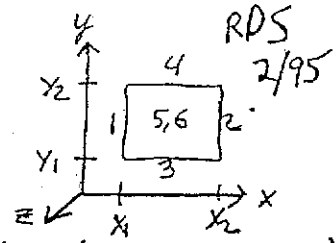

for a charge sheet $+B_r$ in the x-y plane:

$$\frac{4\pi}{B_r}\begin{pmatrix} B_x(x,y,z) \\ B_y(x,y,z) \\ B_z(x,y,z) \end{pmatrix} = \begin{pmatrix} \ln\left(\frac{\left[(Y_{q2}-Y)+\sqrt{T(X_{q2},Y_{q2})}\right]\left[(Y_{q1}-Y)+\sqrt{T(X_{q1},Y_{q1})}\right]}{\left[(Y_{q2}-Y)+\sqrt{T(X_{q1},Y_{q2})}\right]\left[(Y_{q1}-Y)+\sqrt{T(X_{q2},Y_{q1})}\right]}\right) \\ \ln\left(\frac{\left[(X_{q2}-X)+\sqrt{T(X_{q2},Y_{q2})}\right]\left[(X_{q1}-X)+\sqrt{T(X_{q1},Y_{q1})}\right]}{\left[(X_{q2}-X)+\sqrt{T(X_{q2},Y_{q1})}\right]\left[(X_{q1}-X)+\sqrt{T(X_{q1},Y_{q2})}\right]}\right) \\ -\left\{\arctan\left[\frac{(Y_{q2}-Y)(X_q-X)}{(Z_q-Z)\sqrt{T(X_{q1},Y_{q2})}}\right]\Bigg|_{X_{q1}}^{X_{q2}} - \arctan\left[\frac{(Y_{q1}-Y)(X_q-X)}{(Z_q-Z)\sqrt{T(X_{q1},Y_{q1})}}\right]\Bigg|_{X_{q1}}^{X_{q2}}\right. \end{pmatrix}$$

in the y-z plane: (1,2)

$$\frac{4\pi}{B_r}\left(\vec{B}\right) = \begin{pmatrix} \operatorname{atan}\left[\frac{(Y_{q2}-Y)(Z_{q1}-Z)}{(X_q-X)\sqrt{T(Y_{q2},Z_{q1})}}\right]+\operatorname{atan}\left[\frac{(Y_{q1}-Y)(Z_{q2}-Z)}{(X_q-X)\sqrt{T(Y_{q1},Z_{q2})}}\right]-\operatorname{atan}\left[\frac{(Y_{q1}-Y)(Z_{q1}-Z)}{(X_q-X)\sqrt{T(Y_{q1},Z_{q1})}}\right]-\operatorname{atan}\left[\frac{(Y_{q2}-Y)(Z_{q2}-Z)}{(X_q-X)\sqrt{T(Y_{q2},Z_{q2})}}\right] \\ \ln\left[\frac{\left[(Z_{q2}-Z)+\sqrt{T(Y_{q2},Z_{q2})}\right]\left[(Z_{q1}-Z)+\sqrt{T(Y_{q1},Z_{q1})}\right]}{\left[(Z_{q2}-Z)+\sqrt{T(Y_{q1},Z_{q2})}\right]\left[(Z_{q1}-Z)+\sqrt{T(Y_{q2},Z_{q1})}\right]}\right] \\ \ln\left[\frac{\left[|Y_{q2}-Y|+\sqrt{T(Y_{q2},Z_{q2})}\right]\left[(Y_{q1}-Y)+\sqrt{T(Y_{q1},Z_{q1})}\right]}{\left[|Y_{q2}-Y|+\sqrt{T(Y_{q2},Z_{q1})}\right]\left[(Y_{q1}-Y)+\sqrt{T(Y_{q1},Z_{q2})}\right]}\right] \end{pmatrix}$$

in the x-z plane: (3,4)

$$\frac{4\pi}{B_r}\left(\vec{B}\right) = \begin{pmatrix} \ln\left[\frac{\left[(Z_{q2}-Z)+\sqrt{T(X_{q2},Z_{q2})}\right]\left[(Z_{q1}-Z)+\sqrt{T(X_{q1},Z_{q1})}\right]}{\left[(Z_{q2}-Z)+\sqrt{T(X_{q1},Z_{q2})}\right]\left[(Z_{q1}-Z)+\sqrt{T(X_{q2},Z_{q1})}\right]}\right] \\ \operatorname{atan}\left[\frac{(X_{q2}-X)(Z_{q1}-Z)}{(Y_q-Y)\sqrt{T(X_{q2},Z_{q1})}}\right]+\operatorname{atan}\left[\frac{(X_{q1}-X)(Z_{q2}-Z)}{(Y_q-Y)\sqrt{T(X_{q1},Z_{q2})}}\right]-\operatorname{atan}\left[\frac{(X_{q2}-X)(Z_{q2}-Z)}{(Y_q-Y)\sqrt{T(X_{q2},Z_{q2})}}\right]-\operatorname{atan}\left[\frac{(X_{q1}-X)(Z_{q1}-Z)}{(Y_q-Y)\sqrt{T(X_{q1},Z_{q1})}}\right] \\ \ln\left[\frac{\left[(X_{q2}-X)+\sqrt{T(X_{q2},Z_{q2})}\right]\left[(X_{q1}-X)+\sqrt{T(X_{q1},Z_{q1})}\right]}{\left[(X_{q2}-X)+\sqrt{T(X_{q2},Z_{q1})}\right]\left[(X_{q1}-X)+\sqrt{T(X_{q1},Z_{q2})}\right]}\right] \end{pmatrix}$$

where $T(X_q,Y_q,Z_q)=\sqrt{(X_q-X)^2+(Y_q-Y)^2+(Z_q-Z)^2}$

POINT 2 > POINT 1 IN X, Y, or Z

Hybrid (IRON + PM) 3-D Theory

Represent IRON with $\mu = \infty$; PM with $\mu_{\parallel}, \mu_{\perp}, \rho_{eq}$

Game: Given PMs, V_{pole}=?

Let's start with a point charge Q + 2 iron surfaces:

We construct a solution that satisfies MAXWELL in space outside iron and has total flux $\phi_1 = 0$ entering surface 1. This solution is a superposition of 2 solutions to MAXWELL outside iron:

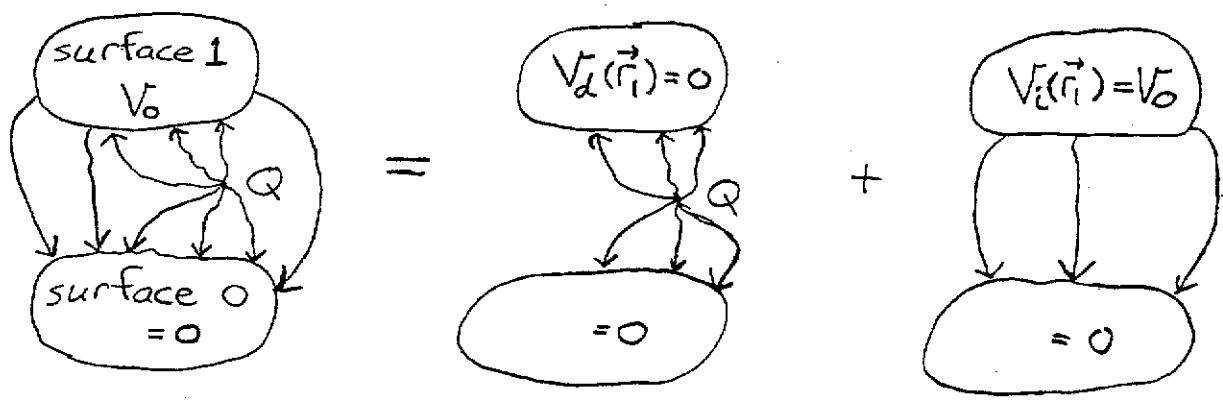

(c) = (a) DIRECT FIELDS + (b) INDIRECT FIELDS

(a) $Q \neq 0$; @1 $V = V_d(\vec{r}_1) = 0$; $V_d(\vec{r}) \rightarrow \vec{H}_d \rightarrow \phi_d = \int_1 \vec{H}_d \cdot d\vec{a}_1 = {}^{+}Q \cdot C_1$

(b) $Q = 0$; @1 $V = V_i(\vec{r}_1) = V_0$; $V_i(\vec{r}) \rightarrow \vec{H}_i \rightarrow \phi_i = \int_1 \vec{H}_i \cdot d\vec{a}_1 = {}^{-}V_0 \cdot C_2$

(c) $V = V_d + V_i \rightarrow \vec{H} = \vec{H}_d + \vec{H}_i \rightarrow \phi_1 = \phi_d + \phi_i = +QC_1 - V_0 \cdot C_2 = 0$

$\therefore V_{SURFACE\,1} = V_0 = QC_1/C_2$

Calculation of C_1: C_1 is just the fraction of Q that goes into surface 1 when both surfaces are on zero scalar potential

RESULT IS INTUITIVE:

$C_1 = V_i(\vec{r}_Q)/V_0$

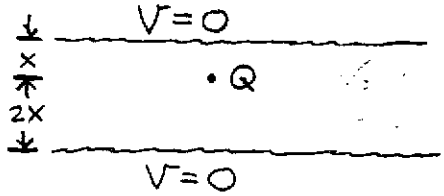

$C_1 = 2/3$

$C_1 = V_i(\vec{r}_Q)/V_0$; Proof: consider $\ell \equiv \int (V_i \vec{B}_d - V_d \vec{B}_i)\cdot d\vec{a}$, $d\vec{a}$ over all surfaces enclosing total volume not iron

on surface 0: $V_d = V_i = 0$
on surface 1: $V_d = 0$, $V_i = V_0$
at infinity : $V\vec{B} \to 0$ faster than $a \to \infty$

$\Rightarrow$ ① $\ell = V_0 \phi_d$

Now $\ell \equiv \int (V_i \vec{B}_d - V_d \vec{B}_i)\cdot d\vec{a} = \int \vec{\nabla}\cdot(V_i \vec{B}_d - V_d \vec{B}_i)\, dv$

② $\ell = \int V_i \underbrace{\vec{\nabla}\cdot\vec{B}_d}_{=\rho_{eq}} - V_d \underbrace{\vec{\nabla}\cdot\vec{B}_i}_{=0} + \underbrace{\vec{H}_d\cdot\vec{B}_i - \vec{H}_i\cdot\vec{B}_d}_{=0}\, dv$ because:

$$\vec{H}_i\cdot\vec{B}_d = \mu_0(\vec{H}_{i\parallel} + \vec{H}_{i\perp})\cdot(\mu_\parallel \vec{H}_{d\parallel} + \mu_\perp \vec{H}_{d\perp})$$
$$= \mu_0(\mu_\parallel \vec{H}_{i\parallel}\cdot\vec{H}_{d\parallel} + \mu_\perp \vec{H}_{i\perp}\cdot\vec{H}_{d\perp}) = \vec{H}_d\cdot\vec{B}_i$$

Equating ① & ②: $\phi_d = \int V_i(\vec{r})\rho_{eq}(\vec{r})\, dv / V_0$

& for point charge Q: $Q c_1 = V_i(\vec{r}_Q) Q / V_0$; $c_1 = V_i(\vec{r}_Q)/V_0$

EXTENSION TO A DIPOLE: $\vec{\Delta r}$: $+Q$, $-Q$

$$\phi_d = Q(V_i(\vec{r}_Q + \Delta\vec{r}) - V_i(\vec{r}_Q))/V_0 = -Q\Delta\vec{r}\cdot\vec{H}_i(\vec{r}_Q)/V_0$$

EXTENSION TO a PM BLOCK: 

$Q = |B_r| \cdot a$

$$Q\cdot\Delta\vec{r} = |B_r| a\cdot\Delta\vec{r} = \vec{B}_r\, dv$$

$$\phi_d = -\int \vec{B}_r\cdot\vec{H}_i\, dv / V_0$$

EXTENSION TO ANY NUMBER OF ISOPOTENTIAL SURFACES – LATER

REMAINING: CALCULATE $C_2 \equiv \frac{\phi_i \text{ SURFACE 1}}{V_i \text{ SURFACE 1}}$; set $\phi_i + \phi_d = 0$

$\Rightarrow$ determines V_0

EM's

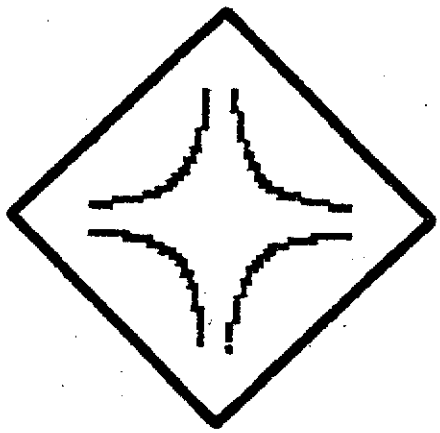

Quadrupole

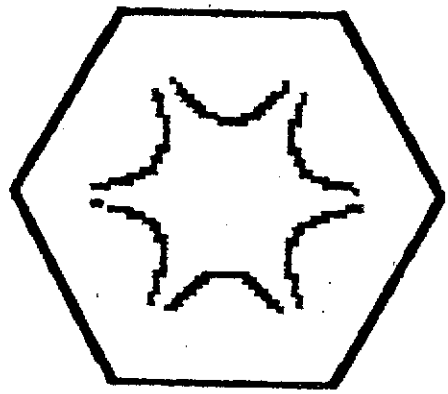

Sextupole

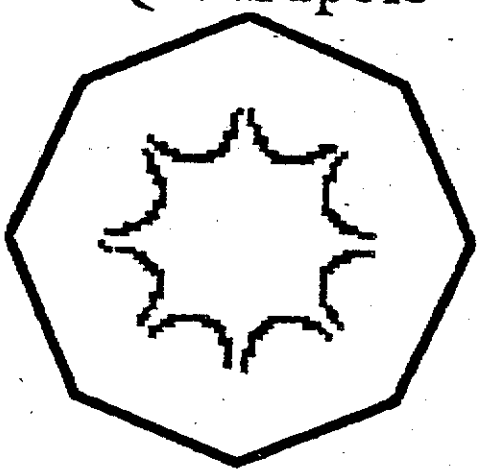

Octupole

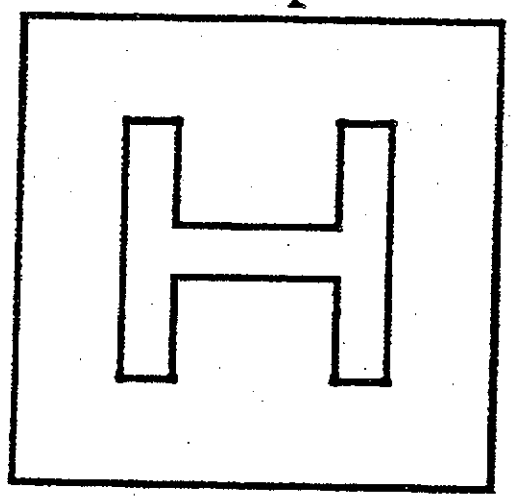

H-Dipole

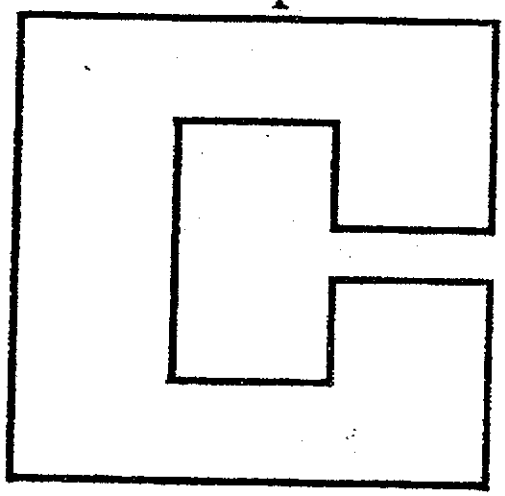

C-Dipole

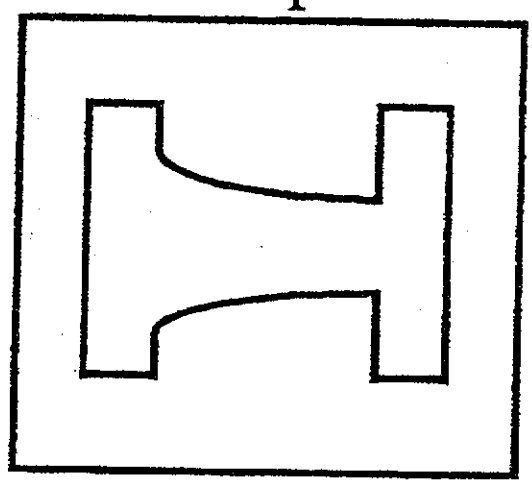

Combined function

EM vs. PM

$\oint H \cdot ds$ vs. fixed flux

YOKED vs. NOT YOKED

THE SILVERTREE HOTEL
P.O. Box 5009, Snowmass Village, Colorado 81615
(970) 923-3520; FAX (970) 923-5192
www.silvertreehotel.com • e-mail: reservations@silvertreehotel.com

① FOR 1/4 geometry windowframe dipole; with $\delta \ll w$:

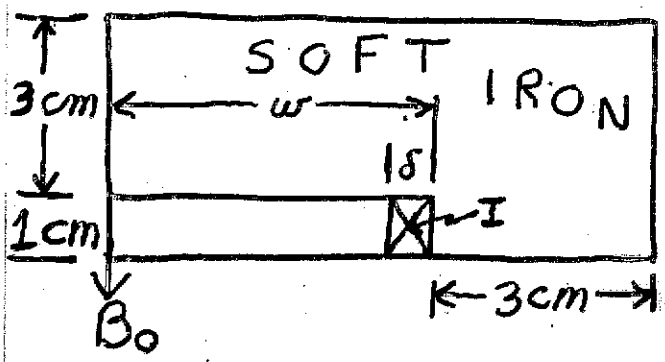

if			then
w [cm]	$I_{UPPER\ HALF}$ [A]	B_o [Gauss]	Comment
4	5000		
8	5000		
12	5000		
4	10,000		
4	20,000		

② For 1/4 geometry P.M.-Hybrid dipole; $B_r = 10{,}000$ Gauss

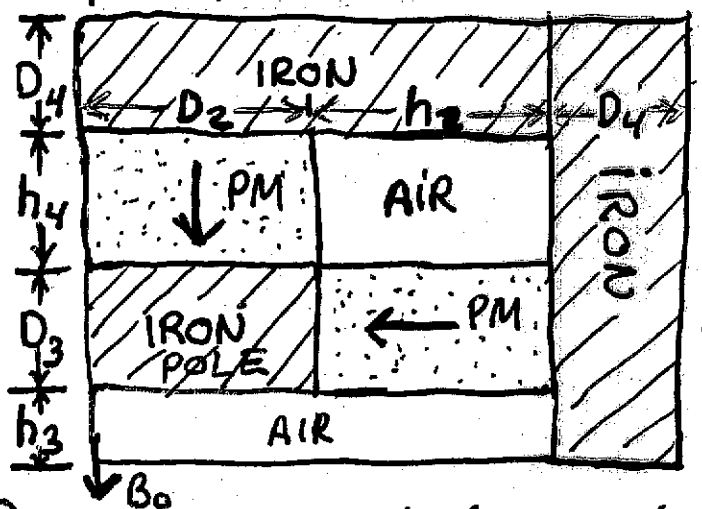

if D_4 is "large-enuf",

- what is the direct flux into the pole? $\Phi_d =$
- neglecting "excess" flux, what is indirect flux out of pole, $\Phi_i = f(V_o, \text{dimensions}) =$
- for $h_3 = 1$, $D_3 = h_4 = D_2 = h_2 = 3$, what is $V_o =$, $B_o =$

③ On the midplane of a magnet we desire: a field $B_x = 0$ & B_y given below. Plot for $|x| \le 2.5$ exact shape & location of the pole pieces of an iron core EM design powered with a total current of 16,000 A-Turns. [top + bottom halves]

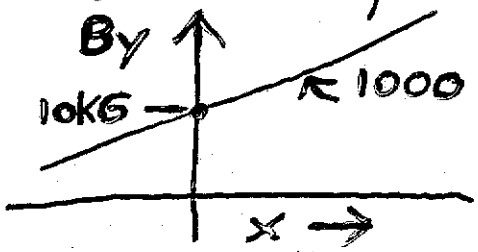

Math details for hybrid design:

- Schwarz-Christoffel Transformation
- analytical expressions for excess flux coefficients (E
- ϕ_3 refinement

Schwarz-Cristoffel Transformation:

What it is: a procedure to derive a transformation that maps the interior of a polygon to a half-plane

What it is good for: establishing closed-form relationships between two relavant complex quantities that are analytical functions of each other (like z, F, B^*)

How we are going to use it: to get closed form expressions for excess flux coefficients

S-C Recipe:

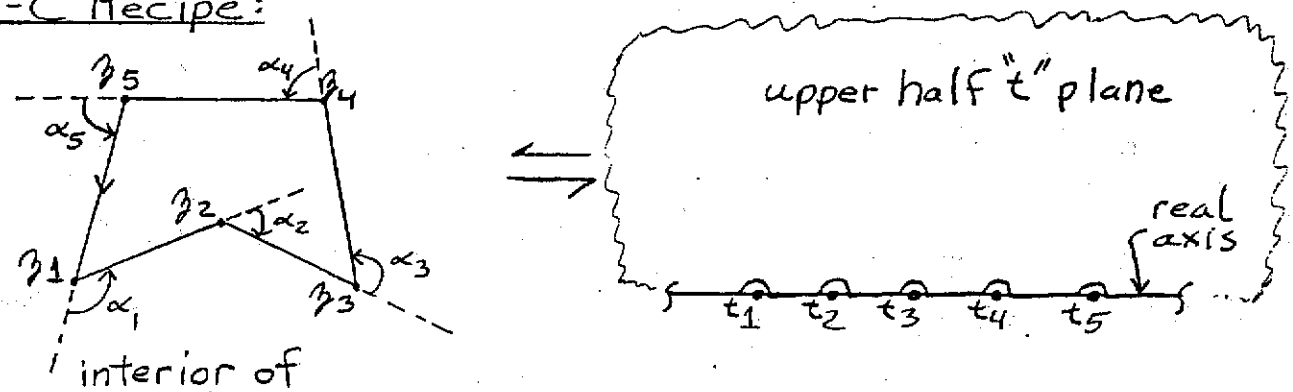

polygon in "z" plane mapped to upper half "t" plane

corners of polygon in z plane numbered sequentially and mapped on sequentially numbered points on the real axis of the t-plane with

$$dz/dt = c_1 \prod_i (t - t_i)^{-\alpha_i/\pi}$$

ifferent
c_1, c_2

S-C recipe, continued: $\frac{d\eta}{dt} = c_1 \prod_i (t-t_i)^{-\alpha_i/\pi}$

- t_i are real, $\sum_{i=1} \alpha_i/\pi = 2$
- $(t-t_i)^{\alpha_i/\pi}$ is real for $t-t_i$ real + positive
- for t real & $t_{i-1} < t < t_i$, the phase of $d\eta/dt$ is invariant $\therefore \eta(t)$ is straight over this segment
- for t real & $t > t_i$: phase of $(t-t_i)^{\alpha_i/\pi}$ is zero

  for t real & $t < t_i$: phase of $(t-t_i)^{\alpha_i/\pi}$ is $e^{i\pi\alpha_i/\pi} = e^{i\alpha_i}$

  $\therefore$ moving along the real axis in t plane from the left to the right of t_i, increases the phase of $d\eta/dt$ by α_i. Therefore along real t axis from $-\infty$ to ∞ phase increases by $\sum_i \alpha_i = 2\pi$. Interior of polygon is mapped to upper ½ t-plane

i's

- choices for t_i (degrees of Freedom)

  1) can pick one t_i at ∞ & it disappears from formula

  2) can choose origin of t plane and scale of t plane and thereby move two more points on the real axis of the t plane to arbitrary locations (convenient to choose @ 0 & ±1) without changing polygon in η plane.

Exercise: Show 1) by picking $t_1 = 0$ and mapping upper ½ plane of to the upper ½ plane of T with the map $T = -1/t$.

HW $d\eta/dT = \frac{d\eta}{dt} \cdot \frac{1}{T^2} = \frac{c_1}{T^2} \frac{1}{(\frac{1}{T})^{\alpha_1/\pi} \prod_2 (\frac{1}{T} - \frac{1}{T_i})^{\alpha_i/\pi}} = c_1 \prod_2 (1 - T/T_i)^{-\alpha_i/\pi}$

$= c_2 \prod_{i=2} (T-T_i)^{-\alpha_i/\pi}$; note: point 1 has disappeared; also $\sum_{i=2} \alpha_i \neq 2\pi$

01/26/2001

DR Quad Cycle = 8

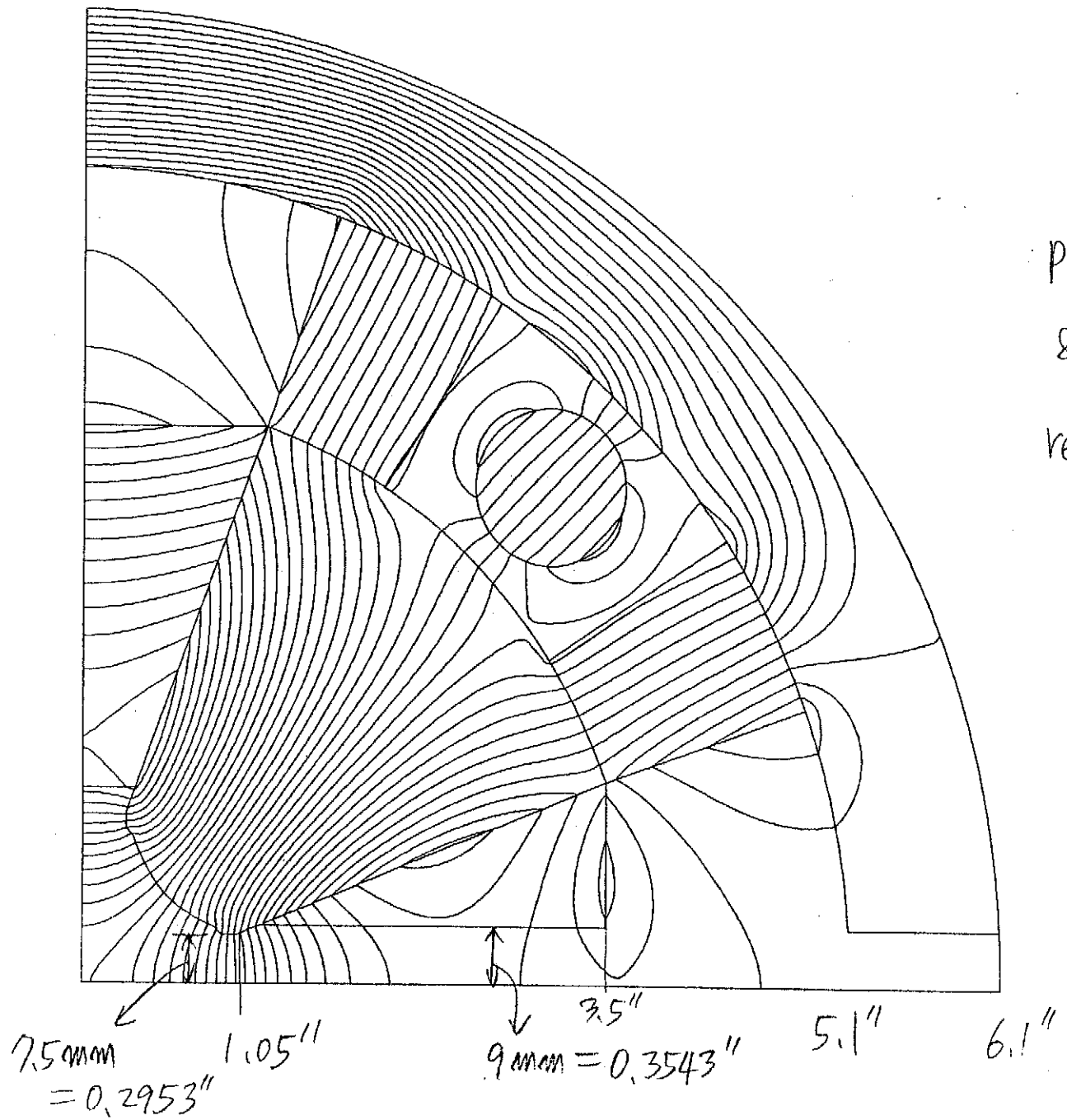

Neo 0.5" radius tuner

pole tip field = 8923 G

$\frac{dg}{g} = 0.42\%$

pole tip field required:

8000 $\xrightarrow{1\%\uparrow}$ 8080 $\xrightarrow{10\%\uparrow}$ 8888

required $\frac{dg}{g} \leq 1\%$

6/29/01

Ferrite

DR Quad Cycle = 6

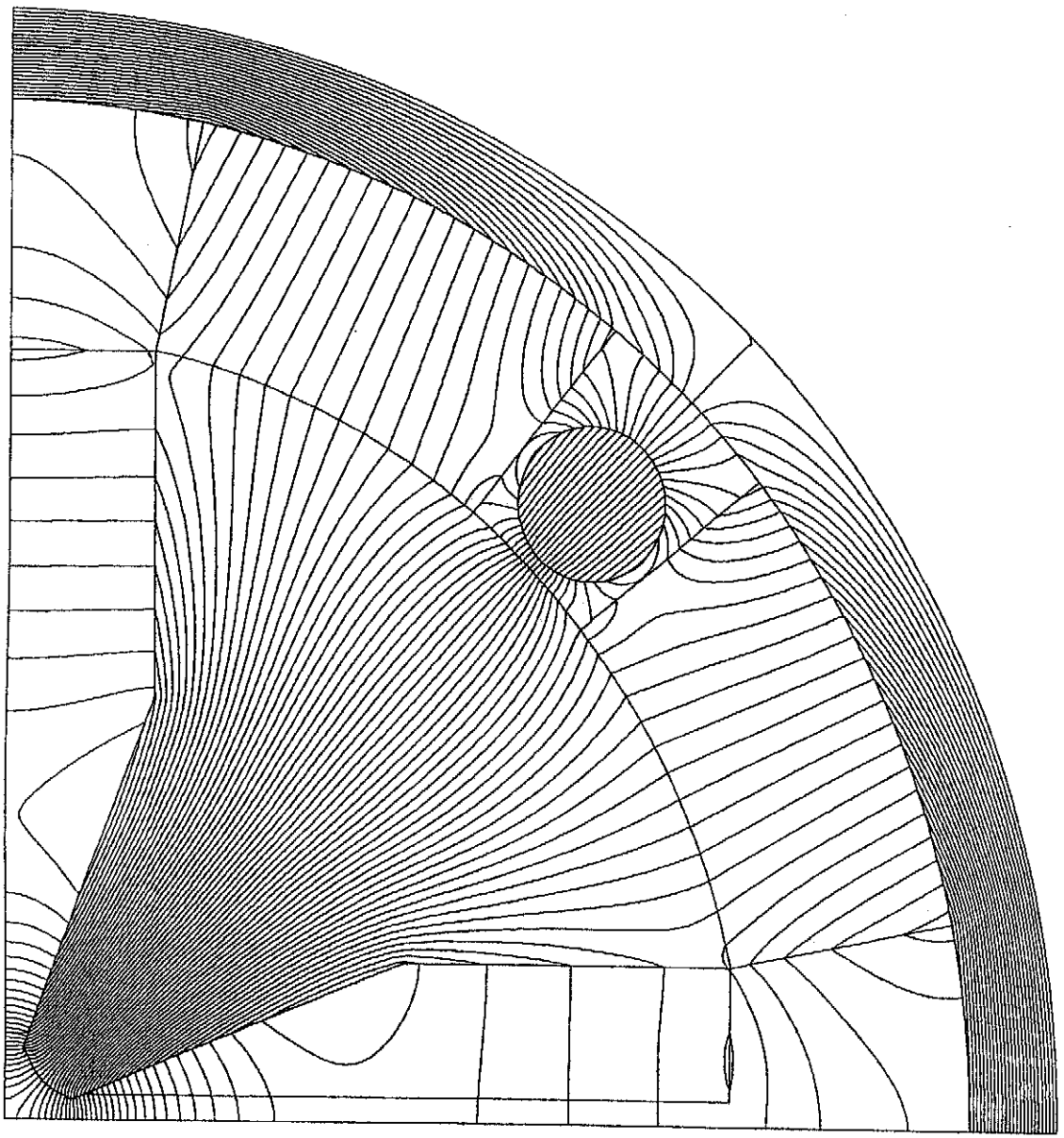

10.9" 14.5" 15.8"

1.1" radius tuner

pole tip field = 9083G

$\frac{dg}{g} = 0.39\%$

pole tip field required:

8000 $\xrightarrow{3\%\uparrow}$ 8240 $\xrightarrow{10\%\uparrow}$ 9064

required $\frac{dg}{g} \leq 1\%$

Handbook of
ACCELERATOR PHYSICS AND ENGINEERING

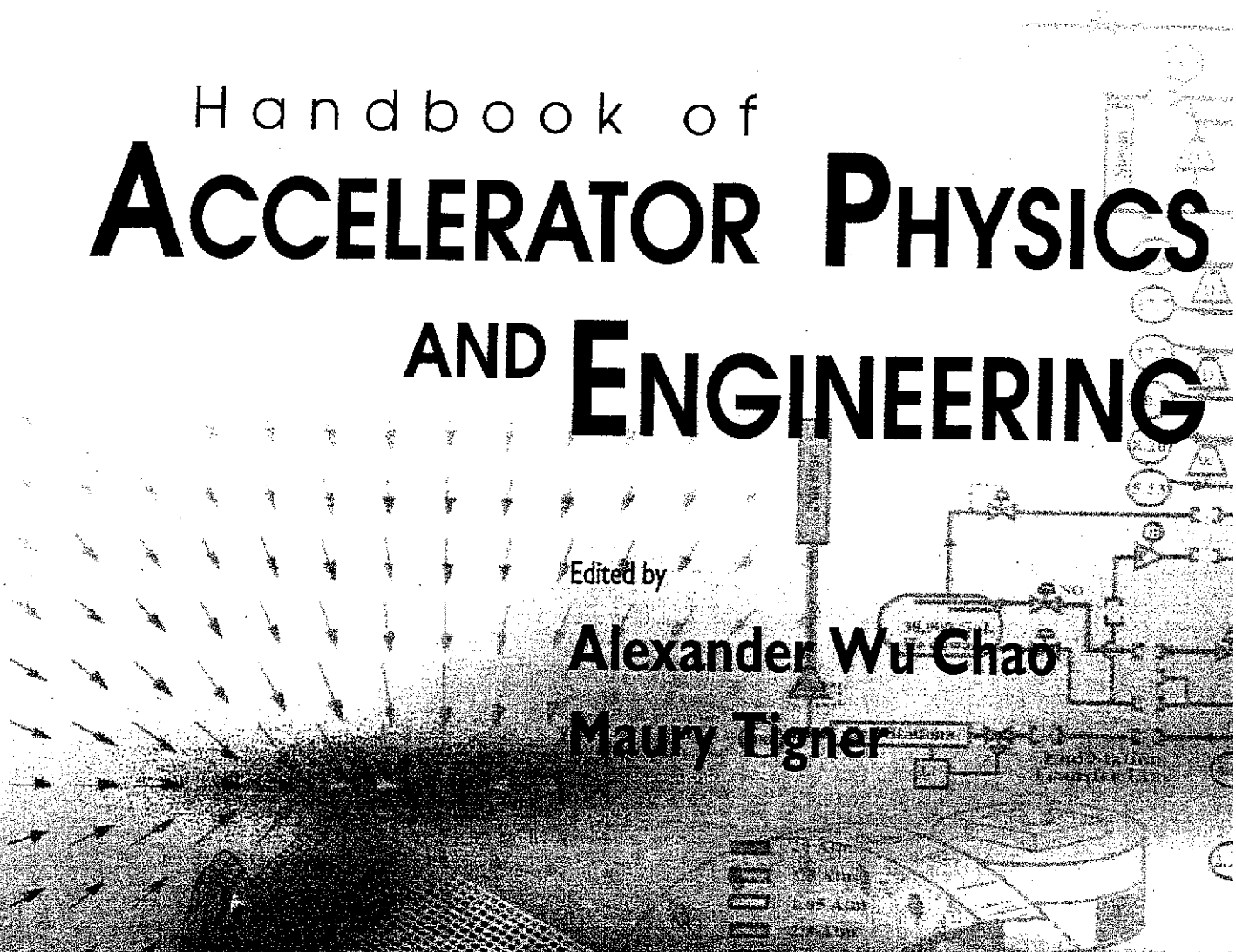

Edited by

Alexander Wu Chao
Maury Tigner

World Scientific

6.4 PERMANENT MAGNET MATERIALS

R.D. Schlueter, LBNL

(See also Sec.7.2.5.)

PMs generally used in accelerator magnets are the rare earths, NdFeB and $SmCo_5$, Sm_2Co_{17} or ferrites, Fe_2O_3. The magnetic properties of these materials are described by

$$B_\parallel = B_r + \mu_0\mu_\parallel H_\parallel \ (B_\parallel > 0), \quad B_\perp = \mu_0\mu_\perp H_\perp \tag{1}$$

where $\parallel$ and $\perp$ refer to the "easy" axis direction, μ_0 is the permeability of free space and $\mu_\parallel, \mu_\perp$ are the dimensionless relative permeabilities (see Fig.1). Typically $(\mu_{\parallel,\perp} - 1) < 0.1$. Uniformly magnetized PM material thus can be represented as a passive material with permeability, $\mu_{\parallel,\perp}$ plus either active currents or charges on PM surfaces parallel or perpendicular to B_r, respectively. Magnetics effects of PM blocks are superposable to the extent that any iron in the system does not saturate. Eq.(1) describing PM material behavior are valid in the second quadrant of the B-H curve; linearity extends near to or somewhat into the third quadrant, where there is a "knee" in the curve. Operation beyond this knee irreversibly changes material properties and is to be avoided.

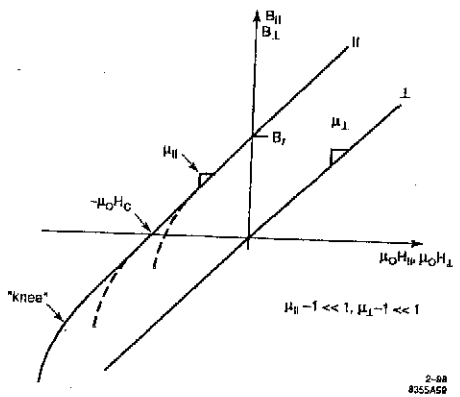

Figure 1: Permanent magnetic material B-H behavior parallel and perpendicular to the magnetization direction.

NdFeB and $SmCo_5$ or Sm_2Co_{17} magnets are employed to achieve high fields in compact magnets. NdFeB PM blocks have the highest available strength, typically B_r = 1.1 - 1.4 T and coercivity $\mu_0 H_c$ = 1.0 - 1.3 T. NdFeB is readily machinable, but its temperature stability and radiation resistance [1, 2, 3], though often acceptable, are inferior to those of the samarium cobalt magnets. NdFeB magnets have experienced significant strength loss after exposure to neutron fluences of as low as 10^{14} n/cm^2. (See also 3.3.8) PM materials exhibiting higher remnant fields, B_r, usually experience irreversible flux loss at lower temperatures and the knee occurs earlier in the third quadrant; thus one needs to be aware of the potential for demagnetization both in the final design configuration and during magnet assembly [4]. Typical costs are \$5/cm^3 or \$150 per 2 cm × 4 cm × 4 cm block used in a PPM or hybrid multipole or insertion device. Typical easy axis (i.e. magnetization vector) orientation error and block-to-block magnetization uniformity are 1° and 1% B_r, respectively. Tab.1 displays typical NdFeB properties. Major NdFeB suppliers include Sumitomo Special Metals Co., Shin-Etsu, Vacuumschmelze and Ugimag.

Table 1 Typical properties of PM materials

Property	NdFeB	SmCo	Fe_2O_3
B_r [T]	1.1 - 1.4	0.9 - 1.2	0.2 - 0.44
$\mu_r H_c$ [T]	1.0 - 1.3	0.7 - 1.1	0.16 - 0.35
$\mu_\perp$, $\mu_\parallel$	1.03 - 1.10	1.01 - 1.03	1.05 - 1.07
$\partial B_r/\partial T$ [%/deg.C]	- 0.10	- 0.04	- 0.2
$\partial H_c/\partial T$ [%/deg.C]	- 0.40	- 0.2	+ 0.35
T_{oper}^{max} [deg. C]	60 - 180	>200	250
T_{curie} [deg. C]	350	800	450
c_p [J/kg deg.C]	450	350	715-835
K [W/m·K]	6.4	10 - 23	4.5
$\alpha_{T,\perp}$* [10^{-6}/ deg.C]	- 0.4	11 - 13	10
$\alpha_{T,\parallel}$* [10^{-6}/ deg.C]	7	8 - 9	14
ρ [g/cm^3]	7.5	8.4	4.8
ρ_r [$10^{-6}\Omega$·cm]	200	84	>10^{14}

* directional thermal expansion coefficients

For $SmCo_5$ or Sm_2Co_{17} one has B_r = 0.9-1.1 T, $\mu_0 H_c$ = 0.8-1.0 T. It is more brittle than NdFeB, but exhibits better temperature stability and radiation resistance [5, 6]. It is thus used in more rugged thermal and radiation environments but attainable field strength is somewhat lower than for the NdFeB magnets. Typical cost is \$5/cm^3. Tab.1 displays typical properties of this material. Major suppliers include Shin-Etsu, Vacuumschmelze and Ugimag.

Ferrites are much cheaper (\$0.02/cm^3). Their remnant field and coercivity are 0.20 - 0.44 T and 0.16 - 0.35 T respectively and thus are not used for compact, high field applications. However, their low cost makes them especially suited for lower field applications. Larger, high field hybrid devices using ferrites are also feasible. Such magnets comprise the dipoles, quadrupoles and combined function hybrid magnets in Fermilab's 8 GeV transfer line and recycler ring [7, 8]. These materials exhibit no magnetic degradation up to 250°C, enabling bakcouts without insulating the permanent magnet material. A disadvantage is their high temperature coefficient, - 0.20%/°C, sometimes necessitating some form of temperature compensation or control. Major suppliers include Crucible Magnetics, Hitachi and Arnold.

References

[1] J. Pfluger, G. Heintze, RSI 66-2 (1995) 1946.
[2] O-P. Kahkonen et al, PRB 49-9 (1994) 6052
[3] J.R. Cost et al, IEEE Trans. Magnetics 24-3 (1988) 216
[4] K. Robinson et al, NIM A250 (1986) 100
[5] A.F. Zeller, J.A. Nolen, 9th In. Wkshp. Rare-Earth Mag. WP32 (1987) 157
[6] H.B. Luna et al, NIM A285 (1989) 349
[7] H.D. Glass et al, PAC 97
[8] W.B. Fowler, B. Brown, J.T. Volk, PAC 97

6.5 PROPERTIES OF LOSSY MATERIALS

M. Tigner, Cornell U.

General Several UHV compatible materials are now available for absorption of microwave energy. They range from resistive pastes that can be fired onto a ceramic substrate through ferrites to "artificial" dielectrics in which micron sized dissipative materials are dispersed within a ceramic matrix serving to concentrate the fields at the dissipating particles. Several types of UHV compatible microwave loads, on-beam-line and off line, have been devised, some capable of kilowatts dissipation. The material for on-beam-line loads must have a finite dc resistivity for charge drainage.

Physical properties Tab.1 displays physical properties of typical ferrites and artificial dielectrics.

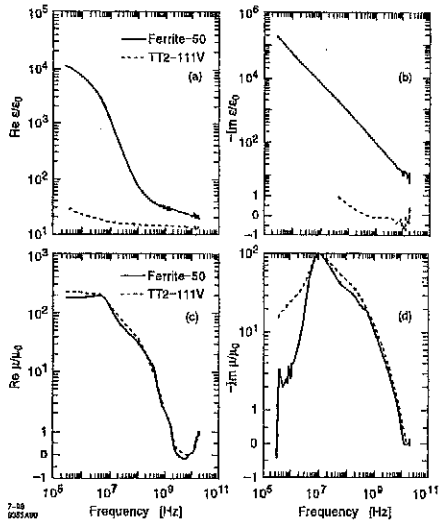

Figure 1: (a) Reϵ_r vs freq., ferrites. (b) Imϵ_r vs freq., ferrites. (c) Reμ_r vs freq., ferrites. (d) Imμ_r vs freq., ferrites.

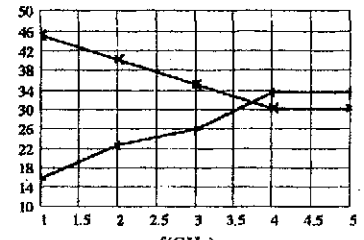

Figure 2: ϵ_r (×) and 100tanδ (+) for AlN-40%SiC.

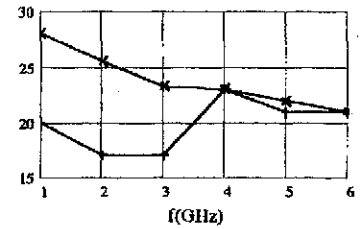

Figure 3: ϵ_r (×) and 100 tanδ (+)for AlN-7%C.

Electrical properties Figs.1 [4], 2 [5] and 3 [6] display the electrical properties of these materials as a function of frequency. The ferrites show ab-

24-d,
10-b

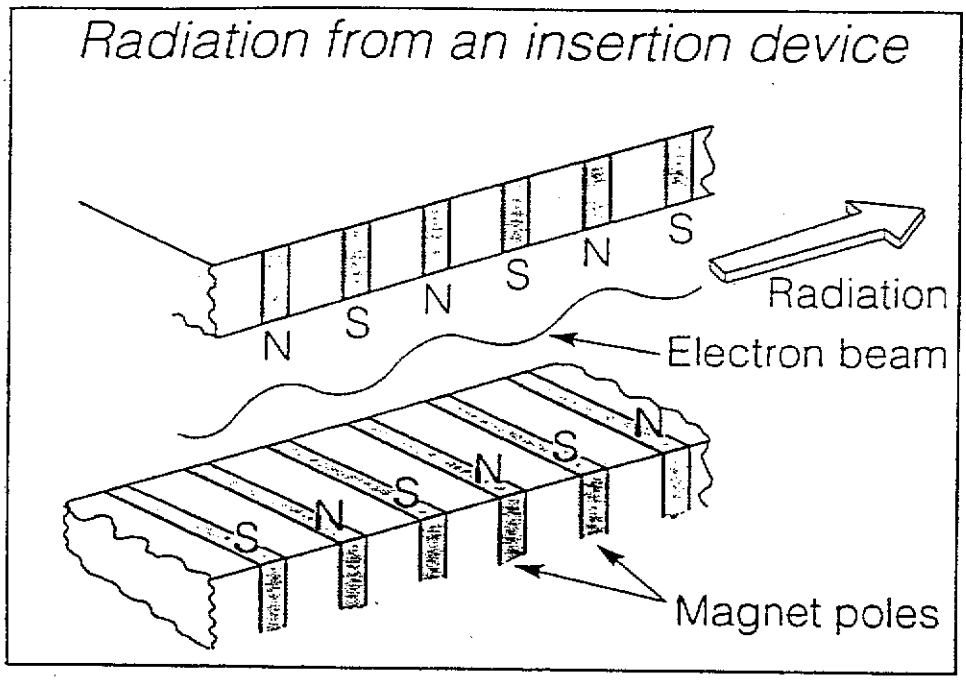

AN INSERTION DEVICE has permanent magnets of alternating polarity that cause electrons moving at nearly the speed of light to follow a sinusoidal path perpendicular to the magnetic field.

HYBRID UNDULATOR DESIGN: (Hybrid ≡ Iron + PM)

GENERAL PROCEDURE:

STEP 1 DESIGN SURFACES TO WHICH $\vec{B}$ IS $\perp$ TO GET DESIRED FIELD DISTRIBUTION

STEP 2 DETERMINE POLE SCALAR POTENTIAL NECESSARY TO GET DESIRED FIELD STRENGTH

STEP 3 DESIGN REST OF IRON + PM TO PRODUCE THESE POTENTIALS

A 2-D Hybrid Undulator Design:

STEP 1

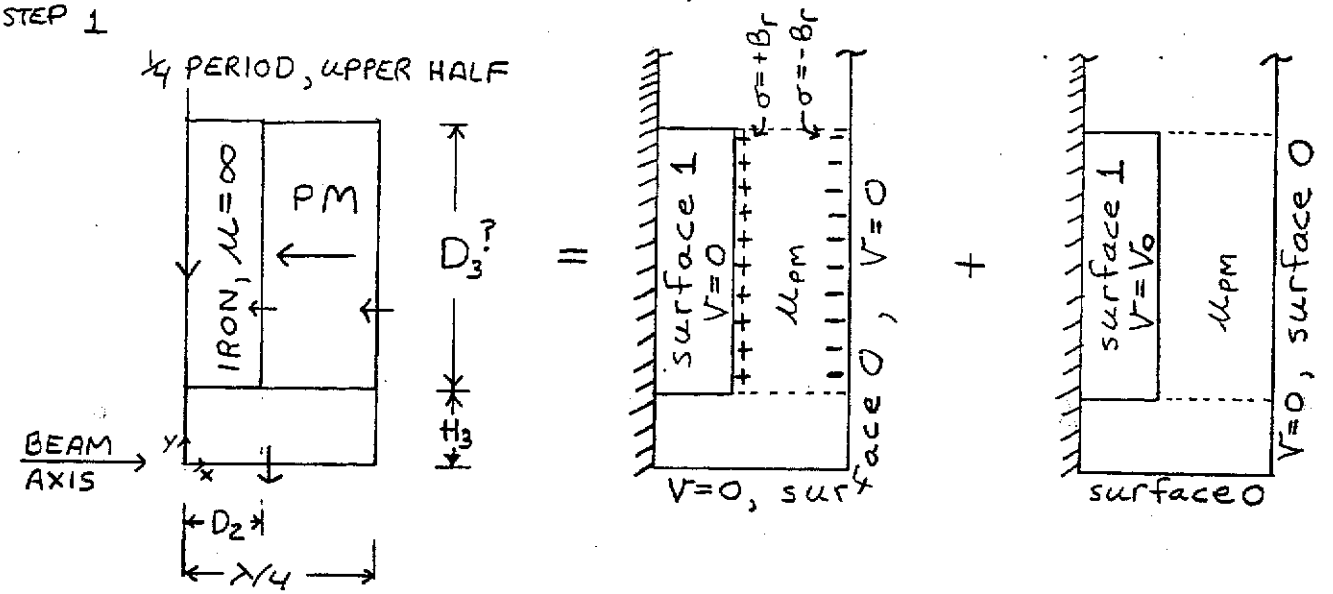

(c) = (a) DIRECT FIELDS + (b) INDIRECT FIELDS

STEP 2

For a peak on-axis field B_0, $B^*(z) \simeq B_0 \cos kz$; $k = \frac{2\pi}{\lambda}$

$$\Rightarrow \tilde{V}_0 \simeq \int_0^{H_3} B_0 \cos ky\, dy = \frac{B_0}{k} \sinh kH_3$$

STEP 3 (a) DIRECT FLUX

for the + charges, $V_i(\vec{r}_{Q^+}) = V_0 \therefore C_1(Q^+) = 1$

for the − charges, $V_i(\vec{r}_{Q^-}) = 0 \therefore C_1(Q^-) = 0$

$$\Rightarrow \phi_d' = \sum Q' C_1 = \sum \sigma D_3 C_1 = B_r D_3$$

where ′ denotes per unit length in 3RD dimension

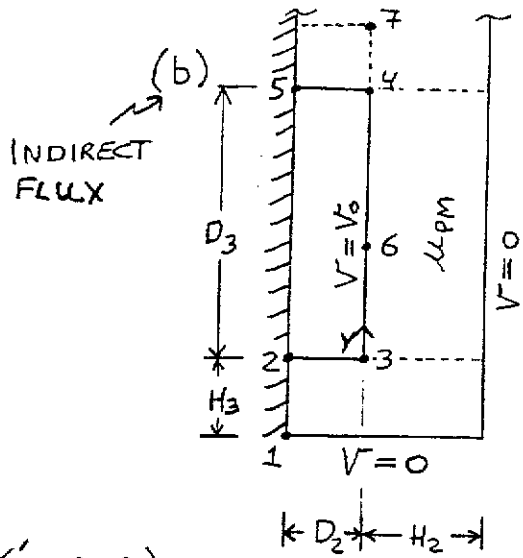

(recall $\phi'_{1-2} = A_2 - A_1$) see pg. 4

We could get ϕ_i' by guessing a D_3, then running a 2-D magnetostatics code to solve boundary value problem, then iterating with different D_3 until $-\phi_i'$, which is $= A_5 - A_2$, becomes equal to ϕ_d' $(= B_r D_3)$ from step 3 (a), above.

Better way is to use capacitance concept (C_2)

- no need for repetitive computer runs
- can do design analytically
- get better understanding of design parameter space
- easy analytical extension to 3-D

Introduce excess flux concept: B ≡ BOTTOM, T ≡ TOP } OF POLE

coordinate system: $(x,y) = (0,0)$ @ POINT 3

$A_1 \equiv 0$ (reference), $\Rightarrow A_2 = 0$ + for y far enough from corners 3+4: $-\frac{\partial \phi_i}{\partial y} = \frac{\partial A(0,y)}{\partial y} = \text{constant} = \frac{\mu_{PM} \tilde{V}_0}{H_2}$

$$\Rightarrow \quad A_6 - A_2 = \tilde{V}_0 \left(E_B + \frac{\mu_{PM} \cdot y_6}{H_2} \right)$$

$$A_5 - A_6 = \tilde{V}_0 \left(E_T + \frac{\mu_{PM} [D_3 - y_6]}{H_2} \right)$$

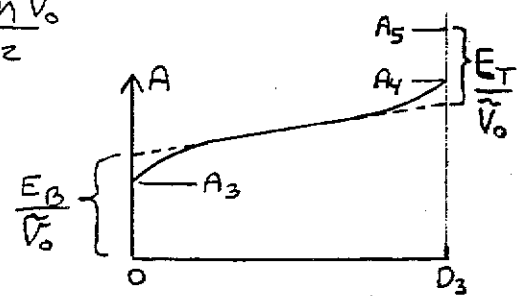

where E_B, E_T are dimensionless coefficients quantifying the excess flux, beyond the uniform portion, due to $\frac{T}{B}$ edges

$$\therefore -\phi_i' = A_5 - A_2 = \tilde{V}_0 \left(E_B + E_T + \frac{\mu_{PM} D_3}{H_2} \right) \equiv \tilde{V}_0 C_2$$

Since $\phi_d' = -\phi_i'$, required $D_3 = \dfrac{\frac{B_0}{B_r} \frac{\sinh k H_2}{k} (E_B + E_T)}{1 - \frac{B_0}{B_r} \frac{\sinh k H_3}{k H_2} \cdot \mu_{PM}}$

12a, 12b, 24-e

Equi-vector potentials

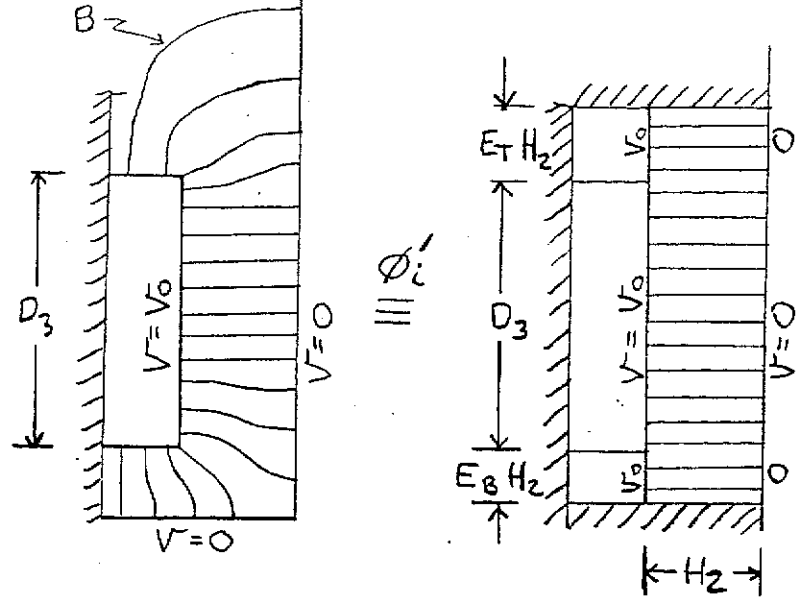

(1) GRAPHICAL REPRESENTATION OF E_T, E_B

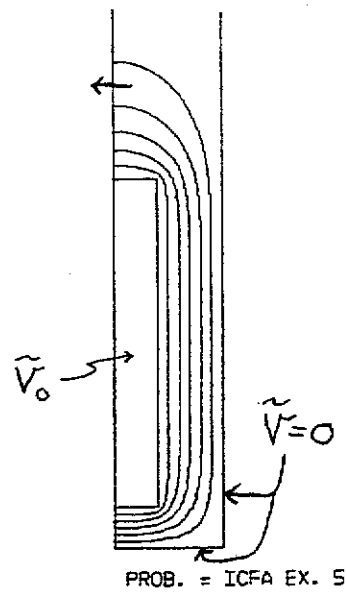

(2) Equi-scalar potentials, as per (b) pg. 11

- $\tilde{V}_o(B_o)$ can be determined exactly from a single POISSON run
- E_B and E_T and thus C_2 can be obtained in closed form or from a single POISSON run ($\neq f(D_3)$)
- Denominator determines lower bound for H_2 (or equivalently, upper bound for D_2), given B_o, λ, H_3

EXTENSION: PM OVERHANG ABOVE TOP OF POLE INCREASES ϕ_d'

$$\phi_d' = \underbrace{\int_0^{D_3} \frac{\tilde{V}_i(y)}{\tilde{V}_o} B_r \, dy}_{\equiv B_r D_3} + \int_{D_3}^{D_3+O_3} \frac{\tilde{V}_i(y)}{\tilde{V}_o} B_r \, dy$$

$$\phi_d' = -\phi_i' \Rightarrow D_3 = \frac{\frac{\tilde{V}_o}{B_r}(E_B+E_T) - \int_{D_3}^{D_3+O_3} \frac{\tilde{V}_i(y)}{\tilde{V}_o} dy}{1 - \frac{\tilde{V}_o \mu_{PM}}{B_r H_2}}$$

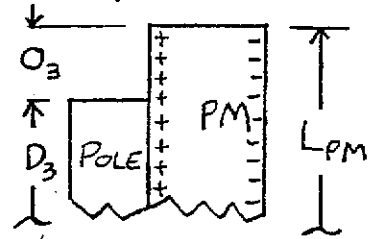

How much overhang is desirable? If $O_3 \uparrow$, then $\phi_d' \uparrow$, right? YES, but this doesn't optimize design, wastes $. Imagine pole height D_3 and PM height L_{PM} are initially the same. Then, with L_{PM} fixed, say we increase pole height by δ_{D_3}: ϕ_d' and therefore ϕ_i' remain unchanged; but since $C_2 \uparrow$, then $V_o \downarrow$. If pole height were decreased by δ_{D_3}: $|\phi_d'|$ + thus $|\phi_i'|$ decrease; but so does C_2. For small δ_{D_3}, C_2 decreases more quickly + thus $V_o \uparrow$; for larger δ_{D_3}, ϕ_i' decreases more quickly + thus $V_o \downarrow$.

Given V_o + H_2: $L_{PM} = D_3 + O_3$, $\frac{\partial L_{PM}}{\partial O_3} = 1 - \frac{\tilde{V}_i(O_3)/\tilde{V}_o}{1 - \frac{\tilde{V}_o \mu_{PM}}{B_r H_2}}$

L_{PM} minimized @ $\frac{\tilde{V}_i(O_3)}{\tilde{V}_o} = 1 - \frac{\tilde{H}_{PM}}{\tilde{H}_c} \Big/ \approx 1 - .8 = .2$ typically

overhanging PM on top reduces amount of PM required.

STEP 1

HYBRID CONFIGURATION GEOMETRY

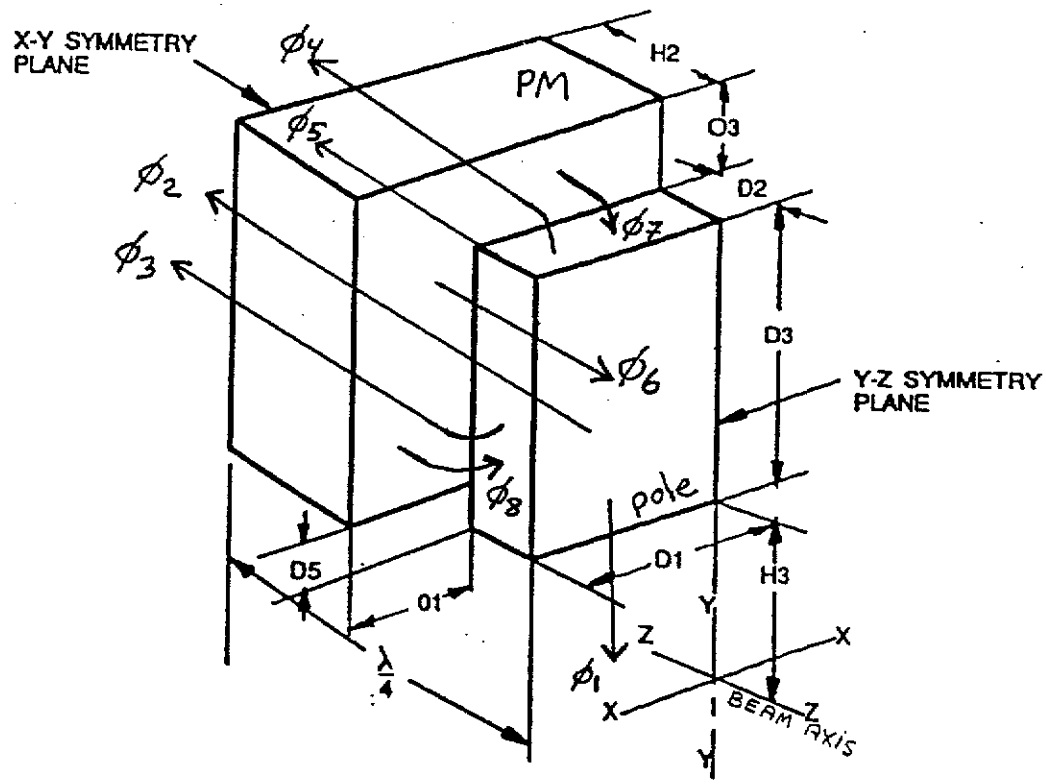

switched coord. system:
$X \to Z$,
3^{RD} DIM $\to X$

STEP 2 $\tilde{V}_0 \approx \frac{B_0}{K} \sinh K H_3$ or exact $\tilde{V}_0(B_0)$ from POISSON

STEP 3

(a) DIRECT FLUX $\phi_d = \phi_6 + \phi_7 + \phi_8$

$\phi_6 = B_r D_1 (D_3 - D_5)$ ↑ from PM overhang on side

$\phi_7 = B_r D_1 H_2 E_{0y}$ ↑ from PM overhang on top; from PM-pole direct contact area

$\phi_8 = B_r (D_3 - D_5) H_2 E_{0x}$ ↑

where E_{0x}, E_{0y} are dimensionless coefficients, $E_0 B_r H_2$ being the 2D flux from the overhang

(b) INDIRECT FLUX $-\phi_i = \phi_1 + \phi_2 + \phi_3 + \phi_4 + \phi_5 = \tilde{V}_0 C_2$

associated with: bottom pole surface facing PM ↑ ϕ_1; side ↑ ϕ_2; top ↑ ϕ_3; corner edges ↑ ϕ_4, ϕ_5

$\begin{Bmatrix} \phi_1 \\ \phi_4 \end{Bmatrix} = \tilde{V}_0 D_1 \begin{Bmatrix} E_B \\ E_T \end{Bmatrix}$ $\qquad \phi_3 = \tilde{V}_0 D_3 E_T$

$\phi_2 = \tilde{V}_0 D_1 D_3 \mu_{PM} / H_2$ $\qquad \phi_5 = \tilde{V}_0 D_2 E_C$

$$\phi_d = -\phi_i \Rightarrow D_3 = \frac{(\tilde{V}_0/B_r)[D_1(E_B+E_T) + D_2 E_C] + D_5(D_1 + H_2 E_{0x}) - D_1 H_2 E_{0y}}{D_1 + H_2 E_{0x} - (\tilde{V}_0/B_r)[\mu_{PM} D_1/H_2 + E_T]}$$

- Overhanging PM on side increases attainable B_o
- E's obtainable in closed form or from a single Poisson run ($\neq f(D_3)$)

excluding ① 3D effects of corners (negligible)
② pole saturation (can include also!)

We have a "nearly" exact 3D model for insertion device magnetics in closed form (or using a single 2-D Poisson run)

- Other design features can be incorporated into above design equation:
  1) PM attached to top &/or side of pole ⇒ incorporate into definitions of E_{oy}, E_{ox}
  2) Tapered (wedged) pole design ⇒ $H_z = f(y)$
  3) pole saturation! ⇒ Make a 2-D Poisson run with desired pole tip geometry, and finite μ_{IRON}, energized with PM plus additional EM coil at top of pole so as to give desired B_o. Since only bottom portion of pole is saturated, read vector potential $A(y_p)$ on pole surface at location $\underline{r} = (D_2, y_p)$. Then modify ϕ_1:

$$\phi_1 = D_1\left[A(y_p) - \frac{\tilde{V}_o \mu_{PM} y_p}{H_z} + B_r(y_p - D_5)\right]$$

Additional possible Hybrid design features:

1) PM on pole top or lateral side

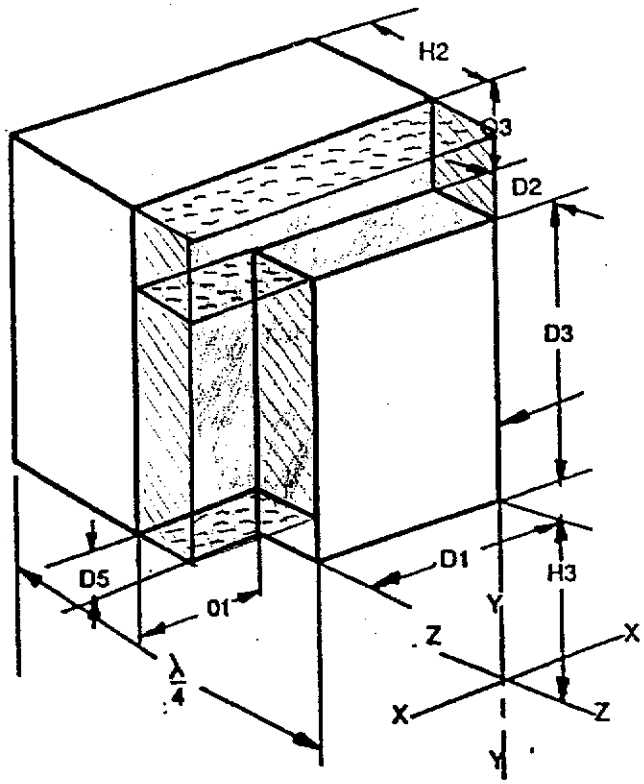

2) tapered pole design

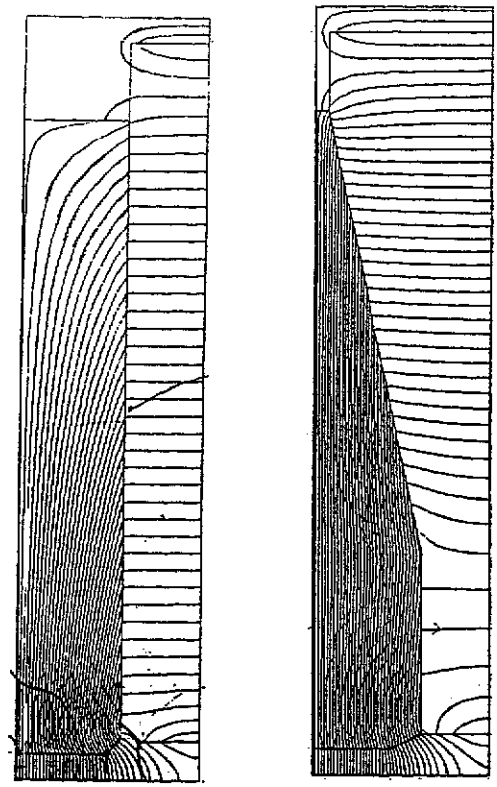

SIDE VIEWS

3) pole saturation: (E_B including saturation effects)

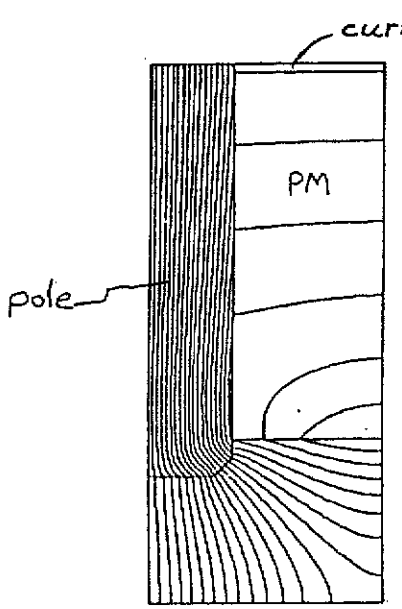

PURE CSEM CONFIGURATION PERFORMANCE

$$B^* = i \cdot 2 \cdot B_r \sum_{\mu=0} \cos(n\,k\,z) \cdot e^{-nkh} \cdot \frac{\sin(n\,\epsilon\,\pi/M')}{(n\pi/M')} \cdot (1 - e^{-nkL})$$

$n = 1 + \mu M'$

$k = 2\pi/\lambda$

$z = x + iy$

Example:

for: $L = \lambda/2$

$M' = 4$

$B_r = 0.9$ Teslas (REC)

$$B^*_{\mu=0}(\text{Teslas}) = i\left[1.55e^{-kh} \cdot \cos(kz) - .36e^{-5kh} \cos 3kz\right]$$

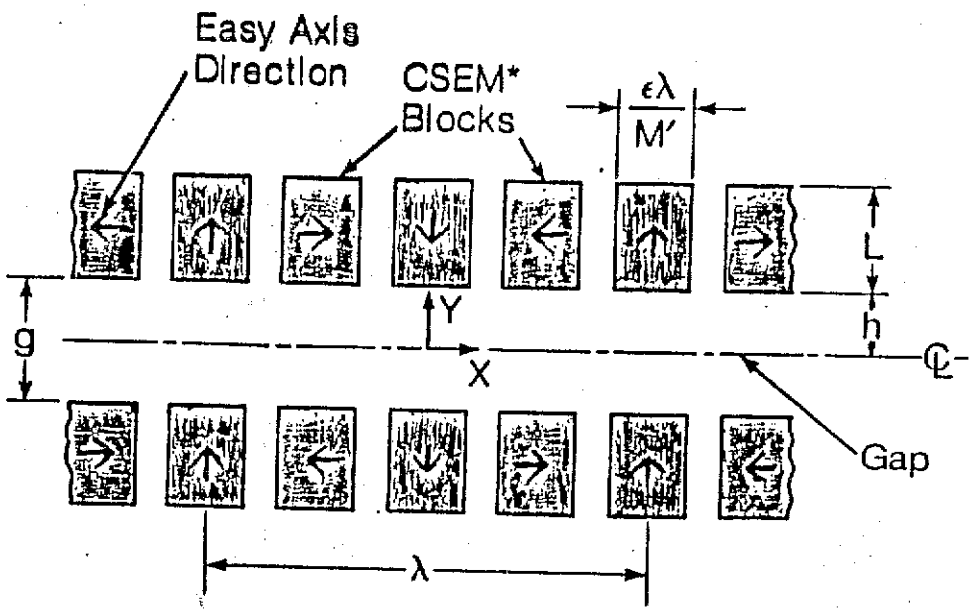

PURE CSEM* W / U CROSS SECTION

*Current Sheet Equivalent Material - e.g. REC

① PAIRS OF KICKS : NET BEAM ANGLE θ & DISPLACEMENT δ

a) for KICKS OF MAGNITUDE ^{+}K & ^{+}K @ $\pm z_0$:

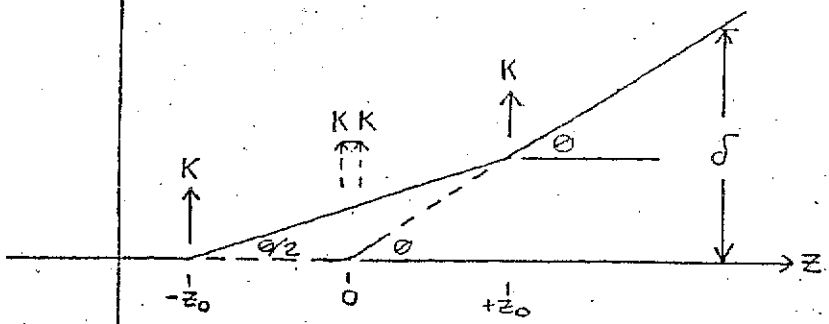

$\theta(\infty) = 2^{+}K$

$\delta(\infty) = 2Kz$

$\delta(\infty)$ DEPENDS ON ΣK & CENTROID, BUT NOT ON DENSITY DISTRIBUTION

b) for KICKS OF MAGNITUDE $^{+}K + {}^{-}K$ @ $\mp z_0$:

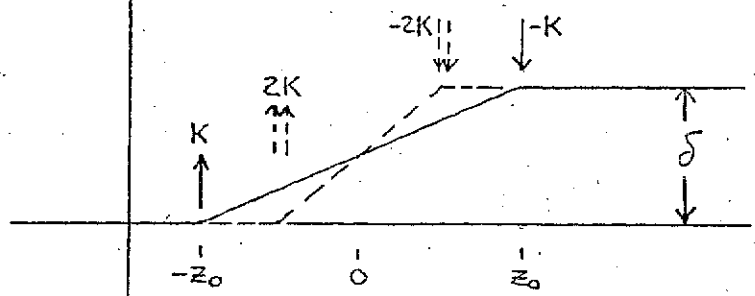

$\theta(\infty) = 0$

$\delta(\infty) = 2z_0 \cdot K$

② PM BLOCKS EQUIVALENT TO CHARGESHEETS ⇒ PAIR OF KICKS ON BEAM

a) FOR $\vec{B}_r$ COMPONENT PARALLEL TO z-AXIS

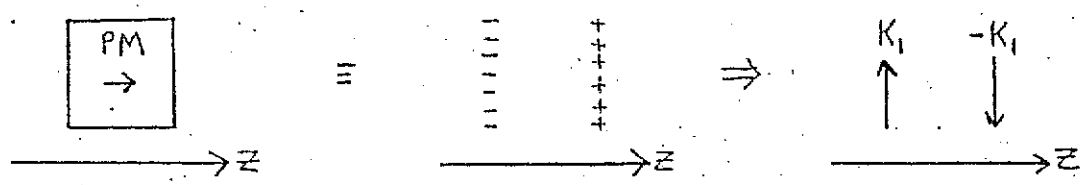

b) FOR $\vec{B}_r$ COMPONENT PERPENDICULAR TO z-AXIS

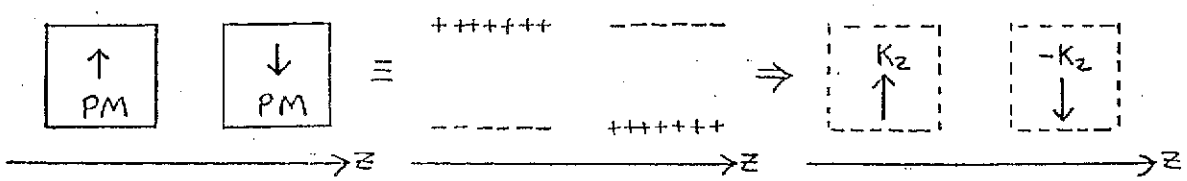

STEERING-FREE, DISPLACEMENT-FREE, GAP-INDEPENDENT

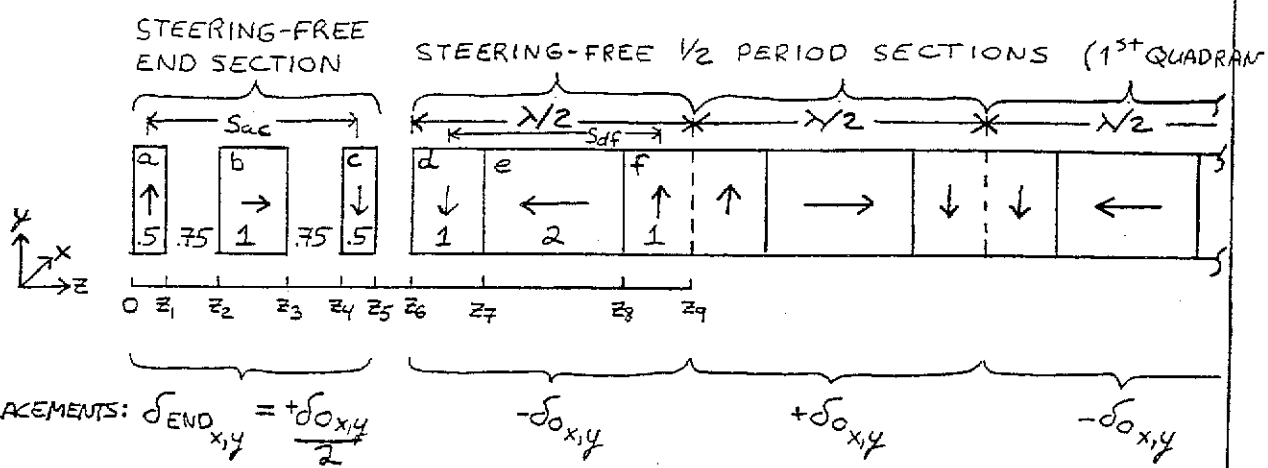

DISPLACEMENTS: $\delta_{END}{}_{x,y} = +\frac{\delta_{0x,y}}{2}$ $\quad -\delta_{0x,y}$ $\quad +\delta_{0x,y}$ $\quad -\delta_{0x,y}$

- ALL BLOCKS HAVE SAME x, y DIMENSIONS & POSITIONING
- PERIODIC $\lambda/2$ SECTIONS, AS SHOWN, ARE INHERENTLY STEERING-FREE IN BOTH x & y WITH DISPLACEMENTS $\pm\delta_{0x,y}$.
- END SECTION, WITH $\vec{B}_r$'s AS SHOWN, IS INHERENTLY STEERING-FREE IF THE "↑" BLOCK + "↓" BLOCK HAVE SAME z- DIMENSION, i.e. $L_a = L_c$
- TO MAKE $\delta_{END} = \delta_0/2$ AT <u>ALL</u> GAPS, REQUIRE KICKS FROM B_R COMPONENTS PARALLEL TO z-AXIS IN END BLOCKS TO PRODUCE 1/2 THE DISPLACEMENT OF THOSE IN THE HALF-PERIOD SECTION, AND LIKEWISE FOR B_R COMPONENTS PERPENDICULAR TO THE z-AXIS.

FOR ALS EPU, WITH ALL BLOCK B_r'S IN A DIRECTION OF ONE OF THE CARTESIAN COORDINATES, THIS REQUIREMENT RESULTS IN

$$\begin{cases} K_b L_b = -\frac{1}{2} K_e L_e \Rightarrow \underline{L_b = \frac{1}{2} L_e} \\ 2 S_{ac} K_a = -\frac{1}{2} 2 S_{df} K_d \Rightarrow \underline{2 S_{ac} L_a = S_{df} L_d} \end{cases} ; \; K_a = -K_c, \; K_d = -K_f, \; L_a = L_c, \; L_d = L_f$$

WHERE: $K \equiv$ KICK, $L \equiv$ LENGTH, $S \equiv$ SEPARATION BETWEEN BLOCK CENTERS, subscripts refer to PM blocks.

- WHEN GAP CHANGES, KICKS CHANGE, BUT RATIOS ARE UNCHANGED. E-BEAM TRAJECTORY THROUGH ID OSCILLATES ABOUT THE FIXED NOMINAL ON-AXIS AT ALL GAPS. OSCILLATION MAGNITUDE IS GAP DEPENDENT.
- TRAJECTORY:

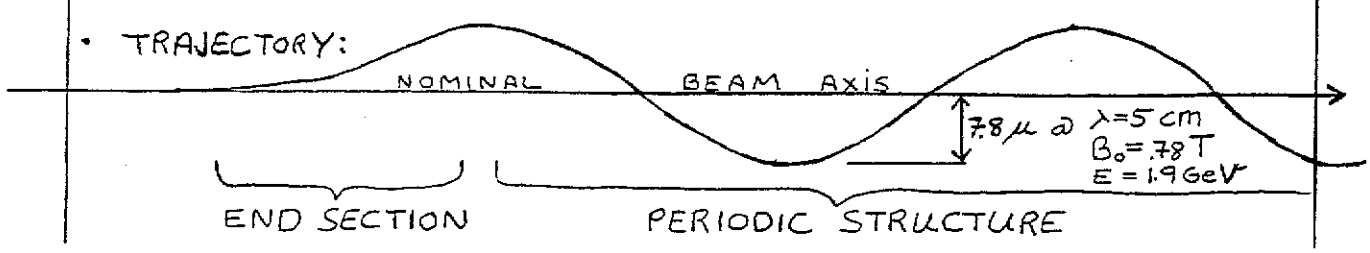

- NOTES

(1) BLOCK "b" CAN BE POSITIONED ANYWHERE IN END SECTION, BUT FOR BEST SPACE UTILIZATION IS PUT BETWEEN "a" + "c", WHICH CAN BE SHORTER WHEN THEIR SEPARATION "S_{ac}" IS LARGER.

(2) SPACE BETWEEN BLOCKS "c" & "d", i.e. BETWEEN THE END SECTION AND THE FIRST HALF-PERIOD SECTION CAN BE ANYTHING, INCLUDING ZERO.

(3) THE END DESIGN ABOVE FEATURES BLOCKS WITH LENGTHS THAT ARE ONE-HALF OF THOSE IN THE PERIODIC SECTION, AND OCCUPIES 3.5 $\lambda/8$ SPACE IN AXIAL DIRECTION.

A SLIGHTLY MORE COMPACT ALTERNATIVE IS TO HAVE NO SPACE BETWEEN BLOCKS "a", "b", + "c". THEN

$$S_{ac} = (L_b + L_a) \Rightarrow \frac{L_a}{L_d}\left(1 + \frac{L_a}{L_d}\right) = \frac{3}{2} \Rightarrow L_a = 0.8229\ \lambda/8$$

ALTERNATE DESIGN FOR END SECTION

a	b	c
↑	→	↓
.823	1	.823

THIS OPTION OCCUPIES 2.65 $\lambda/8$ SPACE IN AXIAL DIRECTION, SAVING ~ 0.5 CM PER END IN A DEVICE OF $\lambda = 5.0$ CM

EPU5.0 END MAGNETIC DESIGN

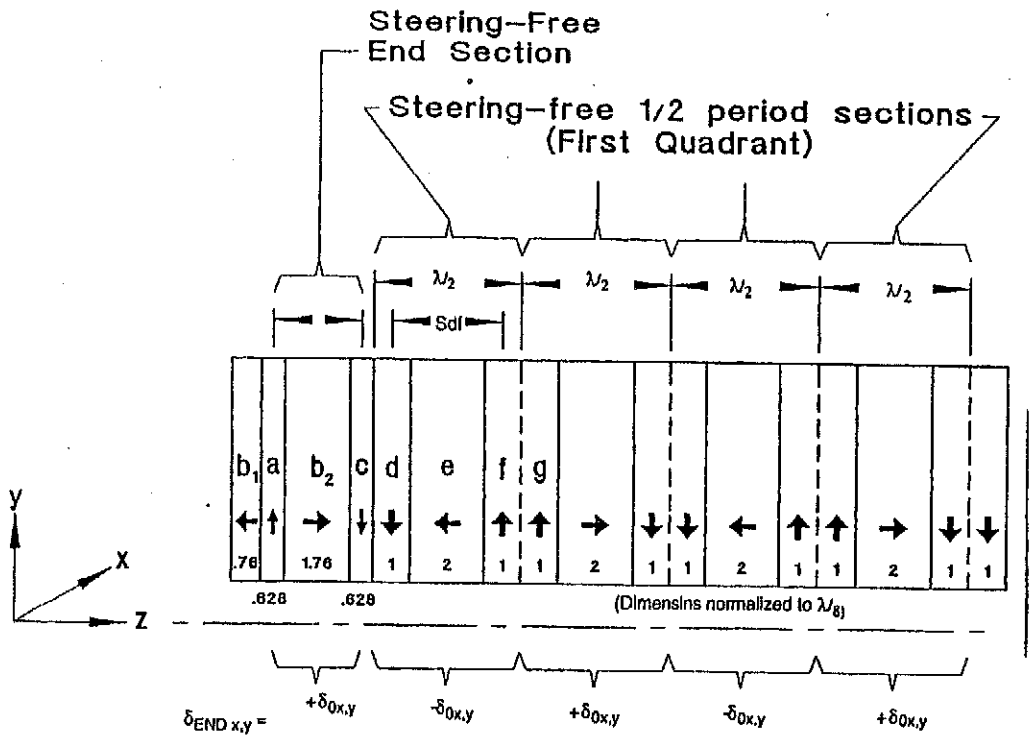

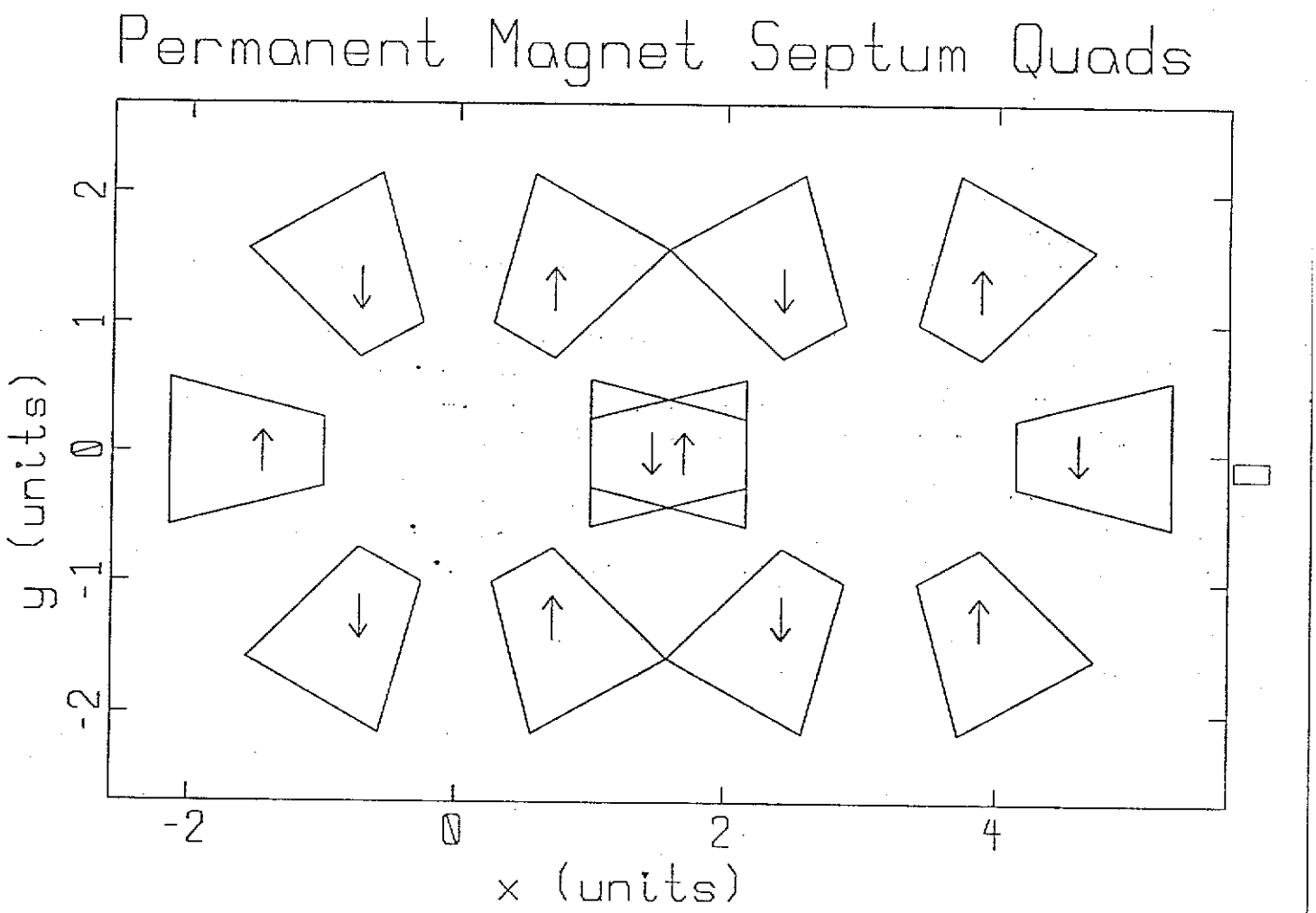
Permanent Magnet Septum Quads
y (units)
x (units)
2
1
0
-1
-2
-2
0
2
4

Pure Permanent Magnet Harmonics Corrector Ring

R.D. Schlueter, D. Humphries, and J. Tanabe
Lawrence Berkeley Laboratory, Berkeley, California 94720

Abstract—A concept for creating any desired harmonics mix in a pure permanent magnet (PM) corrector ring is presented. Useful for nulling various harmonics simultaneously, such a device is versatile for many accelerator applications. The harmonic mix can be changed without redesign or replacement by a new ring or parts and, if desired, can be accomplished in-situ via remote control of rotor motors. Harmonics suppression of greater than a factor of 100 or even 1000 are possible; exact functional dependencies of harmonics suppresion capability versus magnet geometry are given. Sensitivity to positioning and corrector ring PM errors are given, and shown to be themselves nullable.

I. Introduction

Presently, much effort is put into designing magnets with tight harmonics specifications. In the case of electromagnets this entails laborious attention to iron/coil design geometry and often tedious and costly experimentation of end chamfers and designs. In the case of permanent magnets, block quality, sorting, and, positioning must be carefully controlled. Furthermore, in both instances these factors limit the attainable level of field quality achievable.

The theory of pure PM design in two dimensions has been described thoroughly [1,2]. Here we present a concept utilizing a PM corrector ring, insertable at any desired location in the beam path, capable of providing any desired harmonic mix. The present application is to null the harmonics of the Q2 septum quadrupole for SLAC's B-factory. Herein, the PM material with $\mu = 1$ is represented by magnetic charge sheets on surfaces [3,4].

II. Field from Homogeneously Magnetized PM Cylinders

In 2-D, the field at location $z = x + iy$ due to a cylinder of permanent magnet material of radius r_c centered at

First Draft: Nov. 26, 1995. Second draft: March 22, 1996.
This work was supported by the Director, Office of Energy Research, Office of Basic Energy Sciences, Mat. Sci. Div., of the U.S. Dept. of Energy, Contract No. DEAC03-76SF00098.

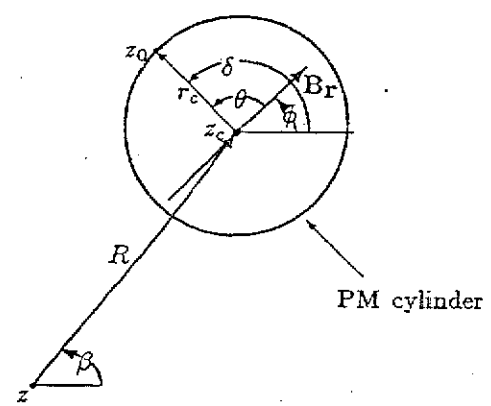

Fig. 1. 2-D geometry for a arbitrarily positioned and oriented PM cylinder (beam axis is into paper, ϕ is magnetization direction w.r.t. horizontal, δ is the integration angle w.r.t. horizontal, and $\theta \equiv \delta - \phi$)

$z_c = z + Re^{i\beta}$ with uniform magnetization $\mathbf{B_r} = B_r e^{i\phi}$ is given by [5] (See Figure 1):

$$B^*(z) = \frac{B_r}{2\pi}\int_0^{2\pi} \frac{r_c \cos\theta}{z - z_0(\delta)} d\delta = \frac{B_r e^{i\phi}}{2}\left(\frac{r_c}{z_c - z}\right)^2, \quad (1)$$

where $B_r \cos\theta(\delta)$ is the equivalent magnetic charge density at the point on the cylinder surface $z_0(\delta) = z_c + r_c e^{i\delta}$, $0 \le \delta < 2\pi$. The derivation is given in the appendix.

The integrated field, $I^*(z) = \int_{-\infty}^{\infty} B^*(z) dZ$, along an axis ($Z$) parallel to that of a lone cylinder of length L is

$$I^*(z) \equiv \sum_{n=1}^{\infty} b_n z^{n-1} = \frac{B_r L r_c^2}{2} \sum_{n=1}^{\infty} \frac{n z^{n-1}}{z_c^{n+1}} e^{i\phi}, \quad (2)$$

where the infinite series on the right is the multipole expansion of Eq. (1) about $z = 0$.

Using two independently rotatable cylinders each of length $L/2$ placed end-to-end, arbitrary net magnetization orientation and strength are achievable by rotation and counter-rotation, respectively, of cylinders in a pair. The effective magnetization orientation of the cylinder pair is adjustable by rotating both cylinders an angle ϕ.

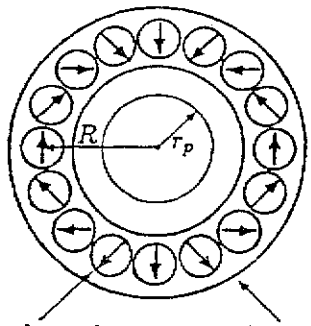

Fig. 2. Pure PM harmonics corrector ring (beam axis at $z = 0$ is into paper at center of ring)

The effective strength $\epsilon B_r L$ of the cylinder pair is adjustable by subsequently counter-rotating cylinders an incremental angle $\pm\eta$:

$$\epsilon B_r L = \cos\eta B_r L \tag{3}$$

For M cylinder pairs spaced uniformly in azimuth (see Fig. 2) $\beta_m = m2\pi/M$, $0 \le m \le M-1$, with net magnetization directions ϕ_m and strengths ϵ_m, the multipole expansion coefficients about $z = 0$ of the integrated field become

$$b_n = k_n \sum_{m=0}^{M-1} e^{-i(n+1)\beta_m} p_m; \tag{4}$$

$$\text{where } k_n \equiv \frac{B_r L n r_c^2}{2R^{n+1}}; \quad p_m \equiv \epsilon_m e^{i\phi_m}.$$

Equivalently, in matrix form:

$$\mathbf{b} = [K][T]\mathbf{p}, \tag{5}$$

where $[K]$ is a diagonal matrix consisting of the elements k_n, $[T]$ is a matrix with elements $T_{n,m} = e^{-i(n+1)\beta_m}$, and $\mathbf{p}$ is an M-element vector quantifying the net orientation and strength of each of the M cylinder pairs.

III. CREATING AN ARBITRARY MULTIPOLE MIX FOR FIELD CORRECTION

To produce a given $\mathbf{b}$, the required $\mathbf{p}$ is given by

$$\mathbf{p} = [T]^{-1}[K]^{-1}\mathbf{b}. \tag{6}$$

where the elements of $[T]^{-1}$ and $[K]^{-1}$ are

$$T^{-1}_{m,n} = e^{i(n+1)\beta_m}/M; \quad K^{-1}_{n,l} = \begin{cases} 1/k_n & \text{if } n = l \\ 0 & \text{otherwise} \end{cases} \tag{7}$$

Thus required orientation and strength of the m cylinder pairs are given by

$$p_m \equiv \epsilon_m e^{i\phi_m} = \sum_n e^{i(n+1)\beta_m} b_n/Mk_n. \tag{8}$$

Let error fields in a magnet be characterized by the multipole expansion a la POISSON Code[6] format:

$$I^*(z) = i \sum_{N=N_1}^{N=N_{max}} \frac{Nc_N}{r_p}\left(\frac{z}{r_p}\right)^{N-1}, \tag{9}$$

where the complex c_N [G-cm^2] $\equiv s_N e^{i\alpha_N}$. Setting $b_{n=N}$ of Eq. (8) equal to the negative of the N error coefficient $is_N e^{i\alpha_N}/r_p^N$ of Eq. (9), the N-pole error term of any accelerator magnet may be nulled in an adjacent coaxial harmonics corrector ring consisting of M cylinder pairs of effective length $\epsilon_N L$ and magnetization orientations defined by ϕ_{m_N}, given by

$$\epsilon_N L = \frac{Ns_N}{r_p}\frac{2}{MNB_r}\left(\frac{R}{r_c}\right)^2\left(\frac{R}{r_p}\right)^{N-1}, \text{ and} \tag{10}$$

$$\phi_{m_N} = (N+1)\beta_m + \alpha_N - \frac{\pi}{2} \equiv (N+1)\beta_m + \phi_{0_N}.$$

To null a single multipole term N_1, the effective length $\epsilon_{N_1} L$ of all M cylinder pairs in the corrector ring are identical. Nulling of an arbitrary number of multipole terms is accomplished by a vectorial superposition, per Eq. (8). Effective lengths $\epsilon_m L$ of the M cylinder pairs are then different, but none are larger than $L\sum_{N=N_1}^{N=N_{max}} \epsilon_N$:

$$L\epsilon_m e^{i\phi_m} = L \sum_{N=N_1}^{N=N_{max}} \epsilon_N e^{i\phi_{m_N}}. \tag{11}$$

where the "N" are the mulipole error terms to be nulled.

Nulling an N-pole term in the corrector ring will in turn introduce higher order multipole errors, per Eqs. (10) and (4):

$$I^*(z) = \frac{B_r \epsilon_N L M r_c^2}{2} \sum_{n=N+\nu M}^{\infty} \frac{ne^{i\phi_{0_N}} r_p^{n-1}}{R^{n+1}}\left(\frac{z}{r_p}\right)^{n-1} =$$

$$\frac{-iNc_N}{r_p} \sum_{n=N+\nu M}^{\infty} \frac{n}{N}\left(\frac{r_p}{R}\right)^{n-N}\left(\frac{z}{r_p}\right)^{n-1}, \tag{12}$$

where $\nu = 0, 1, 2, ..., \infty$. The first $N_1, .., N_{max}$ terms of Eq. (12) (i.e., with $\nu = 0$) are the negative of those that were to be nulled from Eq. (9). The corrector ring should consist of more cylinders than the highest harmonic component to be nulled, i.e., $N_{max} < M$, otherwise nulling the highest terms would introduce lower harmonics. Field contributions from the newly introduced error terms start with the $n = N + M$ term and are relatively small compared with the original N-pole error term (i.e., where $\nu = 0$) that was nulled. For each of the nulled error terms N, at $|z| = r_p$ the ratio f of newly introduced error terms to the corresponding nulled term is:

$$f = \sum_{\nu=1}^{\infty} \left(\frac{N+\nu M}{N}\right) \left(\frac{r_p}{R}\right)^{\nu M} . \quad (13)$$

The largest term is where $N = 1$, and occurs when $\nu = 1$ if $r_p/R < ([1+M]/[1+2M])^{1/M}$ ($\simeq .96$ for $M = 16$), yielding a reduction factor

$$f = (1+M)(r_p/R)^M . \quad (14)$$

IV. PRACTICAL DESIGN ISSUES

A. What level of harmonics reduction is possible?

The number and radial placement of cylinders necessary to achieve a desired level of harmonics reduction follows from Eq. (14).

For the Q2 magnet, assume original B field quality at the normalization radius $r_p = 4.5$ cm is good to 10^{-2} in all harmonics, and that we desire to make it 10^{-4}. For specified stay clear radii $r_1 = 5.0$ cm and $r_2 = 6.4$ cm, choosing for scenario (*i*) $M = 16$, $R = 5.7$ cm, and $r_c = 0.7$ cm, appropriately orienting cylinders would null the N=1 harmonic (as well as others) and would introduce a new $N = 17$ term that contributes a field equal to 39% of that of the original $N = 1$ term at r_p. For scenario (*ii*) let $M = 16$, $R = 5.9$ cm and $r_c = 0.5$ cm, yielding $f = 22\%$. Correction strength capability goes as $r_c^2 r_p^{N-1}/R^{N+1}$; thus the $N = 1$ term strength correction capability of scenario (*ii*) is only 48% of that of scenario (*i*) and marginally less for higher harmonics. Scenario (*ii*) yields a harmonics reduction factor of 5, still far short of the factor of 100 sought.

More effective in the radially restricted Q2 case is increasing the number of rotors. For scenario (*iii*) let $M = 32$, $R = 5.7$ cm, and $r_c = 0.7$ cm, resulting in $f = 1/58$. For scenario (*iv*) letting $M = 32$, $R = 5.9$ cm, and $r_c = 0.5$ cm, gives $f = 1/176$. For the latter design, which more than meets the harmonics reduction criteria, cylinder packing factor $2r_cM/2\pi R = 0.86$, leading to a 1.6 mm spacing between cylinders.

For some instances of quadrupole magnet correction, $N = 1$ and $N = 2$ terms need not be nulled, in which case minimum harmonic reduction is $\sim$ three times better than that of the above scenarios (See Eq. (13).) In cases that are not so radially restricted, much greater harmonics rejection factors are attainable via decreasing r_p/R (e.g., for $M = 16$ and $r_p/R = 0.5$, $f \simeq 1/4000$), though at the expense of harmonic strength nulling capability.

B. What magnitude of harmonic can be nulled?

The length of cylinder pairs to achieve a desired harmonic strength nulling capability follows from Eqs. (10) and (11). Assume a level of $q_N\%$ N^{th}-harmonic at r_p must be nulled, i.e., $Ns_N/r_p = 0.01 q_N N_f s_{N_f}/r_p$, where N_f is the fundamental harmonic and the N are the harmonics to be nulled. We have

$$\epsilon_N L = \frac{0.01 q_N N_f s_{N_f}}{r_p} \frac{2}{MNB_r} \left(\frac{R}{r_c}\right)^2 \left(\frac{R}{r_p}\right)^{N-1} . \quad (15)$$

For the Q2 magnet, $2s_2/r_p = 55800 r_p$ G-cm. Assume for instance that harmonics $N = 1, 3, \& 4$ with magnitudes $q_N = 1\%, 0.5\%$, and 0.25%, respectively at $r_p = 4.5$ cm, must be nulled and other harmonics are negligble. For the parameters of scenario (*iv*) and with $B_r = 10,000$ G, required lengths from Eq. (15) are: $\epsilon_{N=1} L = 2.19$ cm, $\epsilon_{N=3} L = 0.573 q_3 \epsilon_{N=1} L$, and $\epsilon_{N=4} L = 0.564 q_4 \epsilon_{N=1} L$. From Eq. (11), if the regular/skew mixes were such that all three ϕ_{m_N} were identical for some m, the required effective length of that longest cylinder pair would be 3.2 cm.

It is not feasible to use the harmonics corrector ring to null the high order allowed harmonics occuring in a PM device (e.g. the $N = 18$ harmonic of a 16-block PM Q2 quadrupole); these can be nulled or made negligible rather by spacing of the PM blocks [1] (an 11% space penalty), by employing finer block segmentation (e.g. 24 blocks in the Q2 magnet itself), and/or by reducing the ratio r_p/r_1.

It remains then, to be sure to conservatively estimate the magnitude of uncorrected harmonics (i.e., $q\%$ of the fundamental) so that the capacity, i.e., the length L of the designed corrector ring to null them is sufficient. In general, for a given corrector length L, there is a tradeoff between attainable harmonics reduction factor f (Eq. 13) and nullable harmonic magnitude Ns_N/r_p (Eq. 10). Larger M and R/r_p lead to a better harmonics reduction ratio f, but lower the maximum nullable harmonic magnitude (assuming Mr_c is constant). Nonetheless, as illustrated above, both impressive rejection ratios and large absolute magnitudes of nullable harmonics are simultaneously attainable.

C. What if the harmonic mix to be nulled changes?

If the mix of harmonics to be nulled is known and expected to remain invariant, a corrector ring can be designed using cylinders of different lengths per Eqs. (11) and (10). Alternatively, inverting the same matrix of Eq. (5), cylinders of different radii squared $r_{c_m}^2$ (or B_r, were they available) could likewise be employed. Inverting a different matrix, variable radial position R_m could also be employed to null harmonics.

However, the beauty of the counter-rotating cylinder pairs scheme is its flexibility; arbitrary cylinder pair net magnetization strength and orientation allow changing the mix of harmonics to be nulled without resorting to ring or parts replacement. Alternatively, several corrector rings of a standard cylinder pair design can be utilized to null a different error harmonics mix in a series of nominally identical magnets. Furthermore, this robust scheme

provides for self-correction as shown in the following section. The counter-rotation scheme can also be employed with blocks having other shapes, e.g. with square PM cross-sections inside a machined cylindrical sleeve to facilitate rotation, and/or with a different geometrical arrangement of tuning blocks.

A uniform temperature excursion will not alter the harmonic mix of either an accelerator magnet or its companion corrector ring, though it causes a field magnitude change in both of equal percentage. Thus it will not affect harmonic corrector ring performance.

D. Would corrector ring shielding affect performance?

Corrector ring shielding creates additional (virtual) field sources as images of the originals. A dipole or PM cylinder of strength and orientation $p_m = \epsilon_m e^{i\phi_m}$ at location $Re^{i\beta_m}$ in a device with an infinitely permeable annular shield of radius R_s centered at $z = 0$ will produce an image source of strength and orientation $t_m = \epsilon_m (R_s/R)^2 e^{i(2\beta_m - \phi_m)}$ at $R_t e^{i\beta_m}$, where $R_t = R_s^2/R$ and where it is assumed that $r_c/R \leq 0.1$.

Nulling an N-pole term in the shielded corrector ring will introduce further error terms, in addition to those given by Eq. (12). Using the ϕ_{m_N} given in Eq. (10), Eq.(8) gives the coefficient for a single nulled multipole in terms of the uniform effective length ϵ_N and reference orientation ϕ_{0_N}:

$$b_N = M k_N \epsilon_N e^{i\phi_{0_N}}. \tag{16}$$

Error terms created due to image sources, from Eq. (4) are:

$$b_{n=\nu M-N} = M k_n \epsilon_N e^{-i\phi_{0_N}} \left(\frac{R}{R_s}\right)^{2(n-1)}, \tag{17}$$

where $\nu = 0, 1, 2, ..., \infty$. Field contributions from the image source related error terms start with the $n = M-N$ term and are relatively small compared with the original N-pole error term that was nulled. For each of the nulled error terms N, at $|z| = r_p$ the ratio f of image source induced error terms to the corresponding nulled term is:

$$f \equiv \sum_{n=\nu M-N}^{\infty} (nc_n/r_p)/(Nc_N/r_p) = \tag{18}$$

$$e^{-i2\phi_{0_N}} \sum_{\nu=1}^{\infty} \left(\frac{\nu M - N}{N}\right) \left(\frac{R}{R_s}\right)^{2(\nu M-N-1)} \left(\frac{r_p}{R}\right)^{\nu M-2N}.$$

The largest terms are those for which $\nu = 1$ and they increase with N. Thus one must choose M and radii R, R_s, and r_p such that the rejection ratio f is sufficiently small for the highest order terms to be nulled, as is the case for scenario *iv* above.

V. POSITIONING SENSITIVITES AND IMPLICATIONS FOR HARMONICS

Harmonic mix sensitivities due to a perturbation δP in
(1) radial position R_m of the m^{th} rotor pair,
(2) azimuthal position β_m of the m^{th} rotor pair,
(3) angle ϕ_m of magnetization of the m^{th} rotor pair,
(4) length L_m of the m^{th} rotor pair,
(5) cosine of separation angle η_m between magnetization directions of the two cylinders comprising the m^{th} rotor pair,
(6) cylinder radius squared r_c^2 of the m^{th} rotor pair, or
(7) remanent field strength B_r of the m^{th} rotor pair,
is given by (using Eq. (2)):

$$\delta P \frac{dI^*(z)}{dP} = \sum_{n=1}^{\infty} \left\{ g_n \left(\frac{r_p}{R_m}\right)^{n-1} B_{r_m} L_m \left(\frac{r_{c_m}}{R_m}\right)^2 \right.$$

$$\left. e^{i(\phi_m - (n+1)\beta_m)} \right\} \left(\frac{z}{r_p}\right)^{n-1}, \tag{19}$$

where for

$$P \equiv \begin{cases} R_m \\ \beta_m \\ \phi_m \\ L_m, \\ \cos\eta_m \\ r_{c_m}^2 \\ B_{r_m} \end{cases} \quad g_n \equiv \begin{cases} (-n[n+1]/2)(\delta R_m/R_m) \\ (-n[n+1]/2)\delta\beta_m \\ (in/2)\delta\phi_m \\ (n/2)(\delta L_m/L_m) \\ (n/2)\delta\cos\eta_m \\ (n/2)(\delta r_{c_m}^2/r_{c_m}^2) \\ (n/2)(\delta B_{r_m}/B_{r_m}). \end{cases}$$

The kernel of Eq. (17) in brackets {} are merely new inc_n/r_p terms which themselves are nullable via new $\epsilon_N L, \phi_{m_N}$ contributions, calculated from Eq. (10), which when added to the previous summation in Eq. (11) yield new L_m and ϕ_m. Thus, the corrector ring is capable of self-correction!

The magnitude of the corrector ring perturbation-induced harmonics are directly calculable. For the parameters of scenario (*iv*) and with $B_r = 10,000$ G, $L_m = 5$ cm, and a perturbation $\delta P/P = 1\%$ (or $\delta P = 0.01$ rad when P represents an angle or $\delta P = 0.01$ when P represents $\cos\eta_m$), the contribution at $|z| = r_p$ of the new $N = 1$ term s_1/r_p normalized to the Q2 fundamental $N_f = 2$ term is $3.59/251000 = 0.14 \cdot 10^{-4}$ for P representing R_m or β_m, and half that amount for the other perturbation parameters.

The largest multipole contribution at $|z| = r_p$ for P representing R_m or β_m, which occurs at the integer nearest the harmonic

$$n = \frac{2\hat{r}_p}{1-\hat{r}_p}, \text{ is } \frac{(ns)_{max}}{s_1} = \frac{(\hat{r}_p+1)}{(1-\hat{r}_p)^2} \hat{r}_p^{(2\hat{r}_p/(1-\hat{r}_p))} \tag{20}$$

times as large as the $N = 1$ term, where $\hat{r}_p \equiv r_p/R$. For scenario (*iv*) $r_p/R = 4.5/5.9$ and $(ns)_{max}/1s_1 = 5.5$, thus

the largest harmonic contribution at $|z| = r_p$ normalized to the Q2 fundamental is $0.77 \cdot 10^{-4}$ for $\delta R_m/R_m$ or $\delta\beta_m = 0.01$. Actual deviations of these parameters should be much smaller than 0.01 and thus self-correction of these harmonics is most likely unnecessary.

For the other perturbation parameters the largest multipole contribution, which occurs at the integer nearest

$$n = \frac{\hat{r}_p}{1-\hat{r}_p}, \text{ is } \frac{\hat{r}_p^{(\hat{r}_p/(1-\hat{r}_p))}}{1-\hat{r}_p} \tag{21}$$

times as large as the $N = 1$ term. For scenario (iv) $r_p/R = 4.5/5.9$ and $(ns)_{max}/1s_1 = 1.8$, thus the largest harmonic contribution at $|z| = r_p$ normalized to the Q2 fundamental is $0.13 \cdot 10^{-4}$ for $\delta\phi_m$, $\delta L_m/L_m$, $\delta B_{r_m}/B_{r_m}$, $\delta r_{c_m}^2/r_{c_m}^2$, or $\delta \cos\eta_m = 0.01$. These contributions are negligible compared with the target harmonics level of $1 \cdot 10^{-4}$ and need not be corrected if actual perturbation parameters $\delta P/P$ or $\delta P \simeq 0.01$.

VI. SUMMARY

The pure PM harmonics corrector ring described herein enables nulling of an arbitrary harmonic mix in an accelerator magnet. For the B-factory's Q2 septum quadrupole, relatively high harmonic magnitudes ($\sim 1\%$ @ r_p) can be nulled with a compact ($\sim$ 5 cm long) corrector. For Q2, high harmonics rejection factors (> 100) are attainable with reasonable device design complexity (32 PM cylinders). For other magnets, harmonics rejection factors of over 10^3 are possible, limited only by the corresponding absolute strength nulling capability of a specified corrector length. Flexibility for infrequent in-situ harmonics mix changing is easily incorporated in the design and is accomplished by manual rotation and counter-rotation of cylinder pairs. Likewise, several corrector rings of a standard cylinder pair design can be utilized to null a different error harmonics mix in a series of nominally identical magnets. Frequent in-situ harmonics mix changing is possible via remote control of rotor rotation. Harmonics introduced by positioning and magnetization errors are themselves nullable in this robust device. Finally, the need to get the requisite field quality directly from shimming, shaping, or positioning the companion accelerator magnet is obviated, simplifying fringe field design compensation, parts tolerancing, PM quality isssues, etc.

This concept of an independent arbitrary harmonic generating/nulling device embodied in the inexpensive, flexible, robust, high-strength PM design provides a powerful new tool for wide application in accelerator design, tuning, and harmonics suppression.

VII. APPENDIX A: INTEGRAL DERIVATIONS

Eq. (1) becomes, with $\theta \equiv \delta - \phi$; $z_0 - z = Re^{i\beta} + r_c e^{i\delta}$:

$$B^*(z) = \frac{B_r}{2\pi}\int_0^{2\pi} \frac{r_c \cos\theta}{z - z_0(\delta)} d\delta$$

$$= \frac{-B_r}{2\pi}\int_0^{2\pi} \frac{r_c(\cos\delta\cos\phi + \sin\delta\sin\phi)}{Re^{i\beta} + r_c e^{i\delta}} d\delta. \tag{22}$$

Defining $Z \equiv r_c e^{i\delta}$ it follows that $dZ = iZd\delta$, $2\cos\delta = Z/r_c + r_c/Z$, $2i\sin\delta = Z/r_c - r_c/Z$, and

$$B^*(z) = \frac{B_r i}{4\pi}\oint \frac{\cos\phi(Z^2 + r_c^2) - i\sin\phi(Z^2 - r_c^2)}{Z^2(Z + Re^{i\beta})} dZ$$

$$= \frac{B_r i}{4\pi}\oint \frac{e^{-i\phi}}{Z + Re^{i\beta}} + \frac{e^{i\phi}r_c^2}{Z^2(Z + Re^{i\beta})} dZ. \tag{23}$$

The pole at $-Re^{i\beta}$ and the double pole at 0 lie outside and inside, respectively, the circle $Z = r_c e^{i\delta}$. Thus from Cauchy's integral formulas it follows directly that

$$B^*(z) = \frac{B_r i}{4\pi}\left(0 + 2\pi i \frac{-r_c^2 e^{i\phi}}{(Z + Re^{i\beta})^2}\bigg|_{Z=0}\right)$$

$$= \frac{B_r r_c^2 e^{i\phi}}{2(Re^{i\beta})^2} = \frac{B_r e^{i\phi}}{2}\left(\frac{r_c}{z_c - z}\right)^2. \tag{24}$$

ACKNOWLEDGMENT

We are happy to thank Klaus Halbach for teaching us the magnetics fundamentals on which this work is based and for proffering the succinct matrix notation used herein.

REFERENCES

[1] K. Halbach, "Design of permanent multipole magnets with oriented rare earth cobalt material", *Nucl. Instr. Meth.* vol. 169, p. 1, 1980.

[2] K. Halbach, "Physical and optical properties of rare earth cobalt magnets", *Nucl. Instr. Meth.* vol. 187, p. 109, 1981.

[3] K. Halbach, "Insertion device design", LBL Report V8811-1.1-16, 1989.

[4] R.D. Schlueter, "Field errors in hybrid insertion devices", *Halbach Symposium on Magnet Technology* vol. 1, LBL Report 36839, p. 55, 1995.

[5] K. Halbach, "Perturbation effects in segmented rare earth cobalt multipole magnets", *Nucl. Instr. Meth.* vol. 198, p. 213, 1982.

[6] *Reference Manual for the Poisson/Superfish Group of Codes*, LA-UR-87-126, Los Alamos National Laboratory, Los Alamos, NM 1987.

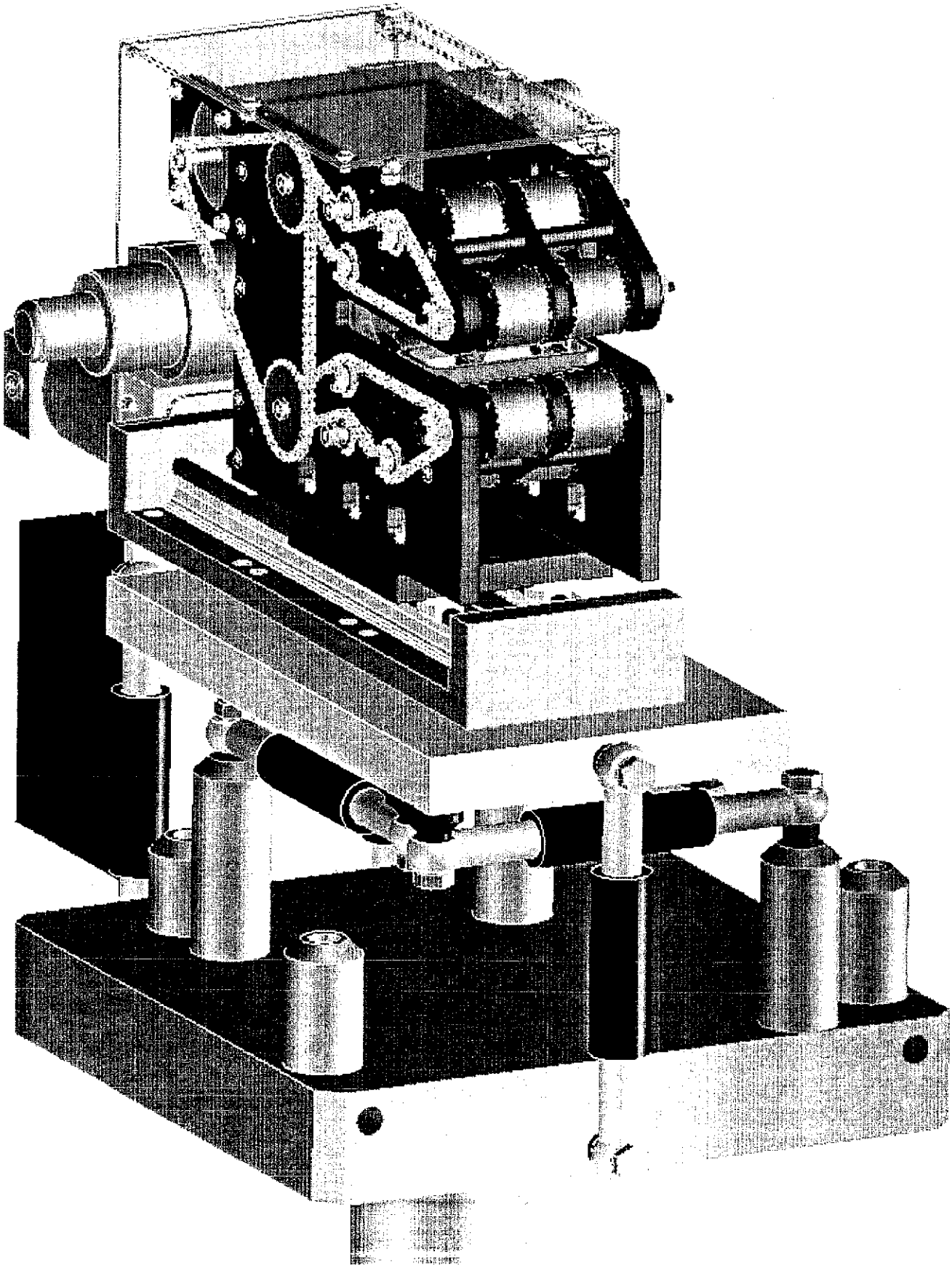

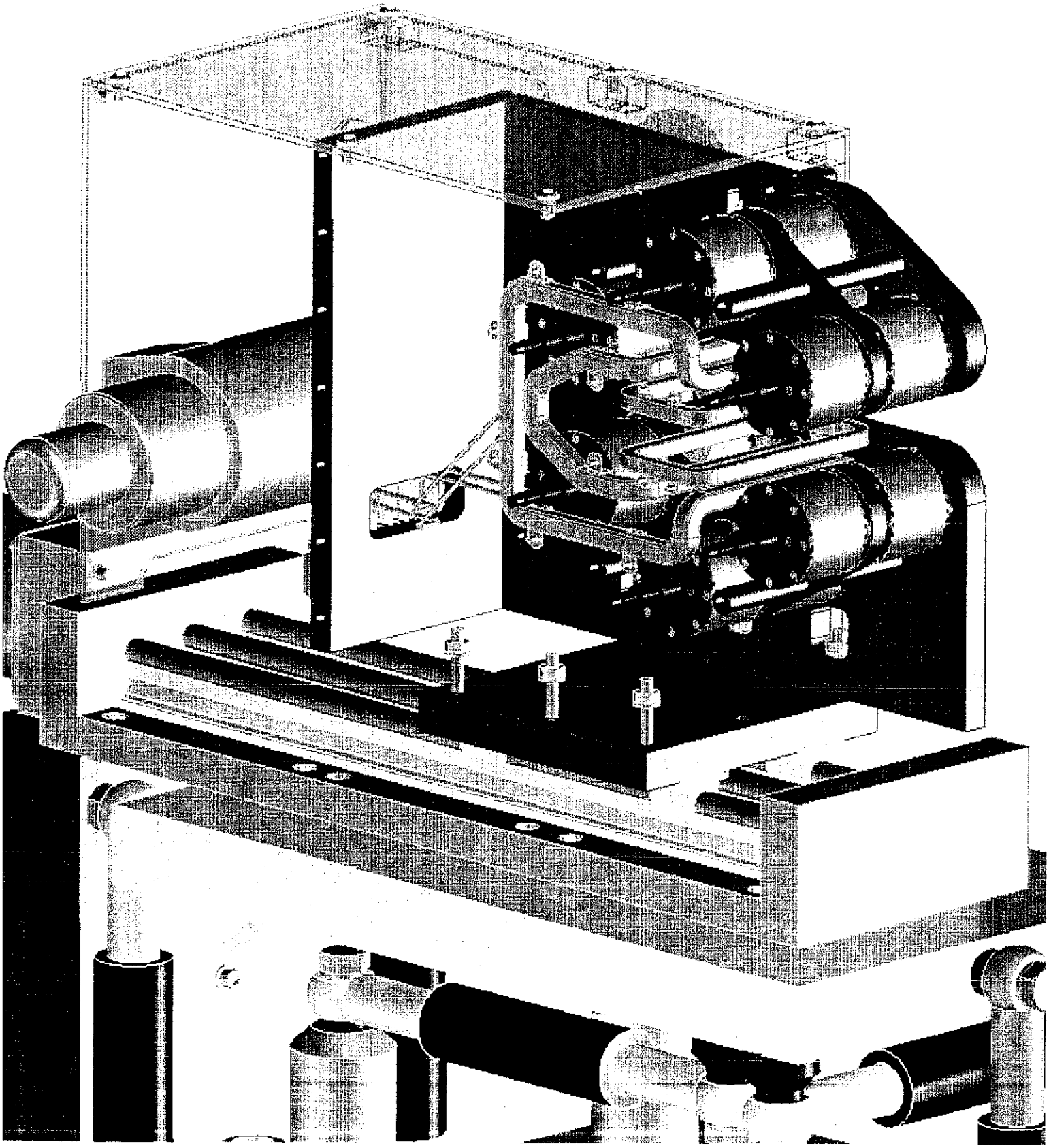

Assume current sheet model: Goal - get $F = f(H \text{ on volume surface})$

$$\bar{F} = \int \bar{j} \times \bar{B}\, dv = \mu_0 \int \bar{j} \times \bar{H}\, dv = \mu_0 \int \bar{\nabla} \times \bar{H} \times \bar{H}\, dv$$

x-comp:

$$\text{now } (\bar{\nabla} \times \bar{H} \times \bar{H})_x = (\bar{\nabla} \times \bar{H})_y H_z - (\bar{\nabla} \times \bar{H})_z H_y = H_z \left(\frac{\partial H_x}{\partial z} - \frac{\partial H_z}{\partial x}\right) - H_y \left(\frac{\partial H_y}{\partial x} - \frac{\partial H_x}{\partial y}\right)$$

$$= H_z \frac{\partial H_x}{\partial z} + H_y \frac{\partial H_x}{\partial y} + H_x \frac{\partial H_x}{\partial x} - \frac{1}{2} \frac{\partial}{\partial x}\left[H_z^2 + H_y^2 + H_x^2\right]$$

$$\therefore \bar{\nabla} \times \bar{H} \times \bar{H} = (\bar{H} \cdot \bar{\nabla})\, \bar{H} - \frac{1}{2} \nabla H^2$$

surface $\int$ for 2nd term: $\int_v \nabla H^2\, dv = \int_a H^2\, d\vec{a}$

surface $\int$ for 1st term: for any vector $\vec{t} \equiv \int \vec{c}\, \vec{\nabla} \cdot \vec{b}\, dv$:

$$t_x = \int c_x\, \vec{\nabla} \cdot \vec{b}\, dv = \int \vec{\nabla} \cdot c_x \vec{b}\, dv - \int \vec{b} \cdot \nabla c_x\, dv$$

$$= \int c_x\, \vec{b} \cdot d\vec{a} - \int \vec{b} \cdot \nabla c_x\, dv$$

then, $\vec{t} = \int_v \vec{c}\, \vec{\nabla} \cdot \vec{b}\, dv = \int_a \vec{c}\, (\vec{b} \cdot d\vec{a}) - \int_v (\vec{b} \cdot \vec{\nabla})\, \vec{c}\, dv$

let $\vec{b} = \vec{H}$ + also $\vec{c} = \vec{H}$:

$$\int_v \vec{H}\, \underbrace{\vec{\nabla} \cdot \vec{H}}_{=0}\, dv = \int_a \vec{H}\, (\vec{H} \cdot d\vec{a}) - \int_v (\vec{H} \cdot \vec{\nabla})\, \vec{H}\, dv$$

$$\therefore \int_v (\vec{H} \cdot \vec{\nabla})\, \vec{H}\, dv = \int_a \vec{H} (\vec{H} \cdot d\vec{a})$$

$$\boxed{\vec{F}/\mu_0 = \int_a \vec{H} (\vec{H} \cdot d\vec{a}) - \frac{1}{2} \int_a H^2 d\vec{a}}$$

UNITS: $\tilde{H} \equiv \mu_0 H$; $\vec{F} = \frac{1}{\mu_0}\left[\int \tilde{H} (\tilde{H} \cdot da) - \int \frac{1}{2} |\tilde{H}|^2 da\right]$

$$[N] = \left[\frac{A}{.4\pi \cdot 10^{-6}\, Tm}\right][T^2 m^2] \quad \checkmark \quad (N = TAm)$$

in my codes $\tilde{H}$ [G], a [cm^2] :

$$\therefore F[N] = \underbrace{\left[\frac{10^{-12}}{0.4\pi \cdot 10^{-6}}\right]}_{\text{!!! conv.}} \int \tilde{H} (\tilde{H} \cdot da) - \frac{1}{2} \int |\tilde{H}|^2 da$$

$$[G]\ [G]\ [cm^2]$$

want to get Forces: F_{1yo}, F_{2yo} (from cpu3) + F_{1xo}, F_{4xo} (from CPU

+ also across horiz midplane: $F_{1yo} + F_{2yo}$

across vert. midplane: $F_{1xo} + F_{4xo}$

on quad. # 1 : $F_{1yo} + F_{1xo}$

2 : $F_{2yo} - F_{1xo}$

3 : $-F_{2yo} - F_{4xo}$

4 : $-F_{1yo} + F_{4xo}$

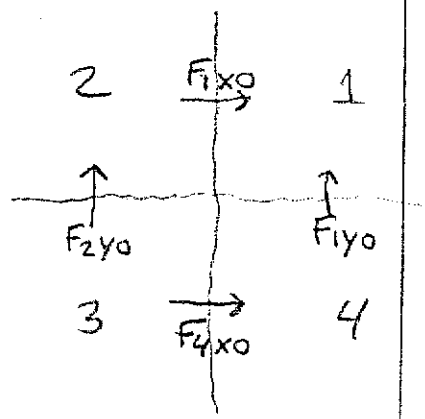

For $F_{1yo} + F_{2yo}$ $d\vec{a} = (0,-1,0)\,da$; ∴

$$F_{1yo} + F_{2yo} = -\frac{conv}{2}\cdot\int\left(2\tilde{H}_x\tilde{H}_y,\ \tilde{H}_y^2 - \tilde{H}_x^2 - \tilde{H}_z^2,\ 2\tilde{H}_z\tilde{H}_y\right)da$$

where $da = dx\,dz$; $-\infty \le z \le \infty$; $0 \le x \le \infty$ for F_{1yo}; $-\infty \le x \le 0$ for F_{2yo}

For $F_{1xo} + F_{4xo}$ $d\vec{a} = (-1,0,0)\,da$; ∴

$$F_{1xo} + F_{4xo} = -\frac{conv}{2}\int\left(\tilde{H}_x^2 - \tilde{H}_y^2 - \tilde{H}_z^2,\ 2\tilde{H}_y\tilde{H}_x,\ 2\tilde{H}_z\tilde{H}_x\right)da$$

where $da = dy\,dz$; $-\infty < z < \infty$; $0 \le y \le \infty$ for F_{1xo}; $-\infty \le y \le 0$ for F_{4xo}

These 2 Eqns. are the "engine" of code fcpu.for. Procedure:

choose (another) geometry: λ, h, Dims, easy-axis orient., $B_r = 1T$ cpu_ind

run cpu3 to get $\tilde{H}(x,0,z)$ over 1 period cpu_out.dat

run cpu5 to get $\tilde{H}(0,y,z)$ over 1 period cpu_out.dat

merge the 2 cpu_out.dat files into fcpu_in.dat

repeat for other geometries, if desired (e.g. diff. zshifts)

run fcpu (hardwired in fcpu are λ, und. length, + B_r, which must be preset correctly)